

**Vibration Damping Property and Flexural Fatigue Behavior of  
Glass/Epoxy/Nanoclay Composites**

Ahmed Kabir

A Thesis

in

The Department

of

Mechanical and Industrial Engineering

Presented in Partial Fulfillment of the Requirements

for the Degree of Master of Applied Science (Mechanical Engineering) at

Concordia University

Montreal, Quebec, Canada

November 2010

© Ahmed Kabir, 2010

**CONCORDIA UNIVERSITY**  
**SCHOOL OF GRADUATE STUDIES**

This is to certify that the Thesis prepared,

By: **Ahmed Kabir**

Entitled: **“Vibration Damping Property and Flexural Fatigue Behavior of Glass/Epoxy/Nanoclay Composites”**

and submitted in partial fulfillment of the requirements for the Degree of  
**Master of Applied Science (Mechanical Engineering)**

complies with the regulations of this University and meets the accepted standards with respect to originality and quality.

Signed by the Final Examining Committee:

_____	Chair
Dr. S. Rakheja	
_____	Examiner
Dr. M. Pugh	
_____	Examiner
Dr. M. Nokken	External
Building, Civil and Environmental Engineering	
_____	Supervisor
Dr. S.V. Hoa	

Approved by:

\_\_\_\_\_  
Dr. A.K.W. Ahmed, MASc Program Director  
Department of Mechanical and Industrial Engineering

\_\_\_\_\_  
Dean Robin Drew  
Faculty of Engineering & Computer Science

Date: \_\_\_\_\_

# ABSTRACT

## Vibration damping property and flexural fatigue behavior of glass/epoxy/nanoclay composites.

Ahmed Kabir

Recently, nano-reinforcement of polymers to form nanocomposites has attracted the attention of researchers for their potential in property developments. This study demonstrates that nanoclay fillers can improve vibration damping property and fatigue behavior of conventional long fiber reinforced composites. Nanoclay was dispersed in epoxy resin by a solvent-free high-speed mixing method using a high speed homogenizer. This modified resin was used to manufacture S-glass/epoxy composite laminates by hand lay-up and autoclave curing. The dynamic properties of the samples were tested using a dynamic mechanical analyzer DMA 983. A maximum of 16.8% improvement in the flexural storage modulus was achieved for adding up to 2 wt.% nanoclay in the unidirectional laminate. The maximum improvement in the loss modulus was 22.5% in a quasi-isotropic laminate for the same amount of clay loading. To see the damping effect of nanoclay at higher frequency and amplitude, a log decrement test was carried out where a maximum of 57% increase in damping ratio was observed. It was also interesting to investigate the significance of property development including damping improvement on fatigue life as vibration represents flexural fatigue load acting on the structure. A fixed amplitude flexural fatigue test method was designed using an MTS machine. 66% and 133% improvement in flexural fatigue life at respectively 1 and 2 wt.% nanoclay

incorporation was achieved in the case of a cross-ply laminate. To validate these results, log decrement tests were done and fatigue damage indexes were calculated after different fatigue cycles. Both of them agree quite well with flexural fatigue test results. Nanoclay increases the fracture resistance significantly which was characterized by optical and scanning electron microscope.

## ACKNOWLEDGEMENTS

I express my sincere and deep gratitude to my thesis supervisor Prof. Dr. Suong V. Hoa for his guidance, encouragement and continued support throughout this work. His enthusiasm, wide knowledge and motivational ability made this journey easier for me. It's been an honor to work with him and I am grateful to Dr. Hoa for giving me this opportunity.

I acknowledge the encouragement, help and continued support of my colleagues. I thank them for providing a dynamic environment to learn and cooperate in every way.

I would like to thank Dr. Ming Xie, Mr. Heng Wang and Mr. Dan Juras for their time and assistance in experimental work and laboratory procedures.

I thank my brother, sister and grandmother for their moral support. At last, but not the least, I am thankful to my parents, Md. Ziaul Haque and Shahnur Haque who brought me to this beautiful world and guided me to the right path of life. To my parents, I dedicate this thesis.

# Table of Contents

<b>List of Figures</b> .....	<b>IX</b>
<b>List of Tables</b> .....	<b>XV</b>
<b>Chapter 1 Introduction</b> .....	<b>1</b>
1.1 Introduction .....	1
1.2 Thesis motivation .....	2
1.3 Content of the thesis .....	3
<b>Chapter 2 Literature Review</b> .....	<b>5</b>
2.1 Nano-layered silicates and organoclay.....	5
2.1.1 Organically modified layered silicate.....	6
2.1.2 Nano-composite structures .....	8
2.2 Fabrication of nano-composites .....	9
2.2.1 In-situ polymerization process .....	9
2.2.2 Solution Process .....	15
2.3 Theories on damping and experimental methods for damping measurements .....	16
2.3.1 Analytical models for damping prediction .....	17
2.3.2 Experimental methods for damping .....	21
2.3.3 Techniques for damping improvement.....	24
2.4 Damping of neat polymer and nano-filler incorporated polymer resins .....	28
2.5 Damping of modified polymer reinforced with long fibers .....	32
2.6 Effect of nano-fillers on fatigue life of composite material .....	36
2.7 Summary .....	40
2.8 Thesis Objectives .....	42
<b>Chapter 3 Materials and Experimental Procedure</b> .....	<b>43</b>
3.1 Materials Selection.....	43
3.1.1 Uni-web S-glass fiber .....	43
3.1.2 Nanomer I.30E .....	44
3.1.3 Epoxy (EPON828).....	45

3.1.4 Hardener EPICURE 3046.....	46
3.2 Dispersion method.....	47
3.3 Sample preparation.....	50
3.3.1 Epoxy + Clay sample preparation .....	51
3.3.2 Epoxy + Clay + S-glass sample preparation.....	53
3.3.3 Autoclave curing.....	56
3.4 Problems associated with sample fabrication.....	58
3.5 Experimental Procedure .....	63
3.5.1 Dynamic Mechanical Analysis (DMA).....	63
3.5.2 Log Decrement Test .....	67
3.5.3 Flexural Fatigue Test.....	70
3.5.3.1 Deflection of Beam .....	73
3.5.3.2 Fatigue Damage Index .....	76
<b>Chapter 4 Vibration Test Results .....</b>	<b>77</b>
4.1 DMA Analysis.....	77
4.1.1 Neat epoxy and nano-clay incorporated epoxy .....	78
4.1.2 Unidirectional Laminate.....	80
4.1.3 Cross-Ply Laminate .....	83
4.1.4 Quasi-isotropic Laminate .....	85
4.2 Log Decrement Test.....	87
4.2.1 Unidirectional Laminate.....	87
4.2.2 Cross-Ply Laminate .....	89
4.2.3 Quasi-isotropic Laminate .....	91
4.3 Conclusion.....	93
<b>Chapter 5 Fatigue Test Results and Fracture Behavior.....</b>	<b>95</b>
5.1 Flexural Fatigue Test.....	95
5.1.1 Cross-ply Laminate .....	96
5.1.2 Quasi-isotropic Laminate .....	108
5.2 Fracture Behavior .....	119

5.2.1 Location A .....	119
5.2.2 Location B .....	121
5.2.3 Location C .....	123
5.3 Conclusion.....	124
<b>Chapter 6 Conclusion, Contributions and Future Work .....</b>	<b>125</b>
6.1 Conclusion.....	125
6.2 Contributions.....	126
6.3 Future work .....	127
<b>References:.....</b>	<b>128</b>

## List of Figures

Figure 2.1 Structure of 2:1 phyllosilicates.....	6
Figure 2.2 Alkyl chain aggregation in layered silicates: a) lateral mono-layer, b) lateral bi-layer, c) paraffin-type mono-layer and d) paraffin-type bi-layer .....	7
Figure 2.3 Schematic illustration of PLS structures: a) phase separated, b) intercalated and c) exfoliated nano-composites.....	8
Figure 2.4 Flowchart showing different steps of “in-situ polymerization” approach.....	10
Figure 2.5A XRD curves of C30B and its EPON828-C30B mixtures after being pre-mixed at different temperatures (a) 0 rpm (by hand) and (b) 24,000 rpm.....	11
Figure 2.5B XRD curves of C30B and its EPON828-C30B mixtures after being pre-mixed at different speeds: (a) room temperature and (b) 120°C .....	11
Figure 2.5C XRD curves of nano-composites pre-mixed at room temperature for different durations and cured at (a) room temperature and (b) 120°C .....	12
Figure 2.6 SEM image of nano-composites: (a) pre-mixed at room temperature with 0 rpm, (b) at 120°C for 0 min with 0 rpm, (c) at 120°C for 2 min with 24,000 rpm, (d) at 120°C for 10 min with 24,000 rpm and (e) at 120°C for 60 min with 24,000 rpm.....	12
Figure 2.7 TEM image of nano-composites: pre-mixed at 120°C for (a) 0 min with 0 rpm and (b) 60 min with 24,000 rpm .....	13
Figure 2.8 Flow chart showing different steps of “solution process”.....	15
Figure 2.9 Schematic diagram of nodal support and coil/electro-magnet drive transducer .....	22
Figure 2.10 Impulse/response test set-up for cantilever-beam specimen .....	23
Figure 2.11 Experimental set-up of free vibration test by using CFRP heater .....	26

Figure 2.12 (a) Principle of applied damping concept and (b) friction ledge assembly ...	27
Figure 2.13 Time history (a) 0% SWNT, (b) 0.5% SWNT and (c) 1% SWNT .....	31
Figure 2.14 S-N diagram obtained from flexural fatigue test.....	39
Figure 2.15 Applied cyclic stress vs. fatigue life curve of glass/epoxy laminates with and without 1 wt.% CNTs .....	40
Figure 3.1 Chemical structure of EPON 828 resin. ....	46
Figure 3.2 Photograph of (a) High speed homogenizer, (b) Rotor-stator assembly (CONCOM Lab) and (c) Rotor-stator working principle.....	48
Figure 3.3 SEM images of fracture surface of epoxy system with 2wt.% nanoclay: (a) lower magnification and (b) higher magnification. ....	49
Figure 3.4 SEM images of fracture surface of glass-fiber-epoxy system with 1 wt.% nanoclay at different magnifications.....	50
Figure 3.5 Epoxy and epoxy + clay sample manufacturing procedure.....	52
Figure 3.6 Flow chart for sample manufacturing with glass fiber.....	53
Figure 3.7 Photograph of a typical Autoclave (CONCOM Lab).....	54
Figure 3.8 Lay-up sequences for (a) Unidirectional, (b) Cross-ply and (c) Quasi-isotropic laminates. ....	55
Figure 3.9 Typical cross-section of a vacuum bag. ....	56
Figure 3.10 Cure cycle for S-glass/epoxy composite laminate.....	58
Figure 3.11 Schematic illustration of vacuum bagging sequence.....	59
Figure 3.12a Optical microscopic image of cross section of quasi-isotropic laminate without nanoclay: (i) lower magnification and (ii) higher magnification.....	60

Figure 3.12b Optical microscopic image of cross section of quasi-isotropic laminate with 1 wt.% nanoclay: (i) lower magnification and (ii) higher magnification. ....	61
Figure 3.12c Optical microscopic image of cross section of quasi-isotropic laminate with 2 wt.% nanoclay: (i) lower magnification and (ii) higher magnification. ....	62
Figure 3.13 Sinusoidal oscillation and response of, (a) purely elastic material and (b) linear viscoelastic material.....	64
Figure 3.14 Photograph of (a) a 983 DMA with TA 2100 Thermal analyzer and (b) a sample clamped with 983 DMA (CONCOM Lab).....	65
Figure 3.15 DMA internal components .....	66
Figure 3.16 Experimental set-ups for log decrement test. ....	68
Figure 3.17 Photographs of (a) typical samples, (b) clamped sample with accelerometer and (c) log decrement test set-up. ....	69
Figure 3.18 Schematic illustration of experimental set-up for flexural fatigue test. ....	70
Figure 3.19 Typical fatigue sample with strain gage and wire. ....	71
Figure 3.20 Photograph of experimental set-up for flexural fatigue test.....	71
Figure 3.21 Schematic of (a) free body diagram, (b) shear force diagram and (c) bending moment diagram. ....	73
Figure 4.1 DMA curves of neat epoxy and nanoclay incorporated epoxy; (a) storage modulus, (b) loss modulus and (c) tan delta. ....	78
Figure 4.2 DMA curves of unidirectional laminates with different nanoclay contents; (a) storage modulus, (b) loss modulus and (c) tan delta.....	81
Figure 4.3 DMA curves of cross-ply laminates with different nanoclay contents; (a) storage modulus, (b) loss modulus and (c) tan delta.....	83

Figure 4.4 DMA curves of quasi-isotropic laminates with different nanoclay contents; (a) storage modulus, (b) loss modulus and (c) tan delta.....	85
Figure 4.5 Free decay curves of unidirectional laminates with different nanoclay contents. .....	88
Figure 4.6 Free decay curves of cross-ply laminates with different nanoclay contents. ..	90
Figure 4.7 Free decay curves of quasi-isotropic laminates with different nanoclay contents. ....	92
Figure 5.1 Flexural fatigue test results of cross-ply laminates: (a) no clay, (b) 1 wt.% nanoclay and (c) 2 wt.% nanoclay. ....	97
Figure 5.2 Flexural fatigue test results of cross-ply laminates: (a) Sample set# 1, (b) Sample set# 2 and (c) Sample set# 3. ....	98
Figure 5.3 Average test results of three cross-ply laminates with scatter in strain values: (a) no clay, (b) 1 wt.% nanoclay and (c) 2 wt.% nanoclay. ....	99
Figure 5.4a Optical micro-graph of the cross section of cross-ply laminate without nanoclay after 200,000 fatigue cycles.....	100
Figure 5.4b Optical micro-graph of the cross section of cross-ply laminate with 1 wt.% nanoclay after 200,000 fatigue cycles.....	101
Figure 5.4c Optical micro-graph of the cross section of cross-ply laminate with 2 wt.% nanoclay after 200,000 fatigue cycles.....	101
Figure 5.5a Free decay curves for cross-ply laminate without nanoclay after different fatigue cycles. ....	103
Figure 5.5b Free decay curves for cross-ply laminate with 1 wt.% nanoclay after different fatigue cycles. ....	104

Figure 5.5c Free decay curves for cross-ply laminate with 2 wt.% nanoclay after different fatigue cycles. ....	105
Figure 5.6 Flexural fatigue test results of quasi-isotropic laminates: (a) no clay, (b) 1 wt.% nanoclay and (c) 2 wt.% nanoclay.....	108
Figure 5.7 Flexural fatigue test results of quasi-isotropic laminates: (a) Sample set# 1, (b) Sample set# 2 and (c) Sample set# 3. ....	109
Figure 5.8 Average test results of three quasi-isotropic laminates with scatter in strain values: (a) no clay, (b) 1 wt.% nanoclay and (c) 2 wt.% nanoclay.....	110
Figure 5.9a Optical micro-graph of the cross section of quasi-isotropic laminate without nanoclay after 200,000 fatigue cycles.....	111
Figure 5.9b Optical micro-graph of the cross section of quasi-isotropic laminate with 1 wt.% nanoclay after 200,000 fatigue cycles. ....	112
Figure 5.9c Optical micro-graph of the cross section of quasi-isotropic laminate with 2 wt.% nanoclay after 200,000 fatigue cycles. ....	112
Figure 5.10a Free decay curves for quasi-isotropic laminate without nanoclay after different fatigue cycles.....	114
Figure 5.10b Free decay curves for quasi-isotropic laminate with 1 wt.% nanoclay after different fatigue cycles.....	115
Figure 5.10c Free decay curves for quasi-isotropic laminate with 2 wt.% nanoclay after different fatigue cycles.....	116
Figure 5.11 schematic illustration of the location of the beam cross-section for SEM. .	119
Figure 5.12 SEM images of cross-section of laminate at location A; (a) without nanoclay, (b) 1 wt.% nanoclay and (c) 2 wt.% nanoclay. ....	120

Figure 5.13 SEM images of cross-sections of laminate at location B; (a) without nanoclay, (b) 1 wt.% nanoclay and (c) 2 wt.% nanoclay..... 122

Figure 5.14 SEM images of cross-sections of laminate at location C; (a) without nanoclay, (b) 1 wt. % nanoclay and (c) 2 wt. % nanoclay..... 123

## List of Tables

Table 2.1 Damping coefficient, natural frequency and amplitude for vibration shape modes .....	34
Table 2.2 Damping factor of first four modes of free vibration .....	35
Table 2.3 Damping factors of hybrid laminate at different impact velocities .....	36
Table 3.1 Typical properties of S-glass fiber .....	44
Table 3.2 Physical and technical details of organoclay Nanomer I.30E .....	45
Table 3.3 Typical properties of EPON 828 .....	46
Table 3.4 Characteristics of EPICURE 3046 .....	47
Table 3.5 Different sample configurations .....	51
Table 4.1 DMA properties of neat epoxy and nanoclay incorporated epoxy .....	79
Table 4.2 DMA properties of unidirectional laminates with different nanoclay contents	82
Table 4.3 DMA properties of cross-ply laminates with different nanoclay contents .....	84
Table 4.4 DMA properties of quasi-isotropic laminates with different nanoclay contents .....	86
Table 4.5 Log decrement values and damping ratios of unidirectional laminates.....	89
Table 4.6 Log decrement values and damping ratios of cross-ply laminates .....	91
Table 4.7 Log decrement values and damping ratios of quasi-isotropic laminates .....	93
Table 5.1 Sample configurations for fatigue test .....	96
Table 5.2 Log decrement values of cross-ply laminate after different fatigue cycles ....	106
Table 5.3 Storage modulus and Fatigue damage index of cross-ply laminate after different fatigue cycles.....	106

Table 5.4 Log decrement values of quasi-isotropic laminate after different fatigue cycles .....	117
Table 5.5 Storage modulus and Fatigue damage index of quasi-isotropic laminate after different fatigue cycles.....	117

# Chapter 1

## 1.1 Introduction

Damping is a very important factor related to the study of dynamic behavior especially related to vibration for fiber reinforced composite structures. This property reduces noise and vibration of the structures thus increases service life. Depending on the different sources of energy dissipation, there are several mechanisms of damping in fiber-reinforced composites as described in [1,2];

- i) The major contribution to composite damping is due to the viscoelastic nature of the polymer matrix. Some of the fibers such as carbon and Kevlar fibers have significant damping compared to other types of fibers.
- ii) Damping due to interphase: Interphase possesses a considerable thickness and its properties are different from those of embedded fiber and matrix. The interphase can be weak, ideal or strong, and accordingly affects the mechanical properties as well as damping of the structure.
- iii) Damping due to damage: It is mainly of two types; a) Frictional damping due to slippage in unbound regions between fiber and matrix interface or delaminations. And b) Damping due to energy dissipation in the area of matrix cracks, broken fibers etc.
- iv) Viscoplastic damping: Usually thermoplastic composite materials have a certain degree of non-linear damping due to the presence of high stress and strain concentration at local regions between fiber and matrix at large amplitude of vibration under high stress levels. So elasto-plastic micromechanical behavior is important even for applied stresses that are intended to remain below the apparent elastic limits of composite materials.
- v) Thermo-elastic damping: It is due to cyclic heat flow from region of compressive stress to the region of tensile stress.

There are different analytical models available for prediction of damping in conventional composite materials. All these analytical models can be classified as micro-mechanical or macro-mechanical level and based on the assumption of linear viscoelasticity [2]. Micromechanical analysis involves contributions from constituents such as fibers, matrix and interface. In the macro-mechanical approach, individual lamina is the element. In this case, the strain energy and dissipation energy of individual lamina give the overall loss factor of the laminate. For the analysis of damping, mostly correspondence principle, strain energy and finite element methods are applied.

Recently, nano reinforcement of polymers to form nanocomposites has attracted the attention of researchers for their potential in property development. Organically modified nanoclay, nano-fiber or carbon nanotubes having ultra-high strength and stiffness became very popular during last decade for nano reinforcement of polymers. Their nano-scale dimensions contribute enormous rheological benefits to the polymer resin systems. Nanoparticles at very low concentration (<5 wt.%) and well dispersed in polymer resins often impart superior mechanical, thermal, barrier and electro-magnetic properties. So nano reinforcement of polymer has opened up a new horizon for different property development and their potentials in structural applications.

## **1.2 Thesis motivation**

Nano particles such as nano layered silicate or nanoclay having thickness around 1 nm and lateral dimensions in the order of few microns, have a very high aspect ratio and specific surface area (around 657 m<sup>2</sup>/g)[3]. So even at very low concentration, these nanoclays can create a huge network of interfacial surface area when well dispersed in a

polymer resin systems. The interface has a tangible thickness having properties different from the constituent materials and is considered as a source of energy dissipation. Another source of energy dissipation related to interface is due to the friction and slippage of unbound regions or delaminated areas of clay platelet and matrix [1,2]. So it can be expected that adding nano-particles (e.g. nano-clay) in a polymer matrix can improve the ability of energy dissipation under dynamic loading thus enhancing the damping property. A number of research studies have been carried out to predict the damping property of nano-particle reinforced polymer. In some recent research, it is pointed out that randomly oriented nano-fillers having high specific surface area, i.e. nanoclay, nanotubes etc. have a significant enhancement on the damping property of composite structures [4,5-7]. So incorporation of nanoclay into conventional continuous fiber polymer matrix composite to enhance the damping property could be a viable choice for structural applications. It is worth mentioning, if vibration damping or dynamic properties are improved, the fatigue life of the structure must be improved. From this motivation, a series of experiments have been carried out to see the effect of nanoclay on vibration damping and fatigue behavior of nanoclay incorporated glass/epoxy composite.

### **1.3 Content of the thesis**

In the first chapter of the thesis, an introduction of vibration and damping, mechanisms of vibration damping and related theories are given. The motivations of incorporating nano-fillers into conventional continuous fiber composites to enhance damping property have also been discussed briefly.

In the second chapter, a detailed literature survey has been carried out. The survey topics include nano-clay, organically treated nano-clay and the reason for organic treatments; clay dispersion, methods of dispersion and their effect on mechanical performance; damping experiments; influence of nano-filler on neat resin and modified resin reinforced with long fiber. A brief summary of the literature survey and objectives of the thesis are given towards the end of this chapter.

Experimental procedures are described in chapter 3. The physical and chemical properties of the materials (i.e. nano-clay, resin, hardener, long fiber) used for this thesis are given at the beginning of the chapter. After that, sample manufacturing procedures are described. Different test methods to determine the damping property and fatigue life are also presented.

Dynamic mechanical analysis and vibration test results are presented in chapter 4. This includes DMA analysis and log decrement test results. The influences of nanoclay on storage modulus, loss modulus and vibration damping property have been discussed based on the results obtained from experiments.

Chapter 5 represents the flexural fatigue test results. The fracture behavior characterized by optical and scanning electron microscope has been discussed in this section.

In chapter 6, a conclusion of the entire work, contributions, achievements and problems are drawn. Recommendations of future potential works are also given in this section.

# Chapter 2

## Literature Review

Use of nano-clay in polymer resins for property enhancement started almost half a century ago. But the most extensive research on nano-technology started in the 1990s. Toyota was the first company to successfully develop a nano-structure incorporating organically-modified montmorillonite in nylon-6 polymer resin [8]. After that, many companies and research institutes became interested to investigate nano-composites. From these investigations, remarkable improvement on mechanical, barrier and thermal properties were reported. As the modified resin system (incorporating nanoclay) shows improved properties compared to pristine matrix, a new trend of reinforcing long fiber with this modified resin system has been started which is called hybrid composite.

The performance of nanoclay-incorporated hybrid composites depend on many factors such as clay structure, type of organic surface modifier, dispersion of clay in resin, fabrication method etc. In this chapter a comprehensive literature survey is presented.

### 2.1 Nano-layered silicates and organoclay

A nano-layered silicate refers to partially or fully synthesized natural clay formed by the weathering of eruptive rock materials and volcanic ash which is usually called bentonite [9]. The most commonly used clay or bentonite are montmorillonite, hectorite and saponite. All these clays belong to the family of 2:1 layered silicates or phyllosilicates. The structure of phyllosilicate is described in [10,11]. According to their study, these phyllosilicates have a crystal structure consisting of layers made of two tetrahedrally coordinated silicon atoms fused to an edge-shared octahedral sheet of either aluminum or

magnesium hydroxide. The layer thickness is around 1 nm, and the lateral dimensions of these layers may vary from 30 nm to several microns or larger, depending on the particular layered silicate. Stacking of the layers leads to a regular van der Waals gap between the layers called the interlayer or gallery. Isomorphous substitution within the layers generates negative charges that are counterbalanced by alkali and alkaline earth cations situated inside the galleries. Figure 2.1 shows the structure of 2:1 phyllosilicates. The surface charge is not constant within the layers but an average value is often considered. The layered silicates are characterized by this average value of surface charge known as the cation exchange capacity (CEC), and generally expressed as mequiv/100 gm.

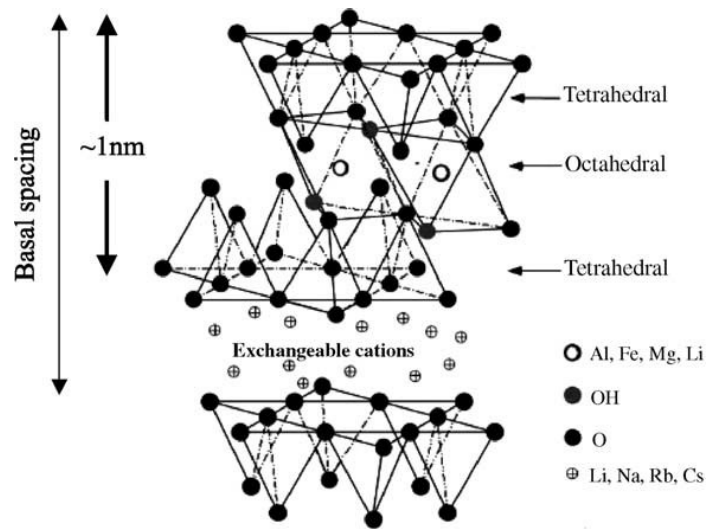
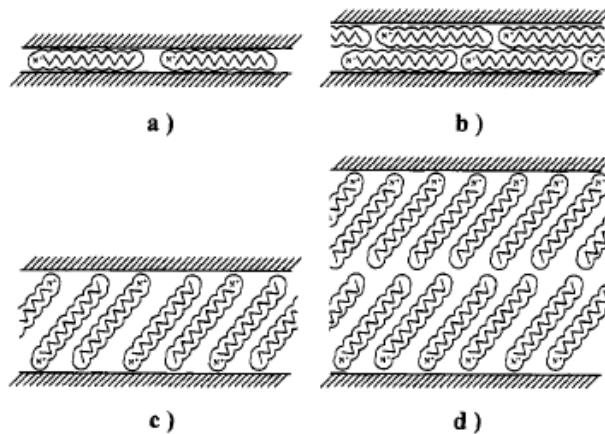


Figure 2.1 Structure of 2:1 phyllosilicates [10].

### 2.1.1 Organically modified layered silicate

Pristine layered silicates are not readily miscible to all polymer resins. The mixing of polymer and layered silicates in the process of nano-composite formation is the most challenging job because of the incompatibility of inorganic layered silicate to organic

polymer. Pristine layered silicates usually contain hydrated  $\text{Na}^+$  and  $\text{K}^+$  ions, so they are mostly hydrophilic. Hydrophilic layered silicates usually have very poor physical interaction with organophilic polymers and after mixing, are mostly separated into discrete phases [10]. Thus the poor physical interaction leads to very poor dispersion of layered silicates into the polymer matrix resulting in poor mechanical and thermal properties. So to improve the physical interaction between layered silicates and organophilic polymer, silicate surface must be modified to organophilic from hydrophilic. This is usually done by ion-exchange reactions with a cationic surfactant including primary, secondary, tertiary and quaternary alkylammonium or alkylphosphonium cations [10,13]. These cations reduce the surface energy of the inorganic layered silicates and increase the wetting capability with polymer matrix. The alkylammonium cations increase the inter-layer spacing thus assist to fill the intra gallery of layered silicates with polymer. Moreover, organic modification leaves functional groups on the clay surface to react with the polymer resulting in improved strength of the interfacial region [10,13].



*Figure 2.2 Alkyl chain aggregation in layered silicates: a) lateral mono-layer, b) lateral bi-layer, c) paraffin-type mono-layer and d) paraffin-type bi-layer [12].*

After the ion exchange reactions, the alkyl chain can be aggregated in different ways in layered silicates. From the X-ray diffraction analysis of modified layered silicates, it was observed that depending on the packing density, temperature and chain length, the chains could lay either parallel to the host layer forming lateral mono- or bi-layer or radiate away from the surface forming extended paraffin type mono- or bi-molecular arrangements [12]. Figure 2.2 shows the alkyl chain aggregations of mica-type layered silicates.

### 2.1.2 Nano-composite structures

Depending on the type of layered silicates, the type of organic modifier cation, polymer matrix and dispersion methods, basically three main types of composites can be obtained when organoclay is incorporated in polymer [10,11,13]. Figure 2.3 schematically shows different types of achievable PLS (polymer-layered silicates) structures.

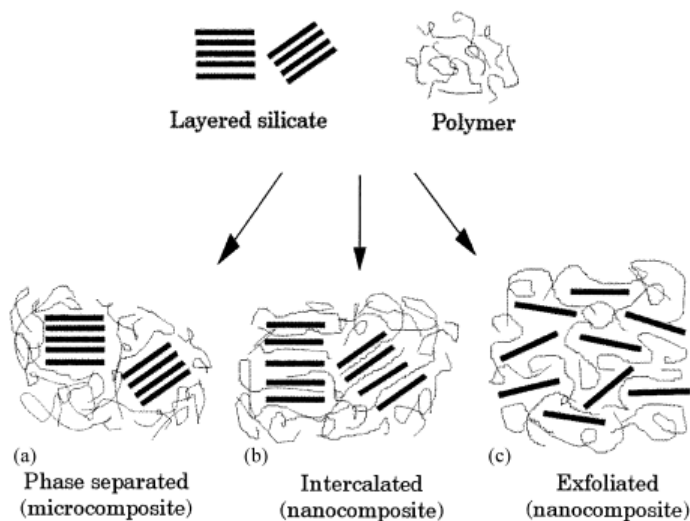


*Figure 2.3 Schematic illustration of PLS structures: a) phase separated, b) intercalated and c) exfoliated nano-composites [11].*

If the polymer cannot intercalate between the silicate layers, a phase-separated structure is formed (figure 2.3a). This type of phase separated nano-composite does not show any improvement in the properties. The reason is, due to large agglomerations of clay, significant interfacial surface area is not created at the clay/polymer interaction compared to the conventional micro-composite [10]. If single or more extended polymer chains are intercalated between the silicates layers forming an ordered multi-layer morphology built up with alternating polymeric and inorganic layers, the material is called an intercalated nano-composite (figure 2.3b) [10,13]. Sometimes silicate layers are flocculated due to hydroxylated edge-edge interaction of silicate layers and called intercalated-and-flocculated nano-composites [10]. When silicate layers are homogenously and completely dispersed in a continuous polymer matrix, an exfoliated nano-composite structure is obtained (figure 2.3c). In an exfoliated nano-composite, the individual clay layers are separated from each other by an average distance and there is no interaction between the layers [10]. An exfoliated structure is the most desirable nano-composite structure and is achievable only when clay loading is very low.

## **2.2 Fabrication of nano-composites**

For thermoset nano-composite fabrication, basically two processes have been applied. The first one is a solvent free “in-situ polymerization process” and the other one is “solution process”.

### **2.2.1 In-situ polymerization process**

In-situ polymerization process is the most popular and conventional method to fabricate polymer nano-composites. In this process, nanoclay is added to the monomer and kept for

a certain period for swelling. The swelling time depends on the polarity of monomer molecules, surface treatment of organoclay and temperature of swelling. After swelling is done, a curing agent is added to the mixture to initiate polymerization [13]. Figure 2.4 shows the flow chart of in-situ polymerization process. After the polymerization reactions, nano-composites are formed. But the dispersion of clay in the monomer does not occur so easily. The nanoclay form aggregates due to the thermodynamic force that holds silicate layers together and do not allow the monomer to diffuse into the silicate layers. Different researchers have applied different techniques to break down the clay aggregates and achieve better dispersion of clay in the polymer.

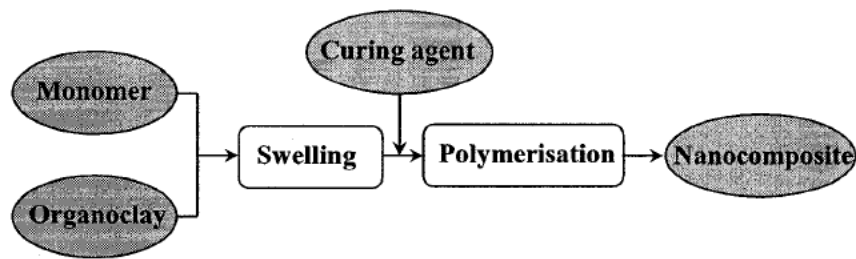


Figure 2.4 Flowchart showing different steps of “in-situ polymerization” approach [13].

Vaia et al. [14,15] have used a polymer melt intercalation approach to fabricate polymer-layered silicate (PLS). Organically modified layered silicates (OLS) and polymer were mechanically mixed and formed into pellets using a hydraulic press at a pressure of 70 MPa. Then the pellets were annealed under vacuum above the glass transition temperature or melting temperature of the polymer. The XRD and TEM investigation confirms the increased layer disorder and spacing towards the polymer-primary particle boundary proving intercalation of polymer into silicate layers.

Ngo et al. [16] developed a high speed mixing technique at CONCOM to disperse organoclay in epoxies. In this process, clay and epoxy are stirred at a very high speed (20,000 ~ 24,000 rpm) with a homogenizer equipped with a cylindrical rotor-stator mixing head of diameter 20 mm. The speed and the temperature were controlled as pre-mixing parameters to understand their effect on dispersion. Very impressive results were obtained using this technique. Figure 2.5 shows the effect of mixing speed, duration and temperature by XRD analysis of EPON828-C30B mixtures. The XRD curves confirms

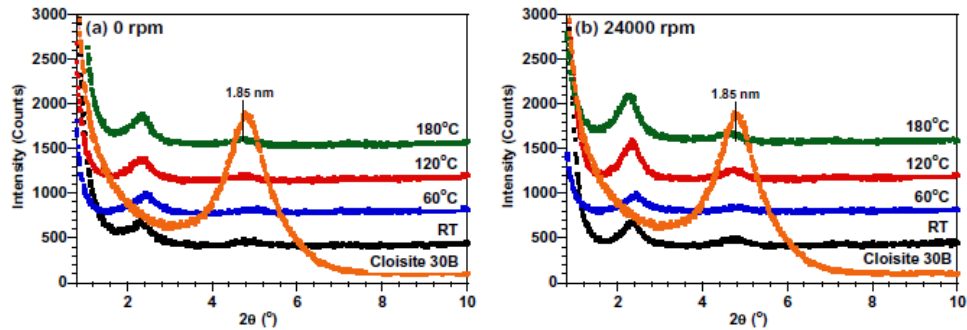


Figure 2.5A XRD curves of C30B and its EPON828-C30B mixtures after being pre-mixed at different temperatures (a) 0 rpm (by hand) and (b) 24,000 rpm [16].

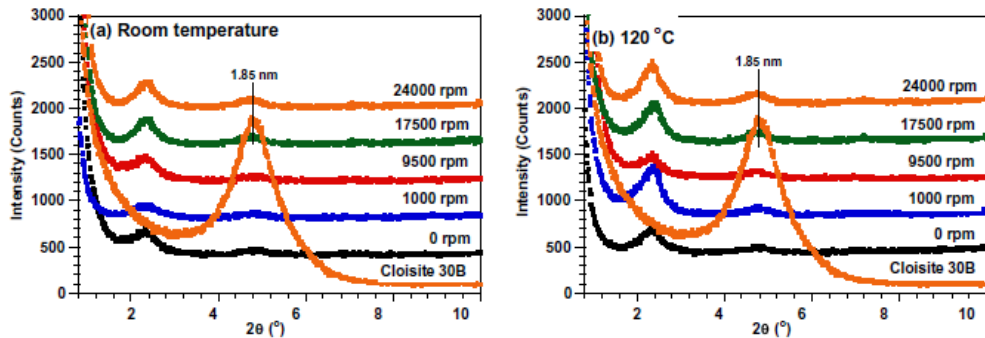


Figure 2.5B XRD curves of C30B and its EPON828-C30B mixtures after being pre-mixed at different speeds: (a) room temperature and (b) 120°C [16].

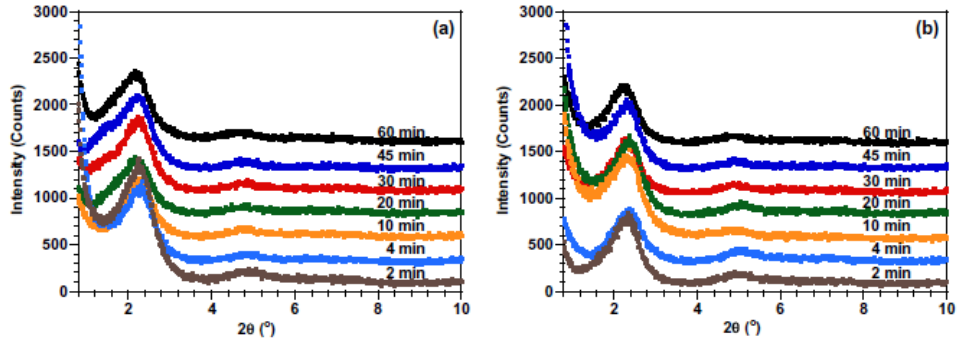


Figure 2.5 XRD curves of nano-composites pre-mixed at room temperature for different durations and cured at (a) room temperature and (b) 120°C [16].

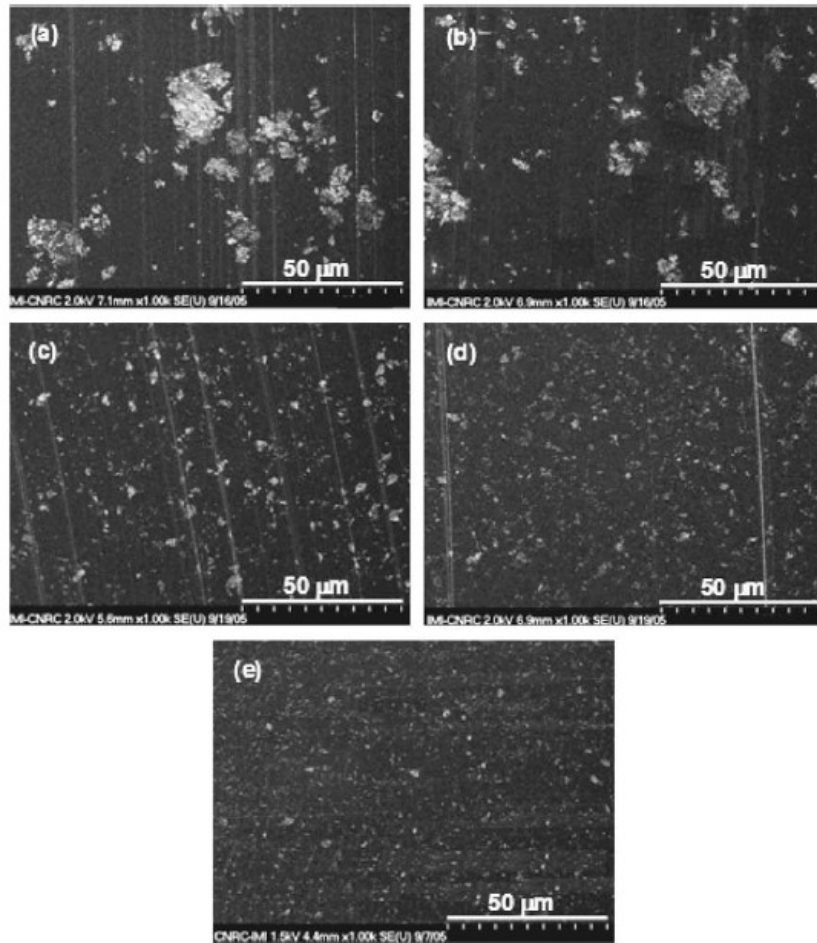
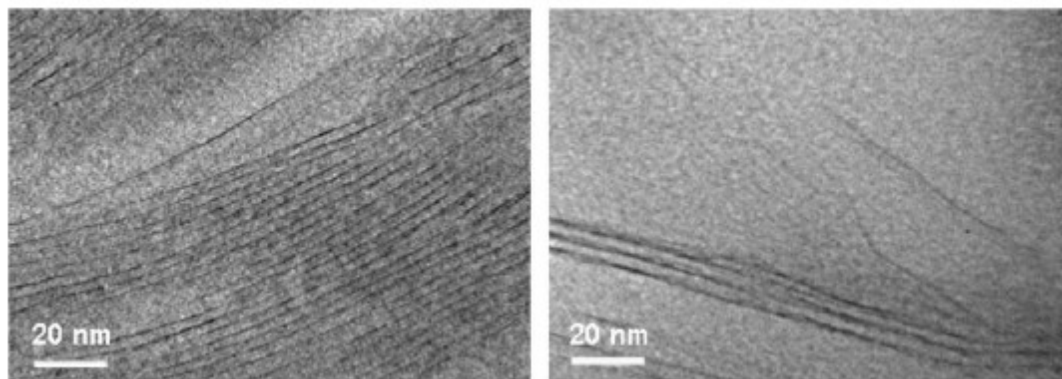


Figure 2.6 SEM image of nano-composites: (a) pre-mixed at room temperature with 0 rpm, (b) at 120°C for 0 min with 0 rpm, (c) at 120°C for 2 min with 24,000 rpm, (d) at 120°C for 10 min with 24,000 rpm and (e) at 120°C for 60 min with 24,000 rpm [16].



*Figure 2.7 TEM image of nano-composites: pre-mixed at 120°C for (a) 0 min with 0 rpm and (b) 60 min with 24,000 rpm [16].*

that, the first peak shifts to lower angle for all epoxy-clay mixtures compared to the peak of the starting clay Cloisite 30B (C30B). This proves that intercalation has taken place. The degree of intercalation was achieved around 3.72 – 3.81 nm which is considerably higher than original C30B (1.85 nm). The SEM image (fig. 2.6) and TEM image (fig. 2.7) show the effect of pre-mixing time, temperature and speed on dispersion. From the images, it was proved that increased pre-mixing speed and duration along with the temperature have a positive effect on the size reduction of the clay aggregates.

Using an excess of silane at the time of surface modification, it is possible to functionalize the clay minerals and at the same time, to intercalate some monomers or oligomers into clay galleries [17-19]. This greatly enhances interlayer distance. Gianni et al. [17] were able to obtain an intercalated/exfoliated structure using montmorillonite modified in this process while a photocurable epoxy was used as matrix. Kornmann [18] et al. successfully synthesized epoxy-layered silicate nano-composites based on tetraglycidyl diamino-diphenyl methane TGDDM resin curing with diamino-diphenyl sulfone

DDS. The layered silicate fluorohectorites modified by means of interlayer cation exchange of sodium cations for protonated dihydro-imidazolines and octadecylamine were used. These leave –OH groups in the molecular structure which has a catalytic effect on polymerization occurring between silicate layers. This helps to diffuse epoxy and curing agent between silicate layers resulting in intercalations. The TEM and SEM investigations confirm better dispersion of clay using this technique. But a systematic decrease of T<sub>g</sub> was observed and the reason for this effect was not clear.

Some researchers have used an ultrasound sonication technique to disperse nanoclay in polymer resin [20,21]. Lam et al. [20] were able to exfoliate silicate layers in epoxy resin using this technique. They added 4% nano-clay in epoxy resin by hand stirring followed by ultrasound sonication for different sonicating time. It was observed that ultrasonic energy can break clay agglomerations and form nanoclay clusters when optimum sonication time is reached. But the XRD analysis confirms that the interplanar distance between nano-clay platelet is not affected by sonication. Mitra [21] et al. prepared highly delaminated clay/poly(dicyclopentadiene) nano-composite by sonicating organically modified montmorillonite clays in dicyclopentadiene (DCPD) monomer.

Epoxy-aided dispersion of nanoclay in a glassy polymer PMMA has recently been studied [22,23]. This involves nano-clay blending in PMMA and epoxy to form a ternary composite using different blending techniques. Hernandez et al. [22] have used both melt-blending and ultrasonic-blending method individually to produce PMMA-epoxy-clay ternary composites. Phase separation between PMMA and the epoxy network was obtained in the form of spherical nodules using both techniques. Organoclay particles were delaminated and finely dispersed into the thermosetting network by ultrasonic-

blending whereas melt-blending produced micrometer-sized aggregates. Park [23] et al. used only melt-blending and was able to obtain a fully exfoliated state in the three-phase composite when epoxy to clay ratio was 10. However, the dispersion of nanoclay to the scale of individual platelets was not achieved as exfoliated clay particles remained as aggregates inside phase separated epoxy domain of approximately 1  $\mu\text{m}$  in diameter.

### 2.2.2 Solution Process

The solution process involves the use of a solvent where organoclay is dispersed in a polar solvent like toluene or acetone. In an organic polar solvent, alkylammonium-treated clay swells very well and forms gel structures. Then the polymer is added to the solution. As the polymer is already dissolved in solvent, it easily intercalates between the silicate layers. Fig. 2.8 shows the flow chart of solution process.

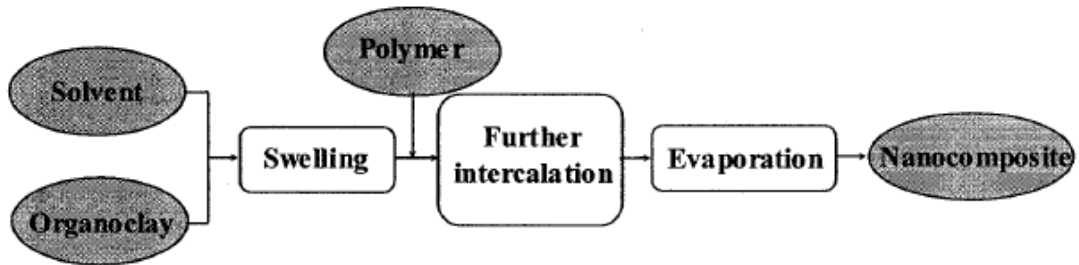


*Figure 2.8 Flow chart showing different steps of “solution process” [13].*

Here organoclays are pre-intercalated with solvent, so the polymer can easily pass through the clay gallery resulting in further intercalation. Next step involves evaporation of the solvent usually done under vacuum. After complete removal of the solvent, the polymerization process is carried out to get intercalated nano-composites. Intercalated

nano-composite structure is achievable using the solution process even if the polymer has a very low polarity [13]. An useful technique has been developed at Concordia University by CONCOM researchers which is called the high pressure mixing method (HPMM) [24,25]. Organoclay is first dispersed in a solvent like acetone to form a paste using a micro-fluidizer machine where a pressure in the range of 15,000 psi is maintained. The mixture is dried at 100°C to have an exact concentration of clay. Then the paste is added to the epoxy according to desired ratio and stirred mechanically for 1 hour at 1,000 rpm and up to a temperature of 120°C. Finally, the mixture is degassed under vacuum at an elevated temperature to remove the solvent. TEM images confirm that the aggregates were broken down to small particles consisting of several clay platelets. But the glass transition temperature  $T_g$  was reported to be slightly decreased with the increase of clay loading [24].

Although the solution process is quite effective to intercalate organoclay in epoxy, it may not be practical to use this process in industries because of its involvement with a significant quantity of solvent that is expensive and requires a cumbersome process of extraction.

### **2.3 Theories on damping and experimental methods for damping measurements**

Many studies have been carried out to develop analytical models for damping prediction of conventional composite laminates at the constituent or micro-mechanical, individual lamina or macro-mechanical and even the structural level. Most of the models developed were based on the assumption of linear viscoelasticity using mechanics of materials and elasticity approaches. For damping prediction, basically three methods have been used:

correspondence principle, strain energy method and finite element method. Using the correspondence principle, linear elastostatic analysis is converted to dynamic linear viscoelastic analysis by replacing elastic moduli with complex moduli. The strain energy method states that total damping loss factor of a system is the ratio of summation of the product of individual element loss factor and strain energy stored in each element to the total strain energy [2]. Numerous models have been developed using the above principle and methods mostly by a micro/macro-mechanical approach. The micro-mechanical approach is applied to find out the effect of constituents, i.e. fiber, matrix and interface whereas the macro-mechanical approach is mostly used to predict the effect of factors such as fiber orientation, laminate configuration, frequency and stress dependence. Some of the popular methods are described below.

### **2.3.1 Analytical models for damping prediction**

Adams and Bacon [26] developed a macro-mechanical model for a unidirectional laminate. According to the Adams-Bacon criteria, energy dissipated in a thin unidirectional lamina is the sum of the separate energy dissipated due to longitudinal, transverse and shear stress. Specific damping capacity is defined by the ratio of the energy dissipated to the strain energy stored. Ni and Adams [27] improved the model given by Adams and Bacon taking bending-twisting coupling into account and considering stress  $\sigma_1$ , strains  $\varepsilon_6$  and  $\varepsilon_6$  in the specimen co-ordinate system while determining the dissipated energy. Excellent agreement between the theoretical prediction and experimental results were obtained. The Adams-Bacon criteria were also utilized to predict moduli and flexural damping of anisotropic CFRP and GFP beams with respect to fiber orientation by Adams and Maheri [28]. Here, effects of aspect ratio

and stress level on damping were taken in account. The test results showed that the SDC (Specific Damping Capacity) of both symmetric angle-ply and off-axis beams at any orientation can be predicted with fairly good accuracy. But for higher angle (of orientation) beams ( $45^\circ$  to  $90^\circ$ ) nonlinearity of SDC was observed which might be attributed from the plastic deformation beyond the critical stress level. Yim [29] utilized the modified classical lamination theory based on the elastic-viscoelastic correspondence principle to develop basic damping of Poisson's ratio for accurately predicting the damping of laminated composites. Six typical symmetric laminated composite with different stacking sequence were employed for this study. Firstly, using the modified classical lamination theory and the elastic-viscoelastic correspondence principle, the [A], [B] and [D] stiffness matrix and the corresponding complex modulus matrix were derived. Then the damping of laminated composites was calculated as the ratio of loss to their storage of each component of [A], [B] and [D]. Ni and Adams theory was used to verify the modified classical lamination theory. The damping loss factors of all six laminated composites were calculated as a function of fiber orientation. The predicted damping values calculated from theoretical models indicate a similar trend with some difference in each damping prediction over a particular range of fiber orientation between  $15^\circ$  and  $35^\circ$ . The damping increases to a maximum value in the range  $15^\circ$  to  $35^\circ$  according to Ni and Adams theory while the maximum value occurs in the range of  $45^\circ$  to  $75^\circ$  in the case of modified classical lamination theory. This discrepancy may occur due to their different assumptions. It was also observed that increasing the percentage of  $0^\circ$  plies within the laminate reduces the damping.

Gibson et al. in their different works used micro-mechanical approach to develop different models for damping prediction to see the effect of fiber aspect ratio, fiber orientation [30] and the viscoelastic properties of constituent materials [31]. All those models were developed based on Cox's stress distribution [32]. From these analyses, it was predicted that very low fiber aspect ratio is required to produce significant improvement of damping but off-axis composite properties are independent of the fiber aspect ratio in the practical range of aspect ratio when the orientation is not close to zero. On the contrary, control of lamina orientation could be a better approach to improve damping in the laminate. Saravanos and Chamis [33] developed an integrated micromechanics methodology for the prediction of damping capacity in fiber-reinforced polymer matrix unidirectional composites. The damping capacities of unidirectional composites subjected to off-axis loading are synthesized from on-axis damping values using explicit micromechanics equations. The hygrothermal effect and contribution from the interfacial friction between broken fiber and matrix are also incorporated for the damping. The predicted values were compared to available experimental data to validate the theory. The on-axis ply damping (longitudinal, in-plane shear, transverse and out-of-plane shear SDC) at different fiber volume ratios show good agreement with the trend of experimental values. Longitudinal SDCs are shown to be insensitive to the temperature and moisture variation due to fiber controlled properties while transverse and shear SDCs increase with the increase of temperature and moisture content. The off-axis ply SDCs have shown wide variation with respect to fiber angle and have excellent agreement with measured values. This indicates that ply angles can be an effective design parameter for tailoring the damping capacity of composite laminate. Interfacial frictional damping has

an important contribution to overall damping capacity of unidirectional composites and its contribution is more significant in case of off-axis loading. White and Abdin [34] again used Cox's stress distribution model [32] to develop a model where loss moduli of aligned short fiber-reinforced plastic was improved through proper choice of fiber aspect ratio and volume fraction while maintaining the high stiffness. But fiber damping was neglected in their analysis. Hwang and Gibson [35] proposed a strain energy/finite element approach to predict damping and stiffness of discontinuous fiber reinforced composites. This model can be used to study several parameters like aspect ratio, fiber volume fraction, fiber matrix modulus ratio, fiber spacing and fiber-end gap size influencing the damping properties of composites and complex structures. The FEM model is based on the actual non-uniform stress distribution unlike Cox's model [32] that is based on equal stress distribution throughout the laminate. So the FEM model is expected to be more accurate. Most of the models did not consider the effect of fiber/matrix interphase even though it has properties different from those of embedded fibers and matrix. Chaturvedi and Tzeng [36] developed three models for damping prediction in aligned short fiber reinforced composite where the interphase was considered as a distinct third phase between fiber and bulk matrix with its own viscoelastic properties. Fiber damping was also taken in account while predicting total damping. The interphase geometric and material properties were interpolated [37] due to their unavailability and there were no experimental values to verify them. Although some of the aforesaid analytical models can be used to predict damping of short fiber (low aspect ratio) reinforced composites but any well defined and accurate analytical model for nano-fiber or nano-filler reinforced composites is scarce where the effects of nano-

fillers are taken into account. Finegan et al. [38] developed a micro-mechanical model based on elastic-viscoelastic correspondence principle to predict damping and stiffness of vapor grown carbon nano-fiber (VGCF)/Polypropylene composites. This model was developed from the theory given by Sun et al. [39]. Predicted and measured value of storage modulus was found to be in good agreement. Predicted and measured damping values of loss modulus were also in the same range but predicted values do not show a decrease in damping with the increase of fiber volume fraction that was found in experiments.

An analytical model that is dedicated to nanoclay reinforced polymer (modified resin system) and long fiber reinforced with modified resin system (hybrid composites) is scarce. All these above mentioned analytical approaches are mostly for conventional composites and have their own scope and limitations regarding composite damping predictions. An accurate and well accepted analytical model is yet to be developed and research on this still in progress.

### **2.3.2 Experimental methods for damping**

There are different measures for damping i.e. damping ratio, specific damping capacity (SDC), loss factor, loss modulus etc. and for measuring these parameters different methods have been developed and used. However, all these parameters are related to each other. Damping capacity can be measured in resonance or sub-resonant frequency. In a high frequency vibration, the resonance technique is mostly applied where damping can be measured from the decay of free oscillations (logarithmic decrement method) or from the width of the resonance peak (power bandwidth method). For low frequency

oscillation, damping can be measured from the phase lag between applied stress and strain response (DMA method) when the sample is subjected to a forced oscillation.

Adams and Bacon [40] developed a resonant frequency technique to measure the flexural damping and dynamic Young's modulus of beam specimens. A coil was attached to the midpoint of the beam and flexural modes of vibration were created by an electro-magnet.

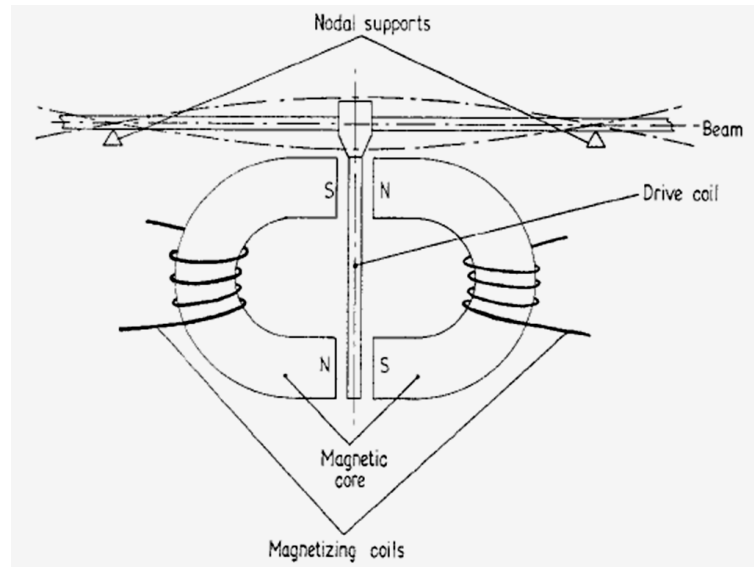


*Figure 2.9 Schematic diagram of nodal support and coil/electro-magnet drive transducer [40]*

Figure 2.9 shows the schematic diagram of the nodal support and coil/electro-magnet drive transducer. A variable-capacitance transducer mounted above the midpoint of the beam was used to measure the amplitude of excitations. Guild and Adams [41] improved the apparatus by clamping both ends of the beam instead of clamping only in the middle and using two coil/magnet pairs. They also used a cantilever apparatus to compare the results. The free flexure mode proved to be more accurate over the cantilever mode. For

both methods, the coil is clamped to the beam which has a considerable weight, which might affect the accuracy of the results. Gibson et al. [42] developed a modal vibration response measurement technique using an impulse/response test set-up for both cantilever-beam specimen and freely suspended plate. Modal testing in either single mode or multiple modes of vibrations can be used to measure elastic moduli and damping factors of composites and their constituents under various environmental conditions. Figure 2.10 shows the impulse/response test set-up for cantilever-beam specimen. Dynamic mechanical behavior of boron/epoxy and SiC/Ti composites at elevated temperature was investigated using this technique. A special apparatus was designed for elevated temperature [43]. Unidirectional laminate of both 0 and 90 degree orientation samples were investigated up to a temperature of 200°C. Quite good agreement between measured and predicted values was found.

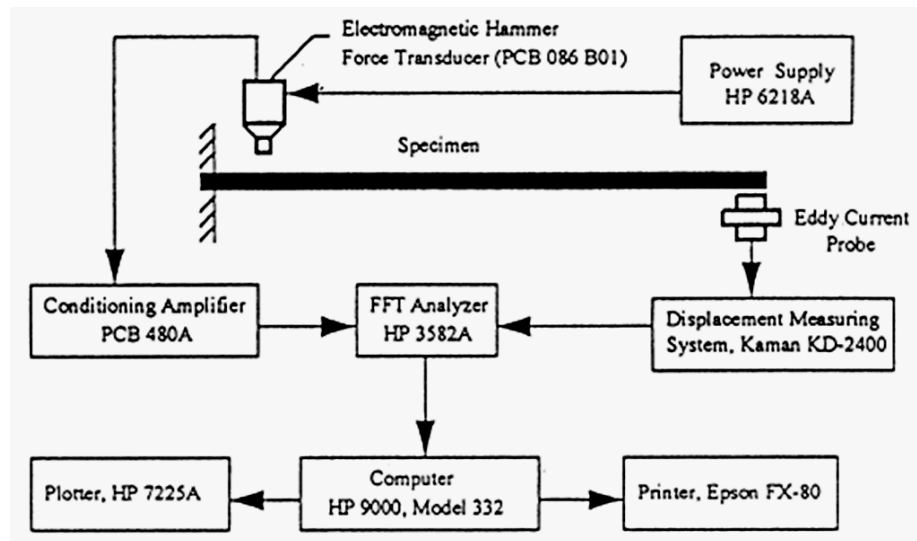


Figure 2.10 Impulse/response test set-up for cantilever-beam specimen [42].

Wei and Kukureka [44] also used resonance technique to measure stiffness and damping properties of pultruded GRP composites and optical fiber cables by both free exponential decay and half-power bandwidth methods. The influence of specimen length and measurement set-up was also investigated. Good agreement between the measured and theoretical values was achieved.

For measuring low frequency and sub resonant vibration damping, the DMA method is the most popular. In the DMA method, the sample is subjected to a forced sinusoidal oscillation which causes a deformation in the visco-elastic material. The deformation is also sinusoidal and phase shifted because of the visco-elasticity. Depending on the apparatus, measurement can be performed at a wide range of temperature (-70 to 600°C) and wide range of modulus ( $10^{-3}$  to  $10^6$  MPa). DMA has also a versatility of sample holder and deformation mode such as three-point bending, dual or single cantilever bending, compression, linear shear, alternated tension etc. The DMA apparatus is also used to measure primary and secondary temperature of relaxation and modulus over a wide range of frequencies [45]. The DMA method is most widely used for polymer composite material to determine dynamic properties.

### **2.3.3 Techniques for damping improvement**

Usually fiber-reinforced materials are very stiff and have very low damping. Although stiffness is very useful for structural applications but its low damping does not often allow it. So a certain form of modification is required for structural application. The most commonly used technique to improve damping is the use of a soft-ply of polymer as a

constrained layer in the laminate (usually called interleave) [46-49] or the use of hybrid composites [50,51].

Moser and Lumassegger [46] first proved analytically that flexural vibrations of laminated fiber reinforced polymer composite structures can be damped as desired by incorporation of a soft ply optimally placed in the zero line of the longitudinal flexural stress. Through the choice of a high shear modulus for the damping ply, the loss factor can be significantly improved with a 20% loss of stiffness. Liao et al. [47] prepared unidirectional and symmetric angle-ply carbon fiber-epoxy laminates as well as their interleaved counterparts with a layer of poly (ethelene-co-acrylic acid) PEAA at the mid plane. Experimental results show that the PEAA layer significantly improves the damping capacity. But the effect of the interleaf on the stiffness was not investigated in this study. Berthelot and Sefrani [48] investigated the effect of a viscoelastic layer as an interleaf in a unidirectional glass laminate with a single viscoelastic layer interleaved in the mid plane or with two viscoelastic layers on the both sides from the mid plane. The effect of fiber orientation and viscoelastic layer thickness was also investigated. For a given thickness of layer, the damping of laminates is increased when the loss factor of the viscoelastic layer increases or when its Young's modulus decreases. Thus the ratio of the loss factor to the Young's modulus of the viscoelastic layer characterizes the laminate damping for a given thickness of the viscoelastic layer interleaved in the mid-plane. The experimental results show a consistent increase in the damping with the frequency in the entire fiber orientation range depending on the vibration mode. Tanimoto [49] developed three different laminates of carbon fiber reinforced plastic composites interleaving viscoelastic thermoplastic films, surface-bonded piezoelectric ceramics and dispersed PZT

particle interlayers. All these damping methods can be used jointly to further improve the damping of CFRP structures. Here the concept is, under vibration the bonded PZT ceramics and dispersed PZT interlayers develop an electric charge and produce a current through the CFRP layers that results in dissipation of energy in the form of heat while running through resistive CFRP layers and this leads to mechanical damping.

A smart hybrid composite laminate has been developed by Oshima et al. [50] where the laminate damping property can be controlled. The hybrid laminate has been manufactured using a carbon fiber reinforced plastic and a glass fiber reinforced plastic interleaving a shape memory polymer (SMP) film in between. Here the CFRP laminate was used as a heater which was connected to a DC power supply. So the temperature of the laminate can be controlled by controlling the power input to the CFRP laminate. Thus the visco-elastic properties of SMP which is extremely sensitive to temperature, can also be controlled. Figure 2.11 shows the experimental set-up of the free vibration test by using a CFRP heater.

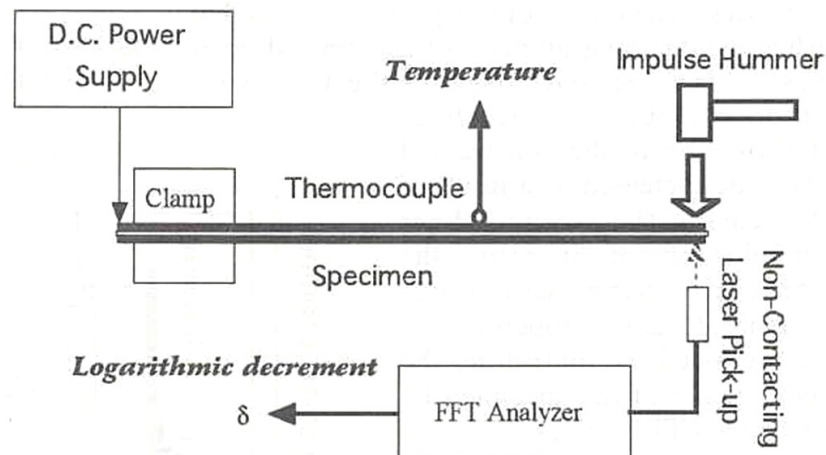


Figure 2.11 Experimental set-up of free vibration test by using CFRP heater [50].

Sandwich structures have also been used extensively for improved passive damping. Romberg et al. [50] have designed a sandwich panel for spacecraft using one casting made of wrapped CFRP, two friction ledges made of CFRP and one spring to generate the normal force between friction ledges and casting. Figure 2.12 shows the principle of applied damping concept and friction ledge assembly. But the experimental results for this structure were not available.

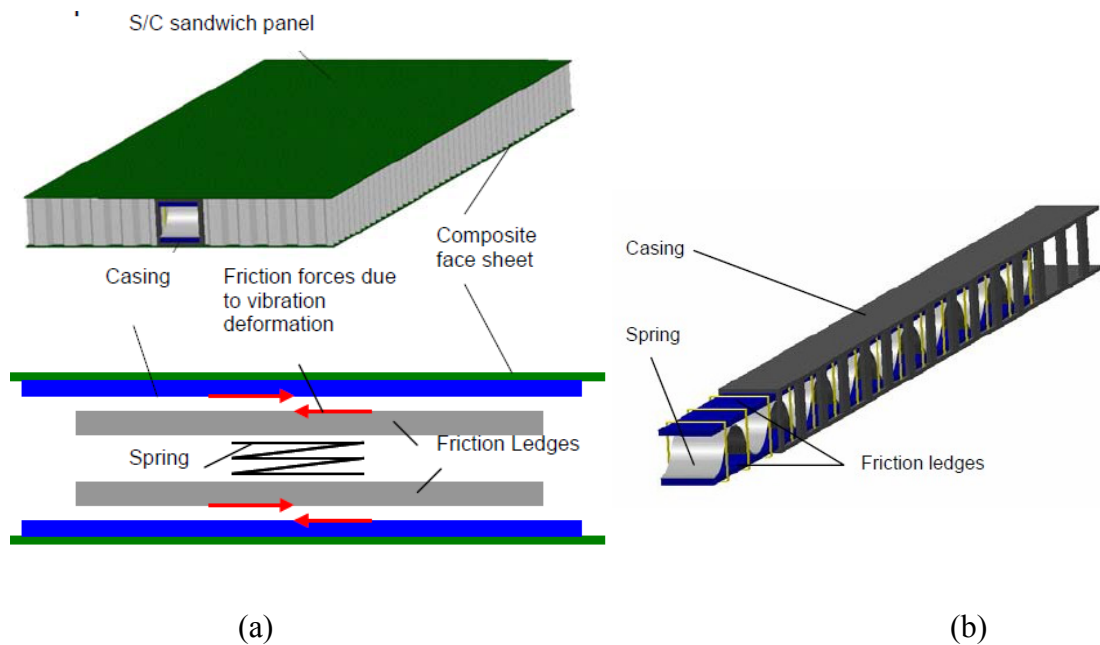


Figure 2.12 (a) Principle of applied damping concept and (b) friction ledge assembly[51].

The method of using soft plies as constrained layer in a laminate always suffers from significant loss of stiffness which is very important for structural application. Also the use of any passive damping technique to any composites structure is not always practical

and feasible. So researchers have recently focused to develop composite structures with improved damping using nano-filler incorporated modified resin system.

#### **2.4 Damping of neat polymer and nano-filler incorporated polymer resins**

Although nano reinforcement of polymer is a relatively recent trend for property development, a lot of work has been carried out during last two decades to find their influence on mechanical and chemical properties like strength, stiffness, chemical resistance, dielectric property etc. But the effects of nano reinforcement on vibration damping are not so extensively studied. The most commonly used nano-fillers in polymer matrix are nanoclay (organoclay) and nano-tubes (vapor-grown single-walled nano-tube SWNT and multi-walled nano-tube MWNT). Because of their nanometer scale size, the specific surface area (surface area to mass ratio) is extremely high and produces a huge interfacial area within the polymer matrix even at a very low concentration of nano-fillers. Interfacial friction between the nano-filler and the polymer resin enhances the energy dissipation ability, so it is anticipated that the damping property can be improved using a nano-filler in the polymer matrix. The elastic properties of nano-filler reinforced composites have been studied by several investigators but comparatively less attention has been given to the damping mechanism of nano-composites.

Messersmith and Giannelis [52] have developed a modified epoxy resin system by dispersing organically-modified mica-type layered silicate in DGEBA resin. The modified resin system was cured in the presence of nadic methyl anhydride (NMA), benzyldimethylamine (BDMA), or boron trifluoride monoethylamine (BTFA) at 100-120°C. Good molecular dispersion of silicate layers and separation of adjacent silicate

layers by 100 Å was verified by XRD and TEM investigation. The dynamic storage modulus was increased by around 58% in the glassy region and 450% in the rubbery region at only 4 vol.% incorporation of silicate. The glass transition  $T_g$  was also increased slightly due to good interfacial adhesion or restriction of molecular mobility of polymeric segments near the silicate surface. The improvement in storage modulus was more significant compared to loss modulus, so the  $\tan \delta$  value was found to be decreased around the glass transition temperature. Chen and Curliss [53] did similar investigation on bisphenol-F (EPON 862) reinforced with organically modified montmorillonite (SC12) and curing with Epicure W curing agent. SC12 was prepared from sodium montmorillonite (SNA) modified with HCL and dodecylammonium chloride. The dynamic storage modulus was improved by 30% in the glass state and about 90% in the rubber state at 3% clay loading. But unlike the previous investigation, the  $T_g$  was decreased by 6°C and below  $T_g$ , the  $\tan \delta$  value was increased compared to pure epoxy. Mohan T. P. et al. [5] investigated the vibration characteristics of DGEBA epoxy resin filled with both alkyl ammonium modified clay and unmodified clay. The nanocomposites were synthesized by mechanical shear mixing at 1000 rpm for 2 hours and cured using diaminodiphenyl methane (DDM). The damping factor was measured using the impulse hammer technique and the logarithmic decrement method. Addition of both organoclay and unmodified clay improves the natural frequency of epoxy polymer and improvement was highest at 3% clay loading for both cases. The log decrement test also confirms that the damping factor significantly improves for both organoclay and unmodified clay up to 3% clay loading. However, natural frequency and damping factor improvement of organoclay is more significant than unmodified clay. For higher clay

content ( $>3\%$ ), both natural frequency and damping factor decreases but still higher than pure epoxy. Sarathi et al. [6] also suggested that 3% clay content is optimum for maximum damping. Here DGEBA resin was reinforced with organophillic MMT and was cured with tri-ethylene-tetra-amine (TETA). Free vibration test was carried out to find out the natural frequency and the damping factor of first four modes of vibration. Experimental results show that, the damping factor and natural frequency increase by adding up to 5 wt.% nano-clay to the base resin. But the characteristic variation in natural frequency of vibration is not so significant between 3 and 5 wt.% of clay in epoxy. Ngo [13] investigated the effect of clay C30B on epoxy EPON 828 cured with Jeffamine D230. Pre-mixing speed, temperature and clay content were the process parameters for the investigation. The DMA analysis showed nanoclay improves both storage and loss modulus of the composites compared to pure resin. Pre-mixing speed and temperature have a significant influence on dynamic properties. High temperature ( $120^{\circ}\text{C}$ ) and high speed (24,000 rpm) mixing of clay has the maximum improvement in dynamic properties. But the improvement is more significant for the case of storage modulus. Some researchers have used carbon nanotubes (CNT) for dynamic property development. Zhou et al. [4] investigated the interfacial damping characteristics of single-walled carbon nanotubes (SWNTs)/epoxy nanocomposites at 0.5% and 1% SWNT loading. A cantilever beam test set-up and the logarithmic decrement method were applied to measure damping ratio. An initial tip displacement was given to the cantilever beam and the response signal was measured by an accelerometer. These signals were converted to strain values and damping ratios were plotted as a function of strain. Experimental results indicate that adding nanotubes greatly enhances damping ratio. For the samples with nanotubes, the

damping increases with strain to a certain value and then decreases for further increase in the strain which supports the “stick-slip” motion between resin and nanotubes as predicted by the author. The time history curves show a significant improvement in the decay of amplitude over time with progressive nanotube loading. Figure 2.13 shows the time history curves for different nanotube contents.

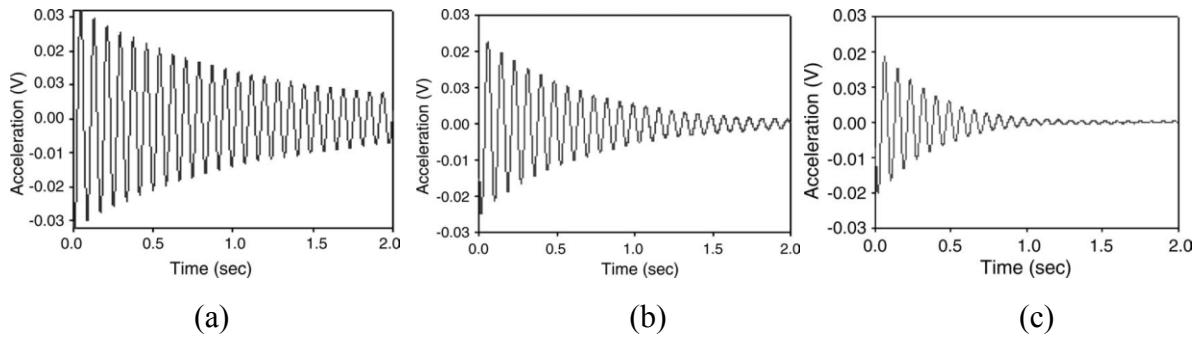


*Figure 2.13 Time history (a) 0% SWNT, (b) 0.5% SWNT and (c) 1% SWNT [4]*

Mantena et al. [7] used a non-destructive impulse-frequency response vibration technique to measure the flexural dynamic storage modulus and loss factor of vinyl ester resin reinforced with 1.25 and 2.5 wt.% of nanoclay C30B and exfoliated graphite nanoplatelets. A 40% increase in the flexural dynamic storage modulus was observed with addition of 2.5 wt.% graphite platelet but the loss factor reduced slightly.

So from the literature, it is quite evident that nano-filler incorporation greatly improves stiffness and modulus and sometimes damping depending on the type of fillers and resin systems. But the improvement in the damping property is not so significant compared to its improvement in stiffness and modulus.

## **2.5 Damping of modified polymer reinforced with long fibers**

Incorporation of nano-fillers in conventional long fiber reinforced composites is the most recent technique for property development. Moreover, ongoing works are mostly focused on the elastic property of materials. Comparatively much less attention has been given to the vibration characteristics of long-fiber/nano-filler/polymer hybrid composites. So papers on this topic are not numerous. Still some available works have been summarized below.

In mid nineties, Hudnut and Chung [54] incorporated submicron (0.1 - 0.2  $\mu\text{m}$ ) diameter carbon filaments into conventional carbon fiber/epoxy composites. The carbon filaments were made catalytically from carbonaceous gases and were different from conventional carbon fiber. Laminate samples were prepared by spreading the carbon filaments as second reinforcement in between every carbon-fiber/epoxy prepreg layers. A total of eight layers of prepreg have been used for sample laminate. The DMA analysis indicates that  $\tan \delta$  value increases greatly for both longitudinal and transverse laminate at only 0.6 vol.% incorporation of carbon filaments. Longitudinal and transverse loss modulus increase to value as high as 2 GPa. Only longitudinal storage modulus was slightly reduced. Haque and Shamsuzzoha [55] investigated the dynamic mechanical properties of S2-glass/epoxy/nanoclay nanocomposites along with other thermal and mechanical properties. Epoxy resin used here is a blend of bisphenol-A and bisphenol-F and has very low viscosity that is suitable for VARIM molding. Plain weave S2-glass fabric was used as the continuous fiber. Various amount of nanoclay I.28E was added to the epoxy blend and vacuum assisted resin infusion molding (VARIM) used to fabricate hybrid composite laminate. Conventional S2-glass/epoxy laminate was also fabricated to compare the

results. DMA analysis indicates that the  $\tan\delta$  value of laminate with 1% and 2% clay increases significantly below  $T_g$  compared to conventional laminate. A  $4^\circ\text{C}$  increase in the  $T_g$  was also observed in case of laminate with 2% clay. This increase in  $T_g$  is usually attributed to the restricted relaxation motion near the interface of inorganic-organic nanocomposites. Modal analysis was carried out to see vibration response to similar glass/epoxy/nanoclay composite laminate by Avila et al. [56]. 16 layers of S2-glass plane weave woven fabric used with various amounts of nanoclay I.30E dispersed in DGEBA epoxy resin by vacuum assisted lay-up method and cured with hardener aliphatic amine. For modal analysis, a sample plate was hanged by a fine nylon wire and excited with random signals by a mini-shaker. Responses were recorded using a Doppler vibrometer and HP data acquisition system. Modal analysis shows that incorporation and dispersion of nanoclay in glass/epoxy composite not only improves the damping coefficients but also changes the shape mode and its natural frequencies. The damping coefficient of mode shape 1 and 7 where bending-twisting is observed was increased by 27%. For bending mode 2 and 6, average increase in damping coefficient was 68%. A new mode shape (mode 5) at frequency of 600 Hz was observed when nanoclay content reached 2%. The results of modal analysis are given in table 2.1.

Table 2.1 Damping coefficient, natural frequency and amplitude for vibration shape modes [56]

Damping coefficient, natural frequency and amplitude for vibration shape modes									
I30E [%]	Mass [g]		Shape modes						
			1st	2nd	3rd	4th	5th	6th	7th
0	66.37	Damping coefficient	0.0297	0.0166	0.0098	0.0112	Not noticed	0.0137	0.0131
		Natural frequencies [Hz]	180.6	344.4	423.6	568.7	Not noticed	692.9	735.2
		Amplitude [m/s/kgf]	57.0	17.0	6.5	4.8	Not noticed	12.1	8.5
1	65.27	Damping coefficient	0.0209	0.0247	0.0088	0.0136	Not noticed	0.0137	0.0138
		Natural frequencies [Hz]	184.9	347.4	424.6	550.1	Not noticed	683.4	728.2
		Amplitude [m/s/kgf]	79.9	14.0	24.1	2.6	Not noticed	17.9	9.6
2	66.92	Damping coefficient	0.0231	0.0248	0.0116	0.0173	0.0052	0.0134	0.0166
		Natural frequencies [Hz]	173.6	361.3	424.0	578.0	655.3	716.1	783.0
		Amplitude [m/s/kgf]	32.9	5.8	4.7	21.5	44.3	15.0	8.1
5	67.46	Damping coefficient	0.0372	0.0445	0.0162	0.0233	0.0134	0.0110	0.0169
		Natural frequencies [Hz]	202.3	336.0	494.6	430.1	645.0	747.6	821.5
		Amplitude [m/s/kgf]	33.3	4.4	2.2	5.0	8.4	10.0	14.7
10	67.89	Damping coefficient	0.0336	0.0413	0.0161	0.0272	0.0138	0.0136	0.0152
		Natural frequencies [Hz]	196.1	331.3	477.5	425.7	610.6	702.4	764.6
		Amplitude [m/s/kgf]	7.6	0.9	1.3	0.8	1.5	4.2	2.8

Chandradass et al. [57] investigated the effect of alkyl ammonium based nonoclay on vinyl ester resin reinforced with E-glass chopped strand mat (CSM). Modal analysis was carried out using a free vibration test by exciting the sample with a modally tuned impulse hammer and recording the response in a PC using an accelerometer and data acquisition (DAQ) card. The free vibration test indicates that natural frequency of glass/vinyl ester composites with organoclay increases for the first four modes of vibrations compared to conventional glass/vinyl ester composite. Maximum increase in natural frequency was observed at 3% organoclay content. Further increase in clay content decreases the natural frequency but always higher than composite without clay. The damping factor of laminate with organoclay also increases for all four modes of vibrations. Table 2.2 presents the damping factor of first four modes of vibrations.

Table 2.2 Damping factor of first four modes of free vibration [57]

Material	Organically modified series			
	I mode	II mode	III mode	IV mode
V-G.F	0.0423	0.0382	0.0302	0.0207
V-G.F+ 1% clay	0.0447	0.0394	0.0321	0.0223
V-G.F+ 3% clay	0.0495	0.0421	0.0334	0.0234
V-G.F+ 5% clay	0.0508	0.0433	0.0349	0.0240

Velmurugan et al. [58] investigated the damping response by low velocity drop weight impact test of hybrid composites using nanoclay and glass fiber as reinforcement in epoxy resin. A fixed weight sharp nose projectile attached to a circular plate was dropped from different heights with maximum velocities as 2.21 and 3.13 m/s at the time of strike. Vibration response was measured using an accelerator attached to sample plate as function of time and from the response curve, damping factor of the laminate was calculated using logarithmic decrement method. The experiment proved that the amplitude of vibration for the samples with clay decays much faster than samples without clay or lower clay content. For lower velocity of impact the contact time between projectile and specimen is more and most of energy is converted to vibration. As the velocity increases, the contact time reduces and part of energy dissipates because of the penetration of projectile into the sample resulting in impact damage. So damping factor increases with the increase of impact velocity for same laminate configuration. Damping factors at two different impact velocities are summarized in table 2.3.

Table 2.3 Damping factors of hybrid laminate at different impact velocities [58]

Specimen	Damping factor at impact velocities of	
	2.21 m/s	3.13 m/s
0 % clay	0.03084	0.03642
1% clay	0.04817	0.05061
3% clay	0.05912	0.06432
5% clay	0.06784	0.08023

So from the above literature review it can be concluded that addition of nano-fillers in conventional long fiber reinforced polymer composite significantly improves its dynamic properties like damping factor and natural frequency along with other mechanical, impact and barrier properties.

## 2.6 Effect of nano-fillers on fatigue life of composite material

Nano fillers well dispersed in polymer matrix improve strength, stiffness, chemical and solvent resistance; reduce water up-take and thermal degradation. And from the above literature survey, it is also proven recently that nano-fillers have a positive dynamic response and better vibration damping properties. So nano-filler reinforced composites subjected to vibration can dampen the amplitude of vibration faster than conventional composites and have improved strength and stiffness. So it is anticipated that nano-filler incorporation can improve the fatigue life of composite structures. A number of research works have been carried out over last few years to see the effect of nano-fillers on fatigue life of composite materials. A few of the recent works are summarized below.

Varadharajan [59] has investigated the fatigue behavior of  $\alpha$ -Zirconium phosphate/Epoxy nanocomposite using a reverse bending fatigue testing method comparable to ASTM

D671-93.  $\alpha$ -ZrP is a synthetic nano structure modified with Jeffamine surfactant with molar ratios of 1:1 and 2:1 to ZrP. A 25% improvement in the fatigue resistance was observed for both type  $\alpha$ -ZrP reinforced epoxies in the experiment compared to neat epoxy. Nanocomposites with two different concentrations of surfactant had the same fatigue life which indicates that there is no effect of surfactant concentration on its fatigue behavior. Analysis of fracture surfaces revealed that crack propagation in ZrP/epoxy system changed its direction frequently. When a ZrP platelet was normal to the crack growth, the crack propagation direction changed and reduced the crack propagation rate. In case of crack aligned parallel to a ZrP platelet, the crack proceeds to extend by the coalescence of void created due to delamination of the ZrP platelet from the matrix. Incorporation of organically modified nano-clay in polyurethane elastomers can significantly improve fatigue life of nanocomposites with 150% increase in static strength and failure strain investigated by Song and Yao [60]. It was observed that nanoclay acts as nano-springs in polyurethane and during fatigue deformation these nano-springs can absorb deformation energy which could cause crack growth leading to failure. Most significant improvement was observed at 3 wt.% clay loading. Blackman et al. [61] added silica ( $\text{SiO}_2$ ) nano-particles in epoxy and performed fracture and fatigue test. Both test revealed significant improvement in the initial toughness and fatigue behavior of nanocomposites at 7.8 wt% clay loading. Wetzel et al. [62] added alumina ( $\text{Al}_2\text{O}_3$ ) and titanium dioxide ( $\text{TiO}_2$ ) nanoparticles in epoxy and investigated different flexural and fracture behavior under cyclic loading. Significant improvements in flexural stiffness, flexural strength and fracture toughness was observed for incorporation of both  $\text{Al}_2\text{O}_3$  and  $\text{TiO}_2$  nanoparticles into epoxy. Moreover  $\text{Al}_2\text{O}_3$  nanoparticles improve the fatigue

crack propagation resistance of epoxy. Crack propagation was also related to different fracture mechanisms i.e. crack deflection, plastic deformation of matrix, debonding and crack pinning.

Nanoparticle incorporated modified resin systems are further reinforced with continuous fiber to see their fatigue behavior. Chisholm et al. [63] incorporated nanosized SiC fillers to conventional carbon/epoxy composite to investigate their effect on mechanical and fatigue behavior. Ultrasonic mixing was used to disperse the nano particles in epoxy and VARTM was used to make sample laminate. Flexural fatigue test was carried out at a stress ratio of 0.1 and frequency of 3 Hz. The S-N diagram shown in figure 2.14 was obtained from the fatigue test. The S-N diagram indicates that the composites with nano-fillers are more sensitive to applied load and above 60% load level neat system has a better fatigue property than nano-filler incorporated carbon/epoxy composite. Below 60% load, 1.5 wt.% filler reinforced system show better fatigue performance. The reason for this reversal fatigue phenomenon was not fully understood. However, 3 wt.% filler reinforced system always shown a very poor fatigue performance over the entire range of loading. From the flexural, tensile and fatigue test, 1.5 wt.% loading of nano-filler was considered as the optimum for maximum property enhancement.

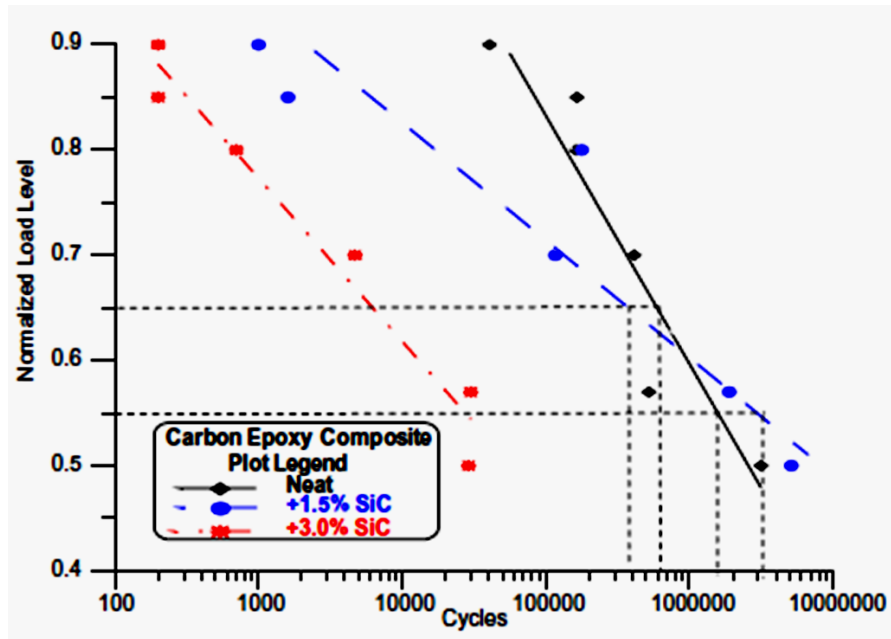


Figure 2.14 S-N diagram obtained from flexural fatigue test [63].

Grimmer and Dharan [64] added only 1 wt.% of multi-walled carbon nanotubes into glass/epoxy composites and investigated the high cycle fatigue behavior in a tension-tension fatigue test using an MTS machine. Samples with specific dimensions were made with both CNT and without CNT by wet lay-up using eight plies of [0/90] woven glass fabric and EPON 826 resin and cured in a heated press. In the centre of sample specimen, a 6.4 mm diameter hole was drilled to create a stress concentration to localize damage. In the fatigue test, a significant improvement of fatigue life was observed for the sample with 1 wt.% CNT which occurred after  $10^4$  fatigue cycles. At low stress level, CNT reinforced glass/epoxy sample showed a fatigue life 2.5 times higher than neat glass/epoxy sample. Figure 2.15 represents the applied stress vs. number of cycles to failure curve.

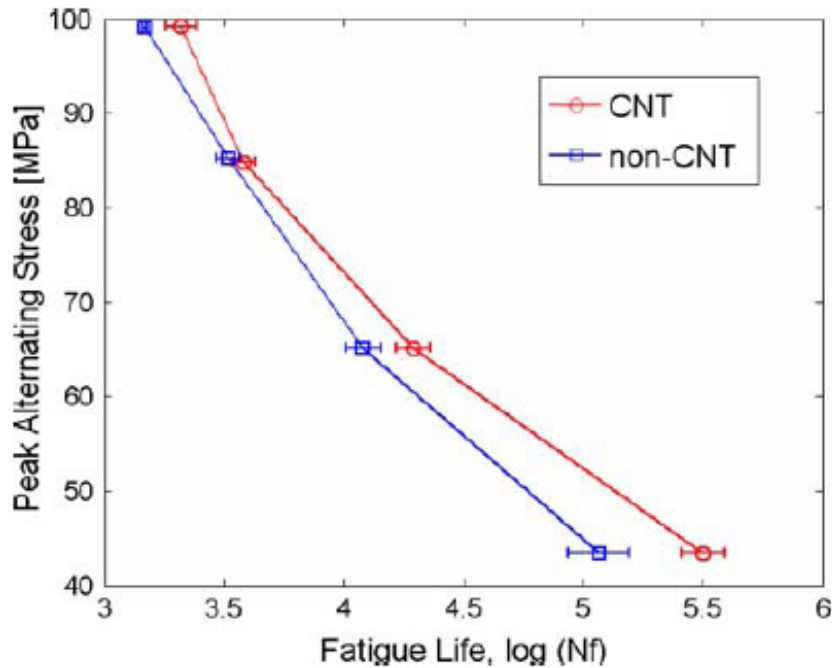


Figure 2.15 Applied cyclic stress vs. fatigue life curve of glass/epoxy laminates with and without 1 wt.% CNTs [64].

From above discussion it can be said that, nanocomposites show better fatigue performance over neat system when the applied stress is below a certain level and deformation is in the elastic region. Nano-fillers incorporated resin system reinforced with conventional long fiber composites also have improved fatigue life at low (~2 wt.%) nanoparticles loading.

## 2.7 Summary

Nano reinforcement in polymers is the most recent trend for property development. Nanoclay or nano layered silicate has a crystal structure with two silicon atoms fused to a sheet of aluminum or magnesium hydroxide. The layer thickness is around 1 nm and has a very high surface area to mass ratio combined with great strength and stiffness. Because

of its hydrophilic nature and incompatibility with organic polymer, it is often needed to modify its surface with alkylammonium cations by ion exchange reactions to make it more compatible with organic polymer. For fabrication of nanocomposites using clay usually direct mixing or “in-situ polymerization process” and “solution process” are used. Mechanical stirring, high shear mixing and ultrasonic sonication technique are mostly used for dispersion of clay in polymer by the direct mixing method. A solvent is used in the solution process for clay dispersion. However solution process is very effective but not always practical because of its involvement with huge amounts of solvent which is costly and requires a difficult process of extraction. For damping prediction, different analytical models have been developed using the correspondence principle, strain energy approach and finite element analysis in both micromechanical and macro-mechanical level and are mostly based on the assumption of linear viscoelasticity. Different experimental methods have been developed for damping measurements but usually for high frequency vibration, the logarithmic decrement method and for low frequency and polymeric composite, the DMA method are used. Conventional composites usually have very high strength and stiffness but always suffer from low vibration damping. So for damping improvement, the use of soft viscous ply as interleave, use of different passive damping device and incorporation of nano-fillers have been tried over last few years. But the use of a soft ply as interleave significantly reduces the strength and stiffness of materials and using passive damping devices are not always practical. So the use of nano-fillers such as nanoclay has a huge potential for enhancement in dynamic properties. Some recent research works also confirm that incorporation of organoclay in polymer resin improves vibration damping and fatigue performance as well as other mechanical,

thermal and barrier properties. Further reinforcement of modified polymer with conventional continuous fiber shows similar improved properties. So incorporation of nanoclay in conventional composite has a great potential for structural applications where vibration is a concern.

## **2.8 Thesis Objectives**

From the above literature review it can be considered that nanoclay reinforced polymer has better dynamic and fatigue behavior along with their mechanical, thermal and barrier properties over pristine matrix. But this improvement in properties depends on several factors like the type of polymer resin and clay, the dispersion of clay in resin, the fabrication method etc. So selecting suitable materials and techniques is very important to fabricate high performance composites. For structural applications, availability and cost of materials and processing should also be reasonable. Considering all these factors the thesis is focused on the following issues:

- To develop a high performance hybrid composite structure using low cost glass fiber and epoxy resin modified with nanoclay with improved vibration damping and fatigue behavior for structural applications.
- To use a solvent-free, low cost and practically feasible but effective dispersion technique and fabrication method.
- To see the effect of nanoclay on the vibration damping and fatigue life of the glass/epoxy composite material.

# Chapter 3

## Materials and Experimental Procedure

There are several factors which must be considered while selecting materials for a composite structure. The most important factors are clay and resin chemistry, dispersion of the clay in resin, compatibility of fiber and resin, matrix formulation, processing parameters and curing conditions. In this chapter, the selected materials, their chemistry and structure, dispersion method of clay in resin, sample manufacturing method, curing conditions and experimental methods are briefly described.

### 3.1 Materials Selection

For this thesis, the following materials have been used for sample manufacturing.

**Fiber:** Uni-web S-glass fiber manufactured by AGY World Headquarters and supplied by Aerospace Composites Products Inc.

**Clay:** Organoclay Nanomer I.30E treated with long chain primary amine intercalant supplied by Nanocor Inc.

**Resin and hardener:** EPON 828 has been used as resin and EPICURE 3046 as hardener. Both supplied by Hexion Specialty Chemicals.

#### 3.1.1 Uni-web S-glass fiber

S-glass fiber is high strength glass fiber for structural applications and offers unique combinations of properties: strength, impact resistance, stiffness, temperature resistance, fatigue resistance etc. S-glass offers around 85% more strength and 25% more linear

elastic stiffness than conventional glass fiber. Uni-web S-glass fiber is all unidirectional structural glass fabric that are held in position by a fine spider web of polymer on either one or both sides for easy handling. The polymer used for the spider web is compatible with epoxy and polyester resin and virtually dissolves when cured. Typical physical and mechanical properties of S-glass are given in Table 3.1.

Table 3.1 Typical properties of S-glass fiber [65]

Bulk density (g/cc)	2.48
Density (g/cc)	2.46
Water absorption (%)	0
Loss on Ignition (LOI %)	0.100 – 1.40
Filament diameter (μm)	5 - 25
Tensile strength (MPa)	4890 @ room temperature
Modulus of elasticity (GPa)	86.9
Elongation at break (%)	5.70
Poisson's ratio	0.22

### 3.1.2 Nanomer I.30E

Nanomer I.30E is a natural montmorillonite based organoclay treated with a long chain primary amine intercalant. Physical and technical details of Nanomer I.30E are given in Table 3.2.

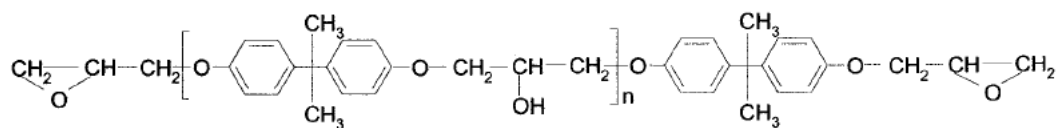
Table 3.2 Physical and technical details of organoclay Nanomer I.30E [66]

Appearance	White powder
Organic modifier or intercalant	ODA (octadecyl ammonium)
Modifier concentration (meq/100g Clay)	100
Basal spacing $d_{001}$ (Å)	23.8
Moisture content (%)	3 max
Specific gravity (g/cc)	1.71
Mean dry particle size (µm)	8 to 10
Supplier	Nanocor Inc.

Nanomer I.30E is commercially available supplied by Nanocor Inc. They developed and commercialized different types of organoclay including I.30E which are quite compatible with epoxy resin. Nanomer I.30E is organically modified with primary amine intercalant that is worth investigating as compared to secondary, ternary or quaternary amine modified nanoclay.

### 3.1.3 Epoxy (EPON828)

Epoxy resin is generally characterized by the presence of a three-member ring containing two carbons and an oxygen. EPON 828 is one of the most commonly used resin among the epoxy family. It is an undiluted clear liquid having reasonably low viscosity (10,000~16,000 cPs) [67]. Di-functional EPON 828 is based on diglycidyl ether of bisphenol-A (DGEBA), a difunctional bisphenol-A/epichlorohydrin derived. The chemical structure and typical properties of EPON 828 are shown in Figure 3.1 and Table 3.3.



$n = 0$  (88%);  $n = 1$  (10%);  $n = 2$  (2%)

Figure 3.1 Chemical structure of EPON 828 resin.

Table 3.3 Typical properties of EPON 828 [67]

Visual Appearance	Clear Liquid
Epoxy equivalent weight (g/eq)	185 to 192
Viscosity @ 25 °C (cPs)	10,000 to 16,000
Density @ 25 °C (g/cm <sup>3</sup> )	1.16
Vapor pressure @ 25°C (mm Hg)	0.03
Refractive index @ 25°C	1.573

EPON 828 has a very good fluidity, easy to process and after curing with suitable curing agent offers good mechanical, dielectric and chemical resistance properties.

#### 3.1.4 Hardener EPICURE 3046

EPICURE 3046 obtained from Hexion Specialty Chemicals is an aliphatic amidoamine containing tri-ethylene tetramine and tall oil fatty acid polyamide. Tall oil fatty acid is produced by the fractional distillation of tall oil, a co-product of Kraft process in wood pulp manufacturing industries. It is a predominately linear chain of 18 carbon mono and di functional unsaturated fatty acids which is mainly oleic and linoleic acid. Some characteristics of EPICURE 3046 are given in Table 3.4.

Table 3.4 Characteristics of EPICURE 3046 [67]

Amine hydrogen equivalent weight (AHEW) (g/eq)	90
Viscosity @ 25 °C (cPs)	120 to 280
phr (parts per hundred)	35

EPICURE 3046 has good compatibility with EPON 828 resin. It has reasonably low viscosity with high amine hydrogen which forms a rigid network with epoxy.

### 3.2 Dispersion method

For this thesis, a high speed stirring method using a high speed homogenizer is used to disperse the clay in resin. The high speed homogenizer consists of an internal rotor and external stator assembly which is called a rotor-stator generator. The rotor is connected with a variable speed electric motor and can be operated at a minimum speed of 6,500 rpm to a maximum of 24,000 rpm. The rotor is designed in such a way that it acts as a centrifugal pump under operation. Due to very high rotational speed a centrifugal force is generated which axially draws the liquid resin as well as the suspended solid additives into its dispersion head which is then forced radially through the slots of rotor-stator arrangement. The differential speed between the rotor and stator produces extremely high shear force which subsequently generates a very high turbulent energy in the shear gap. This energy disperses the clay in the resin. A high speed homogenizer, rotor-stator assembly and its working principle is shown in Figure 3.2. The effectiveness of the dispersion highly depends on the shear gradient and the residence time of particles in the shear zone. Moreover, as the rotor-stator generator produces very high turbulent energy,

it increases the temperature of mixture resulting in the reduction of viscosity to facilitate proper dispersion.

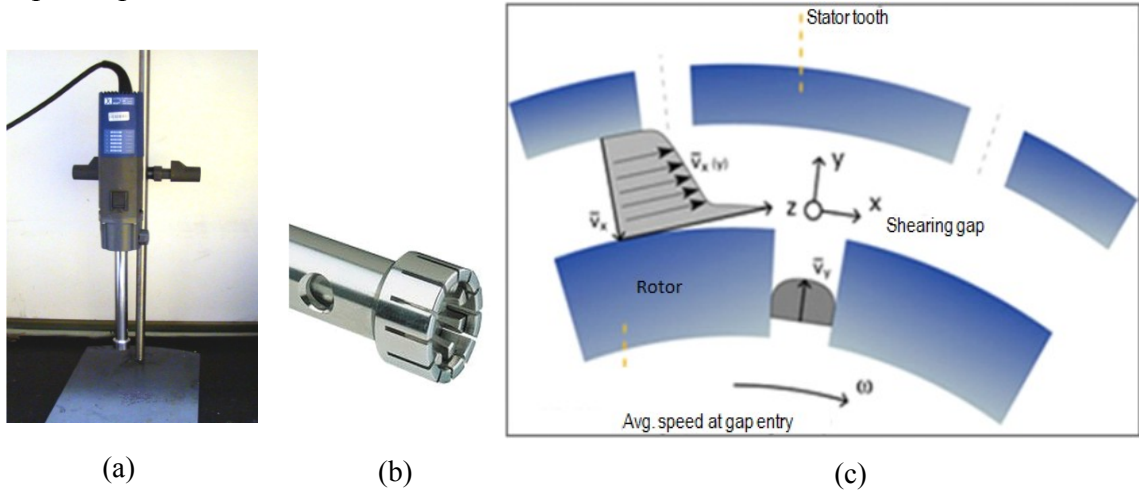
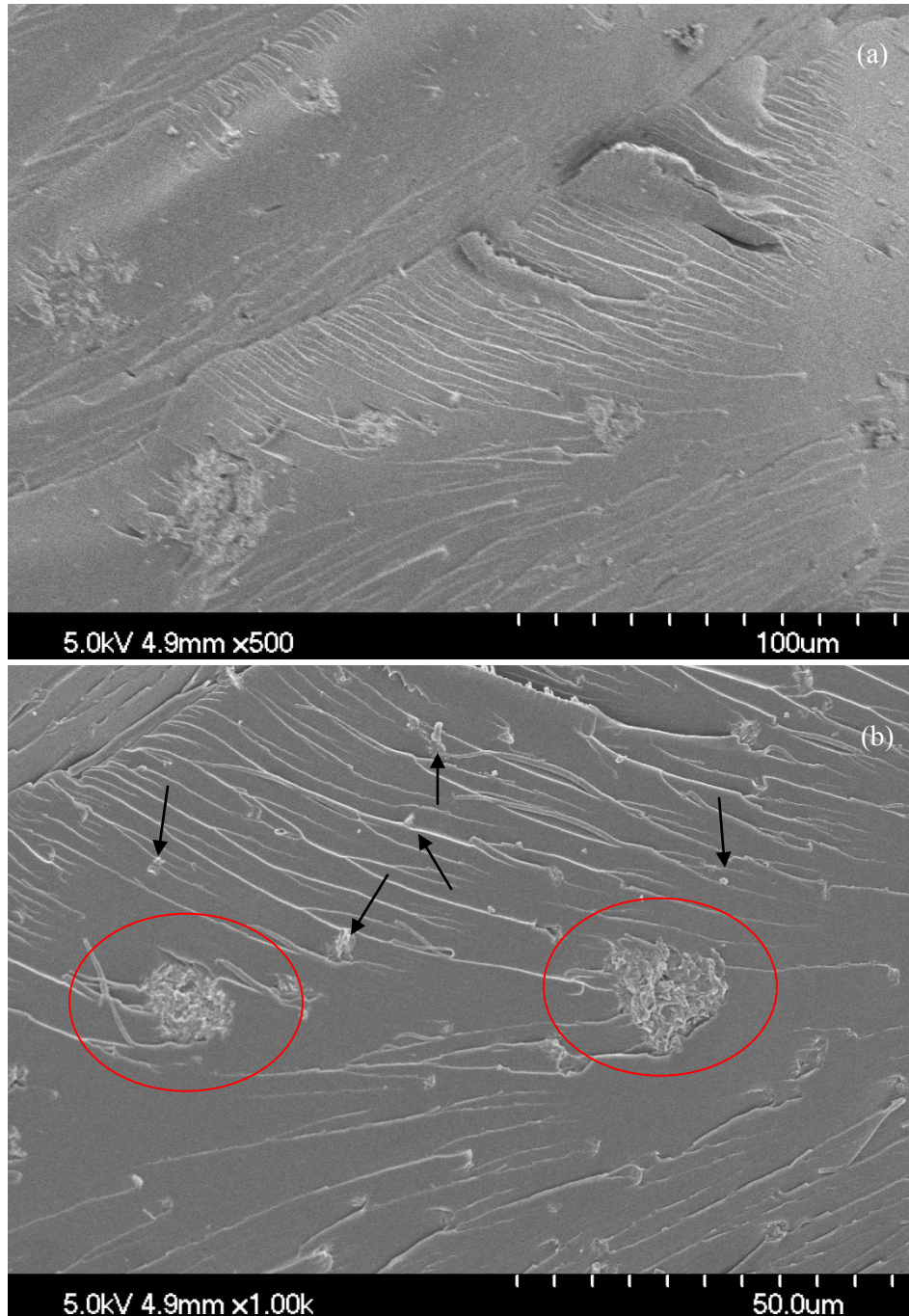


Figure 3.2 Photograph of (a) High speed homogenizer, (b) Rotor-stator assembly (CONCOM Lab) and (c) Rotor-stator working principle [68].

For this thesis, resin EPON 828 was first preheated to 45 °C to reduce the viscosity. The necessary amount (up to 2 wt.%) of organoclay Nanomer I.30E was added to the resin. The clay is mixed into the resin by hand with a spatula. After that, the high speed homogenizer is used to disperse the clay up to a maximum rotational speed of 20,000 rpm for 20 minutes. The temperature of the suspension was closely monitored using a thermometer and kept below 100 °C throughout the process to avoid self-polymerization. Scanning electron microscopy was done to characterize the dispersion of nanoclay epoxy. Figures 3.3 and 3.4 show the SEM images of fracture surfaces of both epoxy/nanoclay and glass-fiber/epoxy/nanoclay systems, respectively. The SEM images indicate that the clay agglomerations are broken into small aggregates (shown by arrow) and in some places complete exfoliation is observed. Also there are a few considerably bigger

agglomerations (shown within circles) observable within the images. On the whole an exfoliated/intercalated structure was achieved using high speed mixing method.



*Figure 3.3 SEM images of fracture surface of epoxy system with 2wt.% nanoclay: (a) lower magnification and (b) higher magnification.*

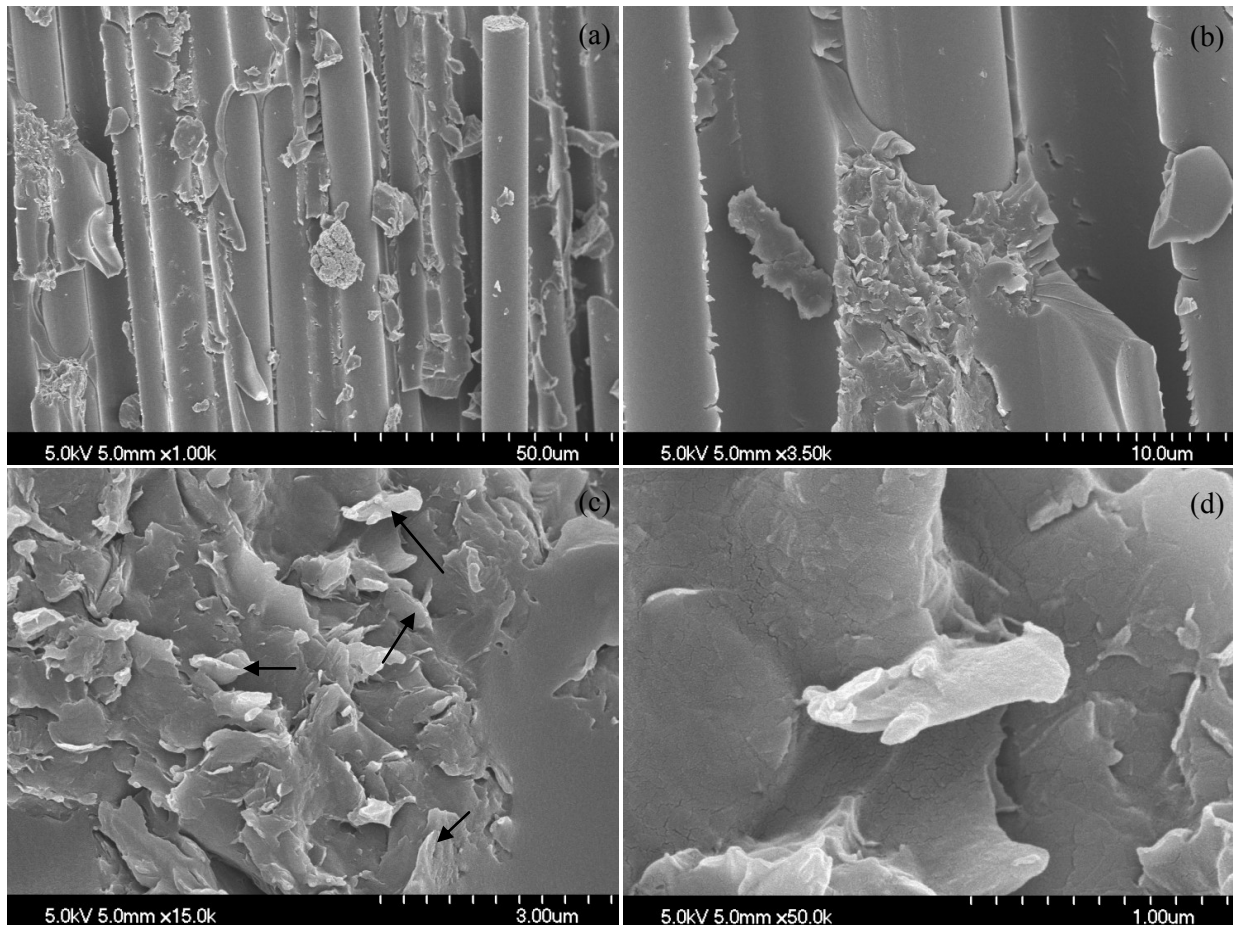


*Figure 3.4 SEM images of fracture surface of glass-fiber-epoxy system with 1 wt.% nanoclay at different magnifications.*

### **3.3 Sample preparation**

The manufacturing process is very important for the composite materials. Manufacturing procedures and curing conditions significantly affect the properties of the structure. In this section, sample manufacturing methods, study parameters and curing conditions are described briefly. Two types of samples have been prepared,

- i) Epoxy + Clay
- ii) Epoxy + Clay + S-glass fiber

For both types of samples, up to 2 wt.% clay have been added. For the samples with continuous S-glass fiber, different fiber orientations have been applied. Table 3.5 shows different sample configurations.

Table 3.5 Different sample configurations

Materials	Fiber Orientation	Clay Loading (wt.%)
i) Epoxy + Clay	-	0
		1
		2
ii) Epoxy + Clay + S-glass	Unidirectional	0
		1
		2
	Cross-ply [0 <sub>2</sub> /90 <sub>2</sub> /0 <sub>2</sub> /90 <sub>2</sub> ] <sub>s</sub>	0
		1
		2
	Quasi-isotropic [0 <sub>2</sub> /90 <sub>2</sub> /±45 <sub>2</sub> ] <sub>s</sub>	0
		1
		2

### 3.3.1 Epoxy + Clay sample preparation

Neat epoxy and clay-incorporated epoxy samples were molded in a silicone rubber mold. First the exact amount of hardener (35 parts per hundred) was added to neat epoxy or epoxy-clay mixture (after dispersion with high speed homogenizer) at room temperature. After that, the mixture and hardener was mixed carefully and slowly with a stirrer for 5 minutes to avoid air entrapment in the mixture. To remove air bubbles, the mixture was then degassed in a vacuum oven at a vacuum of 25 mmHg for 25 minutes at room temperature. The mixture was poured in the pre-heated (50 °C) silicone rubber mold for

curing. Samples were cured at 120 °C for 2 hours in an oven and then post cured at 140 °C for 2 hours. After curing, 6 samples of each configuration were obtained with dimensions 75mm×10mm×2mm approximately. Figure 3.5 shows the sample manufacturing procedure with epoxy and epoxy-clay mixture.

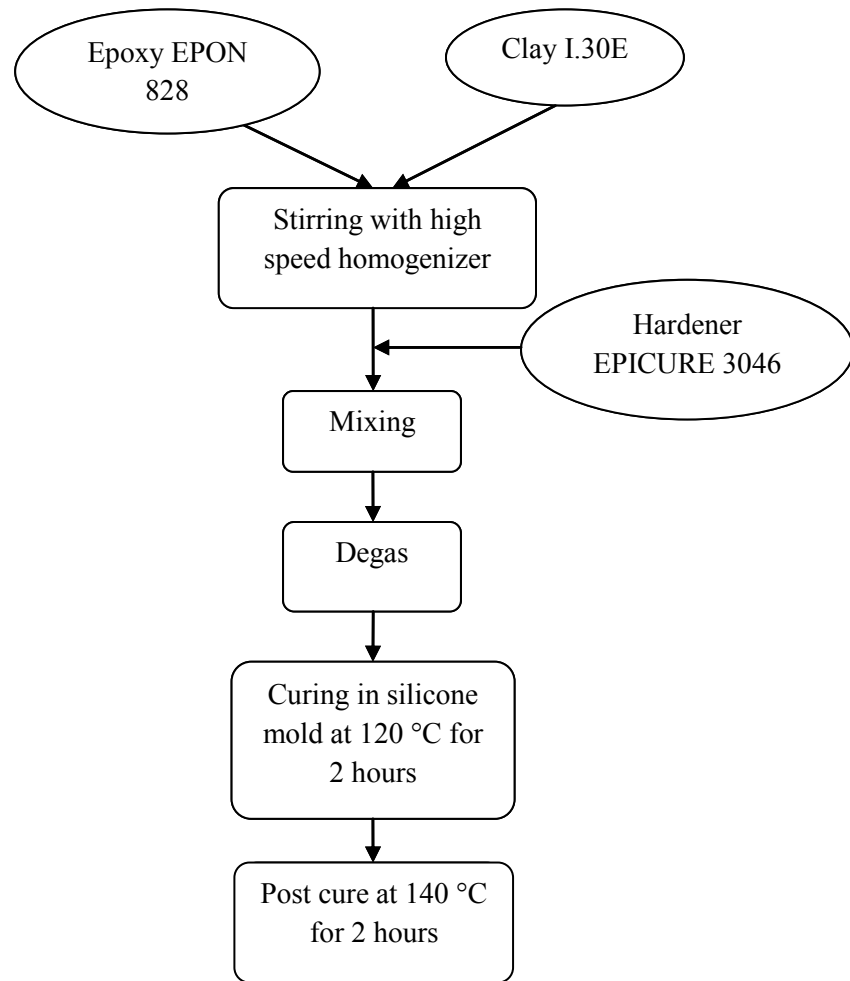


*Figure 3.5 Epoxy and epoxy + clay sample manufacturing procedure.*

### 3.3.2 Epoxy + Clay + S-glass sample preparation

Different manufacturing/fabrication methods can be applied to fabricate continuous fiber composite structure depending on the requirements and parts geometry. Some of the commonly used methods are hand lay-up and autoclave curing, RTM (resin transfer molding), VARTM (vacuum assisted RTM), SCRIMP (Seaman composite resin infusion molding process), Injection molding etc. Filament winding and pultrusion processes are also widely used to produce special shape composite structures especially for cylindrical, spherical and conical shape parts.

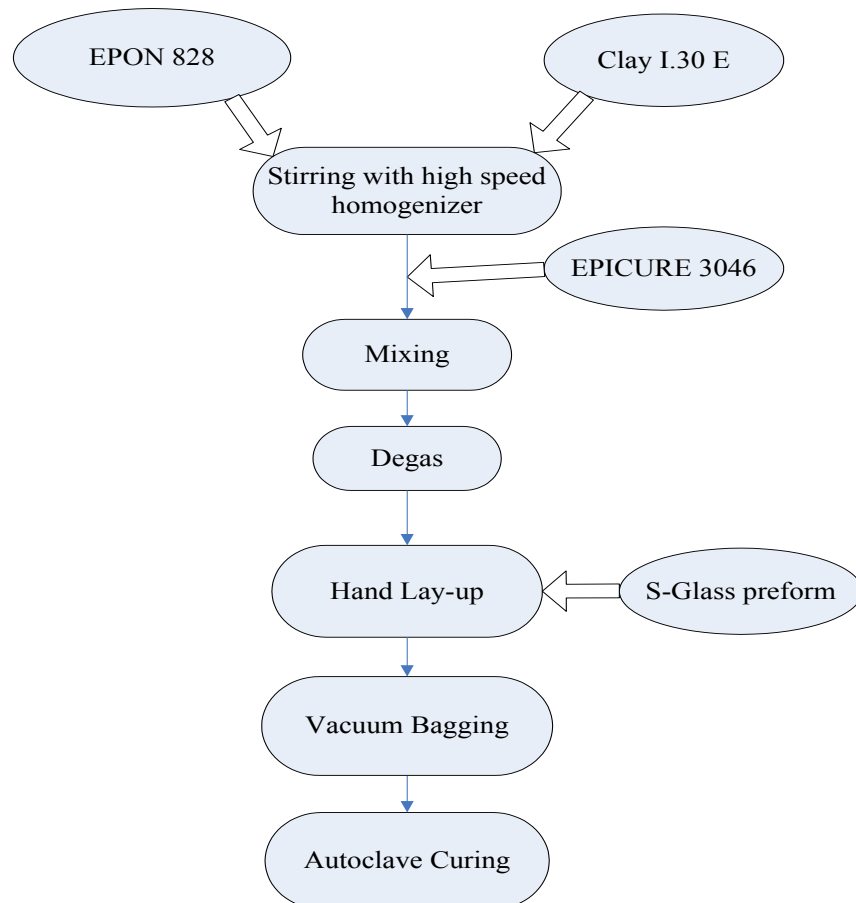
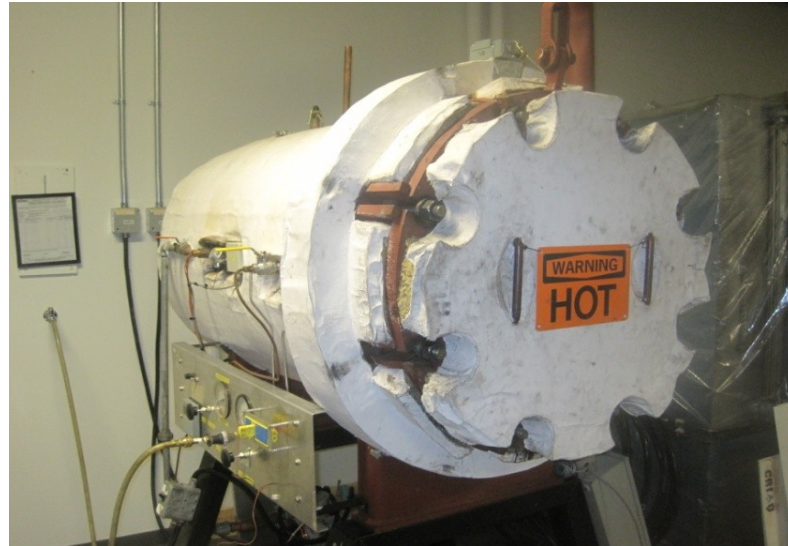


Figure 3.6 Flow chart for sample manufacturing with glass fiber.



*Figure 3.7 Photograph of a typical Autoclave (CONCOM Lab).*

In this research, hand lay-up and autoclave molding process were used to fabricate samples. Figure 3.6 shows the flow chart of sample manufacturing procedure. In the autoclave, a vacuum can be applied inside the vacuum bag and pressure as well as temperature can be controlled as desired. An autoclave is shown in figure 3.7. This provides a compact, consolidated and high quality parts. The Autoclave process has three major steps; tool preparation, lay-up and curing. Tool refers to the mold as autoclave is a molding process. There is secondary tooling materials required to prepare the vacuum bag and to ensure easy removal of the parts after curing. A steel plate of dimensions  $60\text{cm} \times 60\text{cm} \times 1.5\text{cm}$  was used as the tool to fabricate a flat plate laminate. Lay-up was done on this plate then a vacuum bag was prepared and the assembly was subsequently cured in an autoclave. For convenience, a big flat laminate was first manufactured and then the desired size experimental specimens were cut from the laminate using a diamond cutter. The total sample fabrication process and curing is described below:

- First, required size fiber pre-form were cut from the fiber pre-form roll according to the orientation of the lay-up. Here, 16 layers of fiber have been used for all sample configurations.
- The surface of the tool (steel plate) was cleaned and release agent ‘Safe Release 30’ was applied beforehand for easy removal of the parts after curing.
- A layer of fiber was placed upon the tool according to the desired laminate configuration and sufficient amount of resin (after dispersion and mixing with hardener) was applied on the fiber layer. Subsequent layers of fibers were placed on top of the previous layer one by one. After placing every layer sufficient resin was added and enough compaction pressure was applied using a roller to adhere the fiber plies and removal of entrapped air that possibly could form voids within the laminate. The lay-up sequence of all sample configurations is shown in figure 3.8.

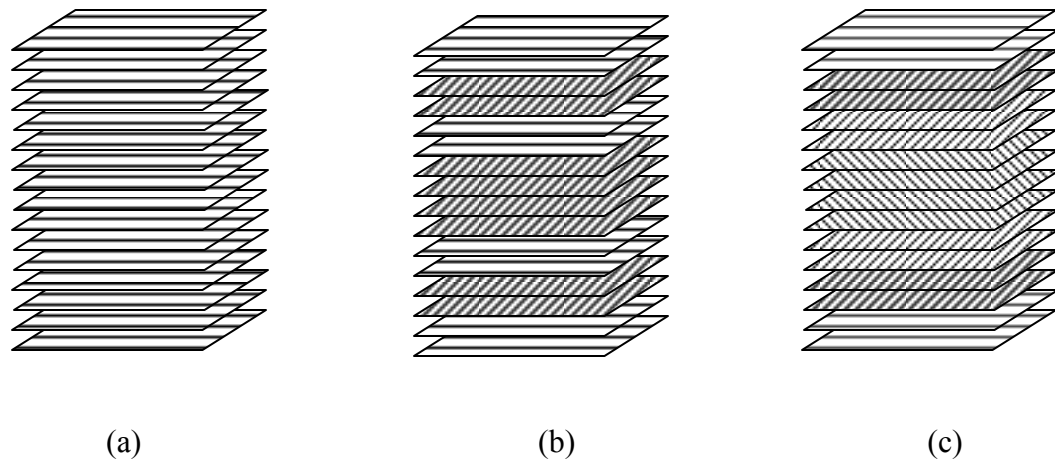
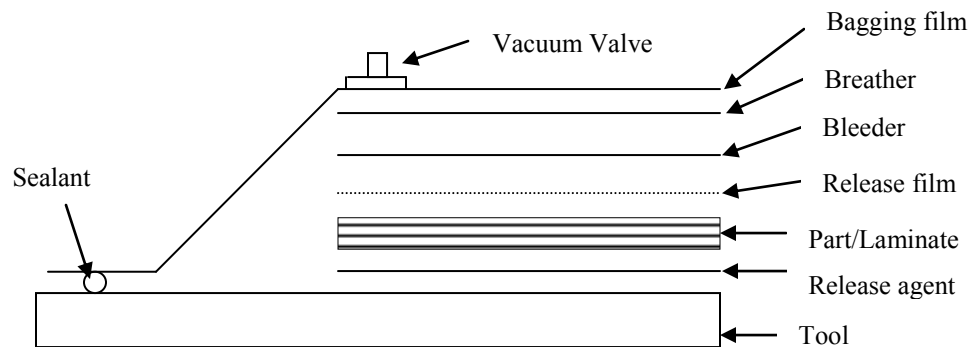


Figure 3.8 Lay-up sequences for (a) Unidirectional, (b) Cross-ply and (c) Quasi-isotropic laminates.

- After completing the ply lay-up, a porous release film, the bleeder ply to absorb excess resin and the breather ply to apply sufficient vacuum were placed on top of the laminate one after another.
- Then sealant tape was placed on the periphery of the plate around the laminate. A vacuum bag connected with a vacuum valve was then placed on the entire lay-up and sealed properly. A vacuum bagging sequence is shown in figure 3.9.



*Figure 3.9 Typical cross-section of a vacuum bag.*

- The entire vacuum bag assembly was then placed inside an autoclave and connected to the vacuum pump of the autoclave. A pressure of 50 psi was maintained inside the autoclave to assist further compaction of the laminate. Then the autoclave is started for curing the laminate.

### **3.3.3 Autoclave curing**

The autoclave is a sophisticated oven in which temperature and pressure can be controlled. It is basically a large cylindrical vessel with thermal insulation. A vacuum pump is always installed in an autoclave to apply necessary compaction pressure to the parts. Even a very complex multi-step curing cycle can be programmed via

computer or controller which precisely maintains the curing temperature inside the autoclave. The flexibility of controlling temperature and pressure is the major advantage of the autoclave. In the autoclave, the temperature plays a very important role to initiate cross-linking and acceleration of curing process. Pressure helps to squeeze out excess resin from the laminate. So the selection of curing temperature and pressure is very important which should meet the following requirements:

- To cure the resin uniformly throughout the laminate.
- To attain a high degree of cure in the shortest possible time.
- To squeeze out all the excess resin from each layer of the laminate before the resin becomes gelled at any location inside the laminate.
- To remove voids from the matrix.

To meet these requirements, a two step curing cycle was used to cure the samples as shown in the Figure 3.10. The laminate is heated from room temperature to 120 °C in 60 minutes then held at this temperature for 2 hours to allow the matrix flow, remove entrapped air and attain a certain degree of cure. In the second step, the temperature is again increased to 140 °C and held for another 2 hours for subsequent post cure.

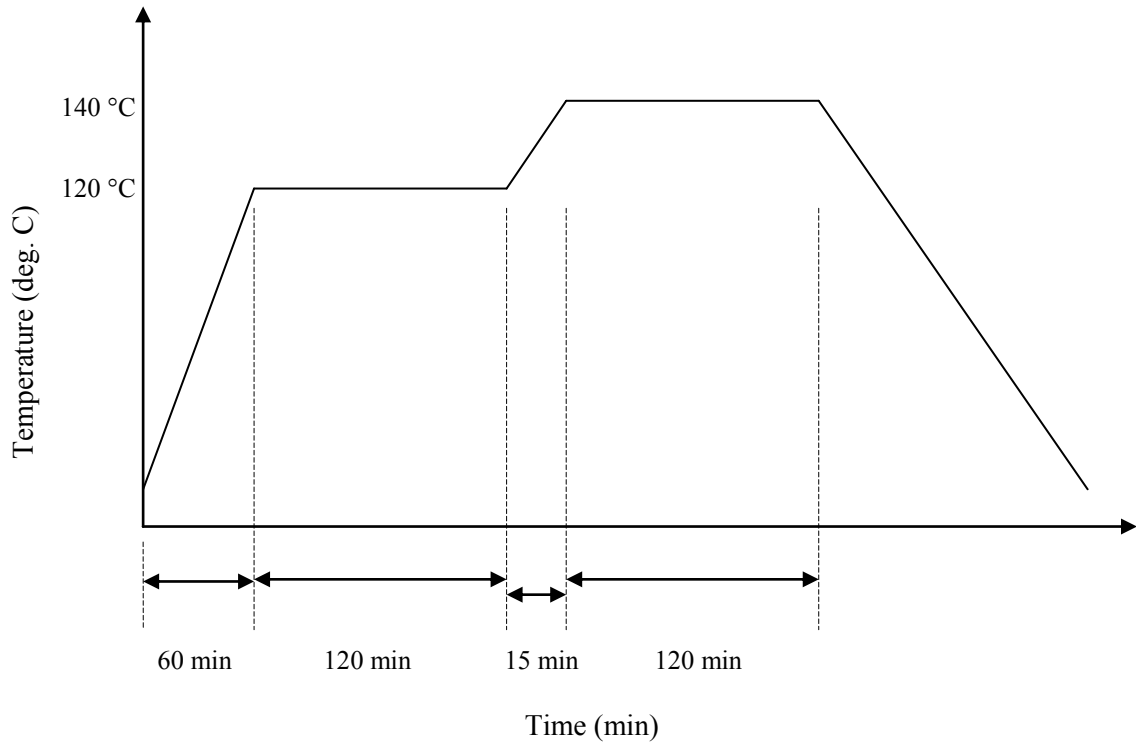


*Figure 3.10 Cure cycle for S-glass/epoxy composite laminate.*

### **3.4 Problems associated with sample fabrication**

The problems associated with the manufacturing of samples are described below:

- The major problem is viscosity of the resin increases after adding nanoclay in it. With increased viscosity, it is very difficult to remove voids from the resin system and extra effort is required to extract excess resin from the laminate at the time of curing. However, there is possibility of dry spots with increased viscosity of resin resulting in degraded quality of the final laminate.
- During high speed mixing, the temperature of the mixture rises very fast. Moreover, Nanomer I.30E is a reactive organoclay with primary amine intercalant

and reacts above 100 °C temperature. So the temperature of the mixture was closely monitored and always maintained below 85 °C while mixing. For this an ice bath was used and an interrupted (stop mixing when temperature reach 85 °C and start again when temperature comes down) mixing technique was applied.

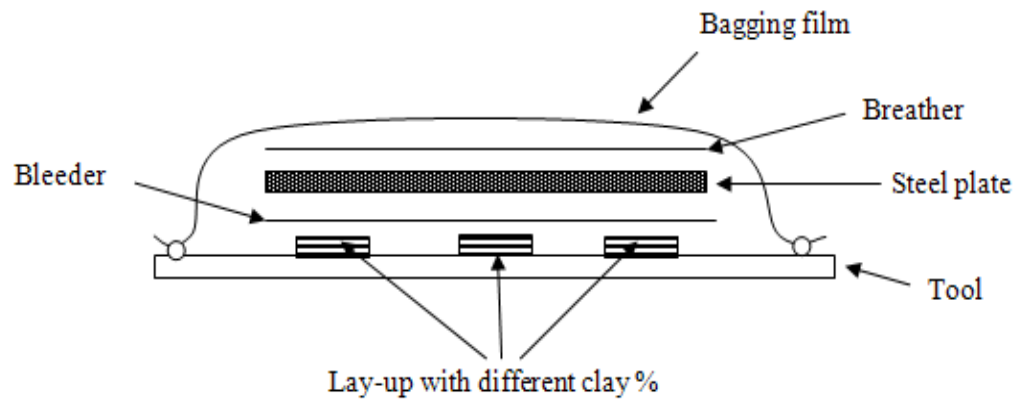


*Figure 3.11 Schematic illustration of vacuum bagging sequence.*

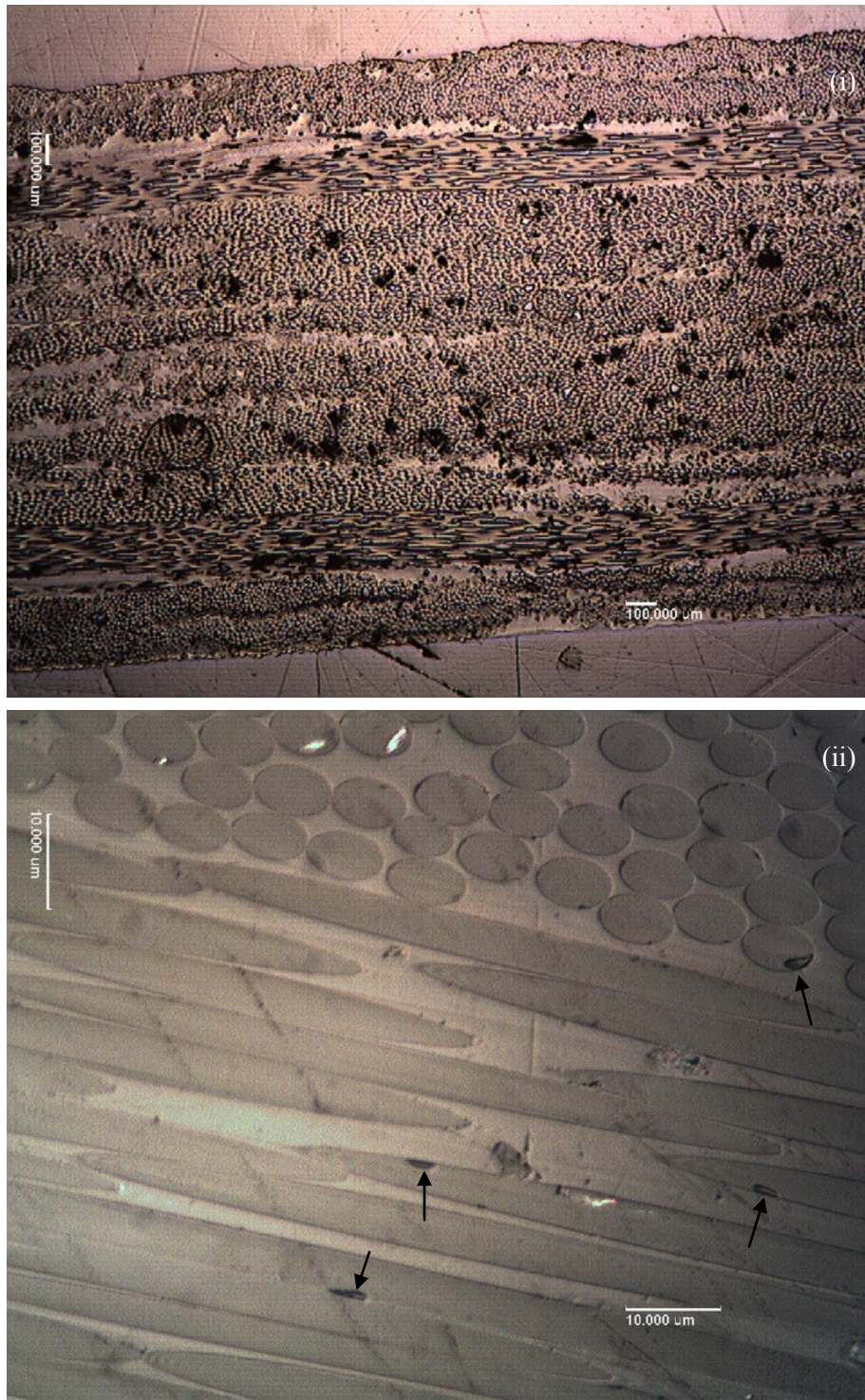


*Figure 3.12a Optical microscopic image of cross section of quasi-isotropic laminate without nanoclay: (i) lower magnification and (ii) higher magnification.*

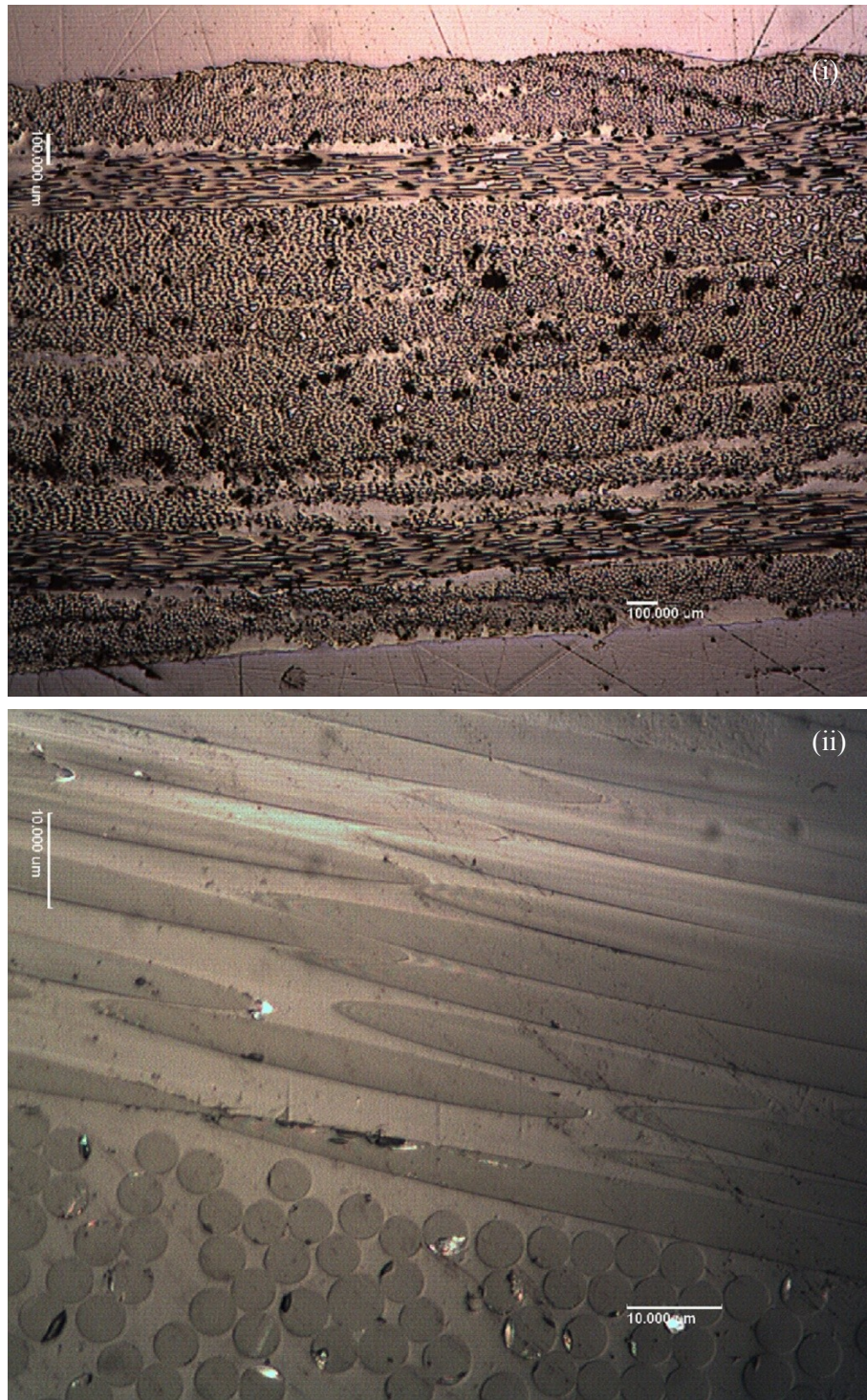


*Figure 3.12b Optical microscopic image of cross section of quasi-isotropic laminate with 1 wt.% nanoclay: (i) lower magnification and (ii) higher magnification.*

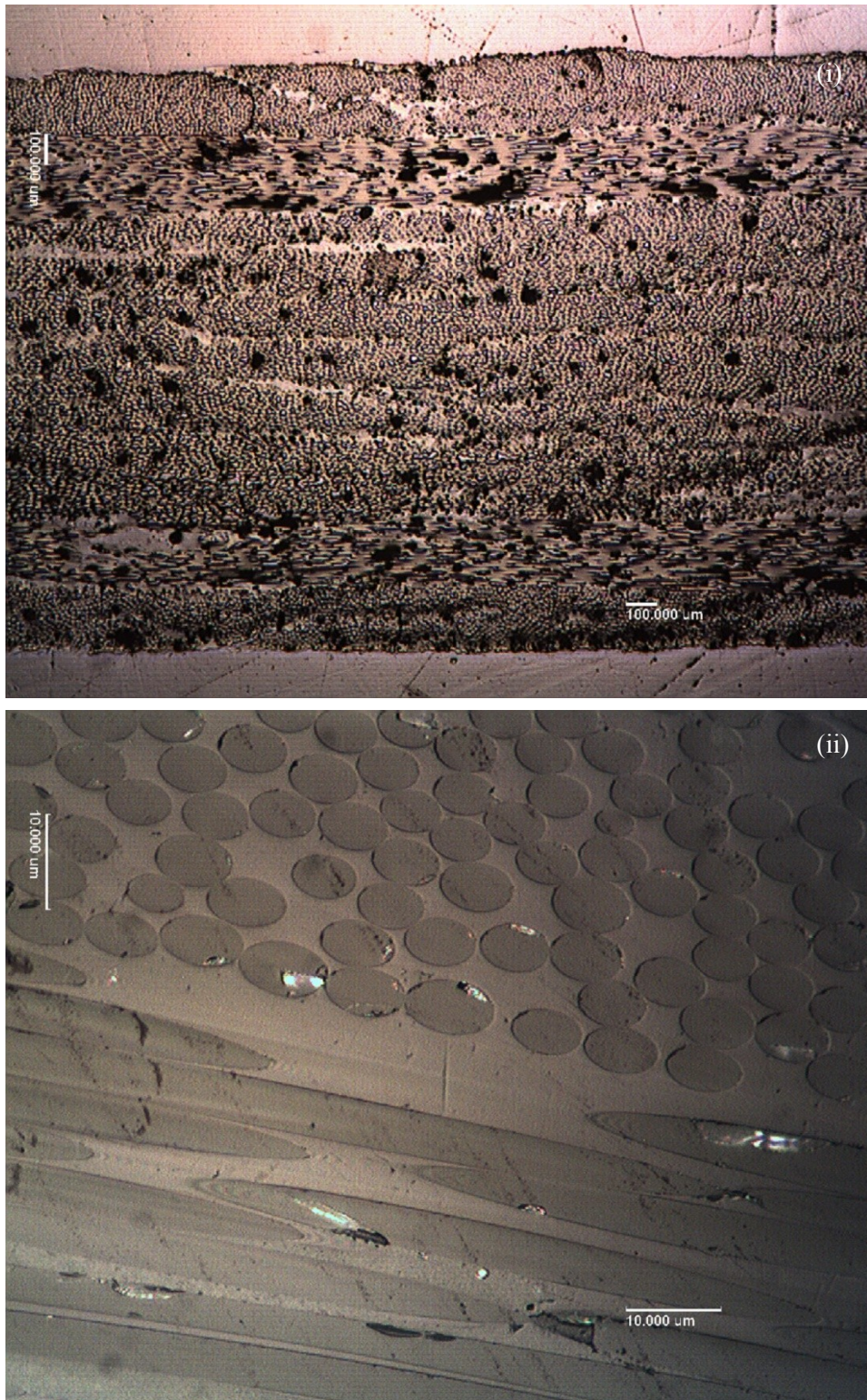


*Figure 3.12c Optical microscopic image of cross section of quasi-isotropic laminate with 2 wt.% nanoclay: (i) lower magnification and (ii) higher magnification.*

- Because of the viscosity difference, the thickness of the laminate with different clay content varied. Thus the laminate with higher clay content had higher thickness although the same curing conditions have been applied. But the number of fiber layers was the same in all laminates. So the volume fraction of the laminates was also varying which is not good for comparative result analysis. This problem was rectified by, laying up all samples with different clay contents of same configuration (unidirectional, cross-ply and quasi-isotropic) on a same tool (steel plate) and after lay-up another steel plate was placed on the top of all samples to apply same pressure on all laminate according to figure 3.11. Using this technique, samples with almost identical thickness and good quality were manufactured as shown in figures 3.12a to 3.12c. From the images, the thickness was measured as  $1.26 \pm 0.02$  mm. There are some black marks observed in the images with higher magnification in figures 3.12a to 3.12c which are mostly on the fibers. These may be induced during grinding and polishing because of very brittle nature of S-glass fibers.

### **3.5 Experimental Procedure**

#### **3.5.1 Dynamic Mechanical Analysis (DMA)**

Dynamic mechanical or viscoelastic properties of material are analyzed by DMA technique. DMA can simultaneously measure elastic or storage modulus and the energy dissipating or loss modulus of the material as a function of several parameters such as temperature, time, and frequency. DMA also can determine the glass transition temperature ( $T_g$ ) and phase transitions. DMA applies a sinusoidal force to the sample and

measures the resulting deformations or strains. Unlike purely elastic material, the strain response of a viscoelastic material always lags behind the input stress by a phase difference which is called the phase angle. Figure 3.13 shows the response to sinusoidal oscillation of purely elastic and viscoelastic material. The ratio of the dynamic stress to the dynamic strain gives a complex modulus which is then resolved into the storage modulus ( $E'$ ) and the loss modulus ( $E''$ ). The storage modulus  $E'$  is usually called the elastic modulus or the stiffness of the material which refers to the ability of the material to retain or store the elastic energy. The loss modulus  $E''$  is the viscous component and refers to the energy absorbing ability of the material. The tangent of the phase angle, usually denoted by  $\tan\delta$ , provides the relation between elastic and viscous components.

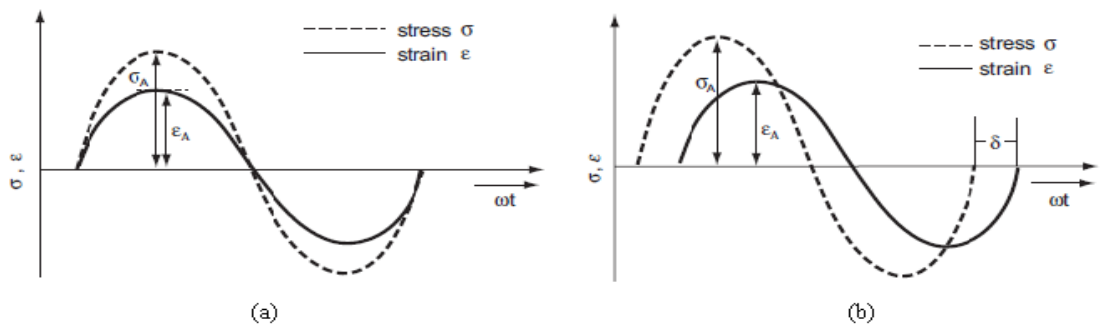


*Figure 3.13 Sinusoidal oscillation and response of, (a) purely elastic material and (b) linear viscoelastic material.*

A Du Pont 983 DMA coupled with TA 2100 thermal analyzer was used to measure the storage modulus, loss modulus and  $\tan\delta$ . Figure 3.14 shows the 983 DMA and TA 2100

thermal analyzer used for this experiment and a sample clamped with the DMA. In 983 DMA, the sample is clamped between two parallel arms and is deformed under a constant stress, oscillating stress or a constant strain, depending on the experiment mode. The behavior of the sample under this deformation is monitored by a linear variable displacement transducer (LVDT). Using 983 DMA, sample can be analyzed in four different modes of operation: resonant frequency, fixed frequency, stress relaxation and creep mode [69]. Figure 3.15 shows the internal components of a 983 DMA.



*Figure 3.14 Photograph of (a) a 983 DMA with TA 2100 Thermal analyzer and (b) a sample clamped with 983 DMA (CONCOM Lab).*

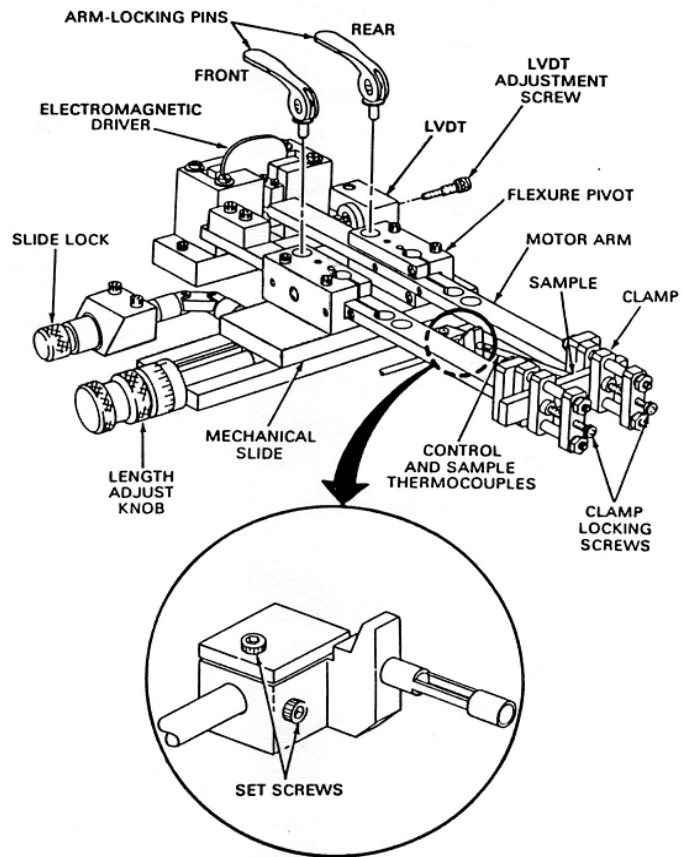


Figure 3.15 DMA internal components [69].

All samples had the width between 8 mm to 10 mm and thickness between 1.25 mm to 2 mm. The dynamic properties were determined using fixed frequency method of 1Hz and amplitude of 0.2 mm. The samples were heated from room temperature to 180°C at a ramp (heating rate) of 2°C/min.

### 3.5.2 Log Decrement Test

The log decrement test is a method to measure damping ratio experimentally of an under-damped system. In an under-damped system, the amplitude of vibration exponentially decays over time and the natural log of amplitudes of any two successive peaks is called the logarithmic decrement or log decrement. So the log decrement, usually denoted by  $\delta$ , can be defined by

$$\delta = \frac{1}{n} \ln \frac{A_0}{A_1} \quad (3.1)$$

Where  $A_0$  is the amplitude of first cycle and  $A_1$  is the amplitude of the peak after  $n$  period.

From this log decrement, the damping ratio  $\zeta$  can be calculated using the following formula

$$\zeta = \frac{1}{\sqrt{1 + \left(\frac{2\pi}{\delta}\right)^2}} \quad (3.2)$$

For the log decrement test, samples were manufactured using the same hand lay-up and autoclave curing method as the DMA test. The length and width of the samples were 20 cm and 2.54 cm respectively and the thickness between 1.25 mm and 1.35 mm. Figure 3.16 shows the log decrement test set-up. One end of the sample was clamped on a rigid support with sufficient clamping force at distance of 20 cm from the free end. An accelerometer (Bruel & Kjaer 4393) was attached on the tip of the sample using wax glue to measure the amplitudes of vibration. The tip of cantilever composite beam is then excited with initial amplitude of 20 mm approximately and let to vibrate freely until the amplitude decays. These amplitude signals were then amplified by a Kistler 504E dual

mode amplifier and the amplitude versus time graph was plotted using an Agilent 54624A oscilloscope. Figure 3.17 shows the photograph of samples and experimental setup for the log decrement test. From the free decay curve, logarithmic decrement  $\delta$ , and damping ratio  $\zeta$  was calculated using equations 3.1 and 3.2 respectively. The experiment was done in air so the results include the effect of air damping. The effect of air damping could be avoided by doing the test in vacuum but for comparative purpose, tests in air are sufficient.

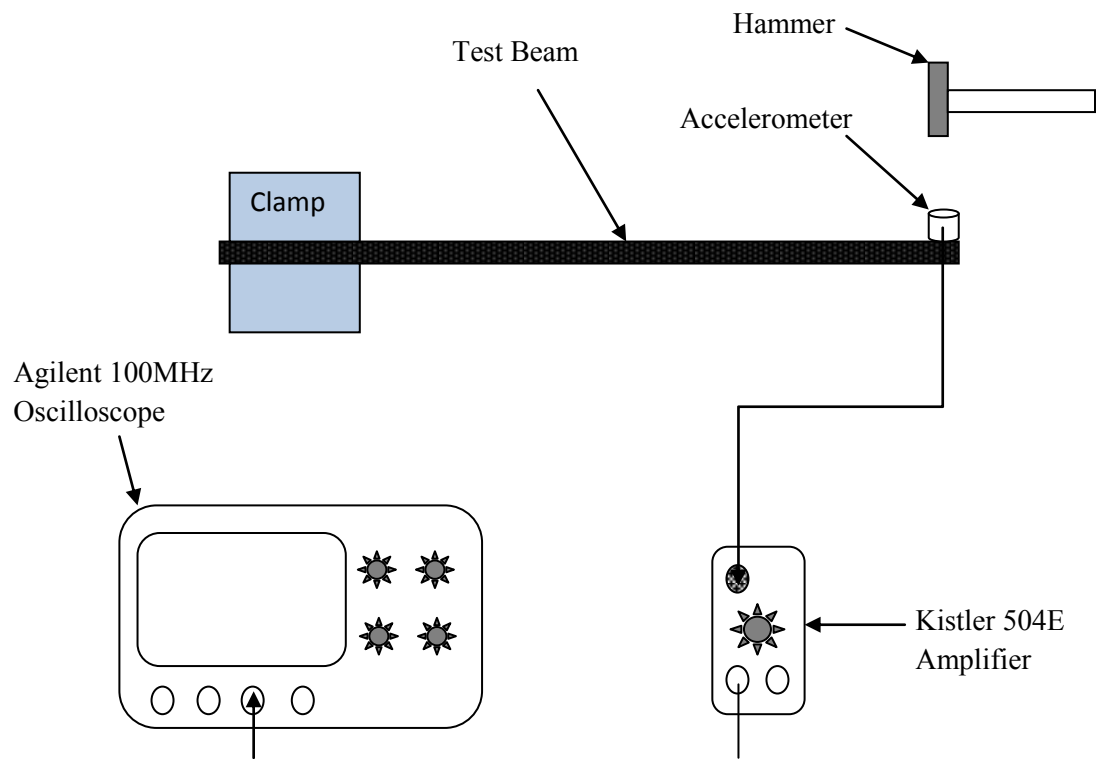


*Figure 3.16 Experimental set-ups for log decrement test.*

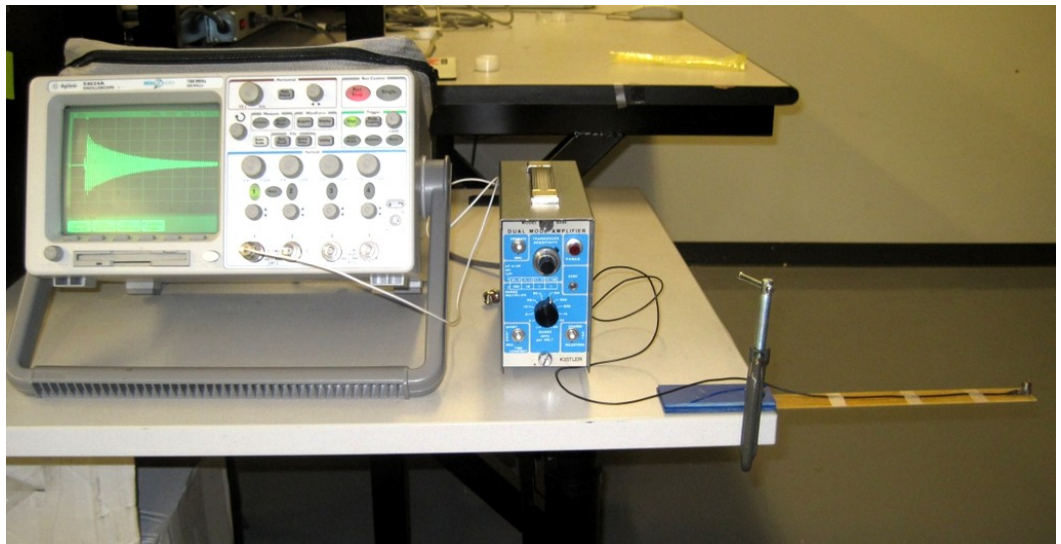
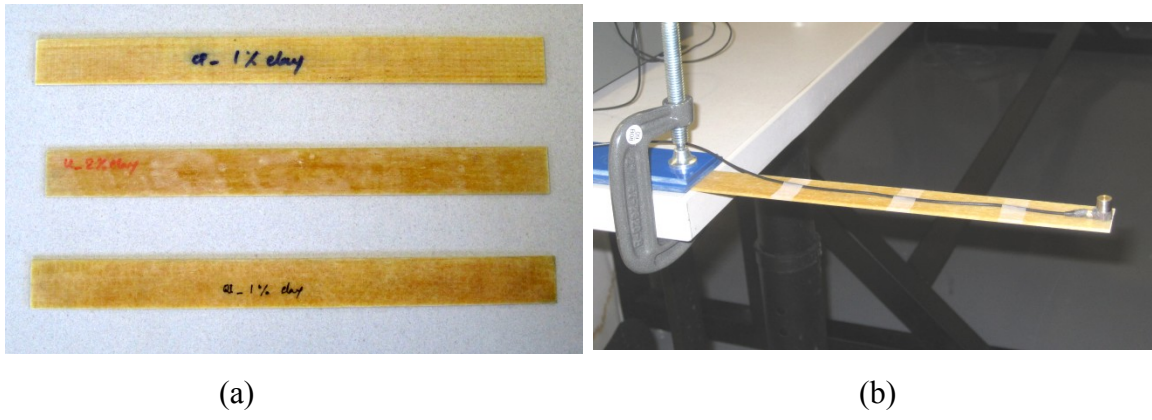


Figure 3.17 Photographs of (a) typical samples, (b) clamped sample with accelerometer and (c) log decrement test set-up.

### 3.5.3 Flexural Fatigue Test

Vibration has a very important influence on the fatigue life of any structure. During vibration, a structure is usually subjected to flexural fatigue load and the amplitude or deflection of vibration is not very high (usually less than  $7^\circ$ ). So to see the effect of damping improvement on fatigue life, a fixed amplitude flexural fatigue test was designed. The flexural fatigue tests were carried out using an MTS machine to measure the fatigue life of glass/epoxy composite laminate with and without nanoclay. Sample manufacturing procedure and dimensions were the same as for the log decrement test samples. Figure 3.18 shows the schematic illustration of experimental set-up for the flexural fatigue test.

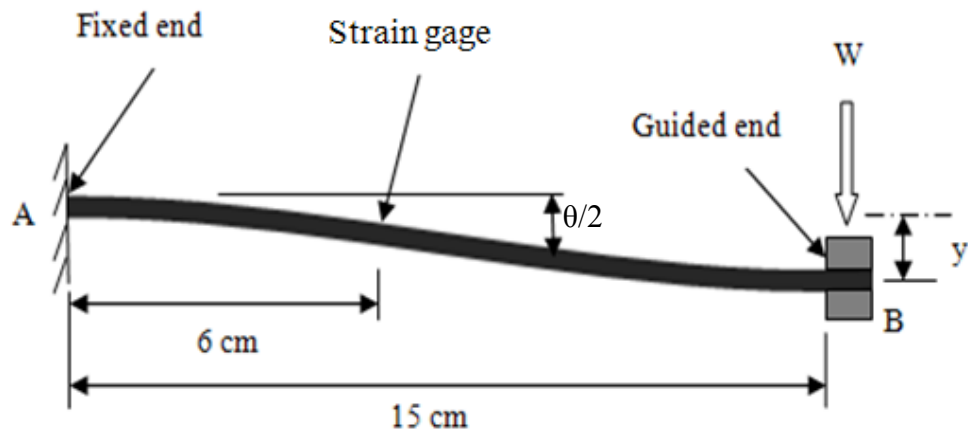
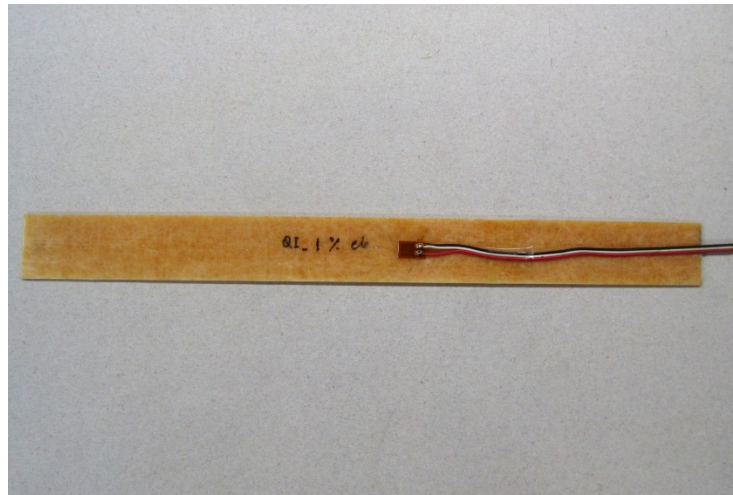
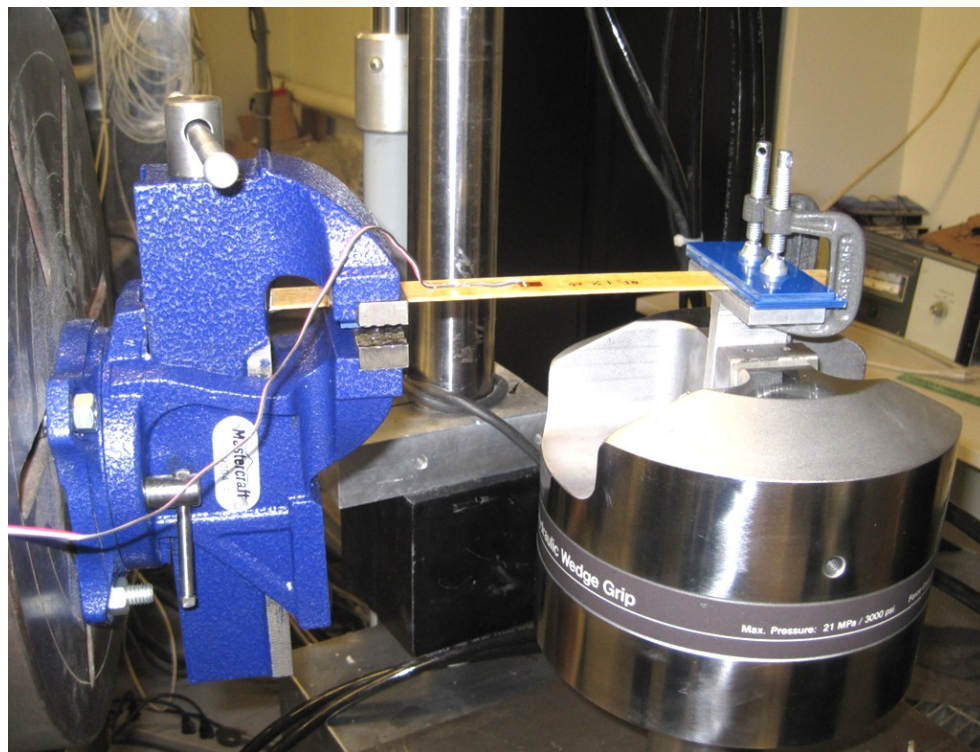


Figure 3.18 Schematic illustration of experimental set-up for flexural fatigue test.



*Figure 3.19 Typical fatigue sample with strain gage and wire.*



*Figure 3.20 Photograph of experimental set-up for flexural fatigue test.*

One end of the sample was clamped with lower grip of MTS machine and the other end was clamped to a fixed and rigid support outside of the machine at a distance of 15 cm. To monitor the damage inside the laminate sample, a strain gage (Vishay CEA-06-125UW-350) was attached to the laminate at a distance of 6 cm from the fixed end. A test sample with strain gage and wire is shown in figure 3.19. The photograph of the experimental set-up is given in figure 3.20. The MTS machine was programmed to deflect the sample to maximum amplitude of  $\pm 6.67$  mm at frequency of 4 Hz. So from figure 3.18, total angle of deflection was measured as,

$$\text{Tan } \left\{ \frac{\theta}{2} \right\} = \frac{y_B - y_A}{x_B - x_A} = \frac{y}{L}$$

$$\therefore \text{Tan } \left\{ \frac{\theta}{2} \right\} = \frac{6.67}{150} \approx \text{Tan } 2.5^\circ$$

$$\therefore \theta \approx 5^\circ$$

For each sample 300,000 fatigue cycles were applied. Strain on the sample was recorded after every 25,000 cycles of fatigue. This is a cantilever beam system with one end fixed and the other end is guided. The theoretical analysis of beam deflection is given in the following section. To see the effect of damage on damping property, logarithmic decrement tests were carried out after every 100,000 fatigue cycles. For better understanding of the effect of nanoclay addition on fatigue life, flexural fatigue tests were carried out only on cross-ply and quasi-isotropic laminate samples because they have less fiber dominant flexural properties compared to unidirectional laminate. For repeatability of results, 3 samples of each configuration were tested.

### 3.5.3.1 Deflection of Beam

This is a cantilever beam arrangement with one end fixed and the other end is guided where a controlled deflection of  $y$  is given. Figure 3.21 represents the schematic of beam deflection, free body diagram, shear force diagram and bending moment diagram. As the end B is guided, the slope of both ends will be zero under deflection.

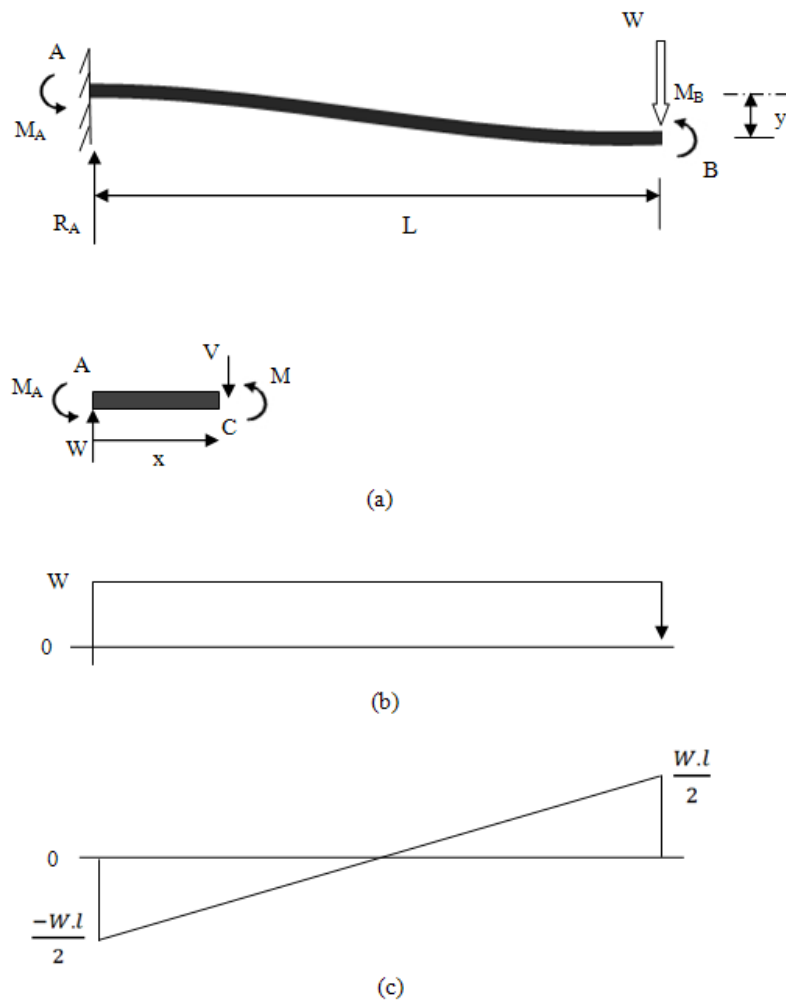


Figure 3.21 Schematic of (a) free body diagram, (b) shear force diagram and (c) bending moment diagram.

In equilibrium,

$$\sum F_y = 0$$

$$\therefore R_A = w$$

Now, taking moment about B,

$$R_A L = M_A + M_B$$

From symmetry condition,

$$M_A = M_B = M$$

Or,

$$wL = M + M$$

$\therefore$

$$M = \frac{wL}{2}$$

Using the free body diagram of portion AC of the beam, where C is located at distance x from end A

$$M = -\frac{wL}{2} + wx$$

$$\langle EI \rangle \frac{d^2y}{dx^2} = -\frac{wL}{2} + wx \dots\dots\dots (i)$$

Integrating equation (i) in x,

$$\langle EI \rangle \frac{dy}{dx} = -\frac{wLx}{2} + \frac{w}{2}x^2 + C_1 \dots\dots\dots (ii)$$

Integrating equation (ii) in x again,

$$\langle EI \rangle y = -\frac{wL}{4}x^2 + \frac{w}{6}x^3 + C_1x + C_2 \dots\dots\dots (iii)$$

Now by applying boundary conditions,

$$\text{At } x = 0, \quad \frac{dy}{dx} = 0$$

$$\therefore C_1 = 0$$

And at,

$$x = 0, \quad y = 0$$

$$\therefore C_2 = 0$$

So equation (iii) becomes,

$$\langle EI \rangle y = -\frac{wL}{4}x^2 + \frac{w}{6}x^3$$

Or, 
$$y = -\frac{1}{12} \frac{1}{\langle EI \rangle} (3wx^2 - 2wx^3)$$

Or, 
$$y = -\frac{w}{12\langle EI \rangle} x^2 (3L - 2x) \dots\dots\dots (iv)$$

Now,

Strain on the surface of the beam, 
$$\varepsilon = \frac{d}{\rho}$$

Where,

$d$  = distance of surface from the neutral axis

and  $\rho$  = curvature of neutral axis

Here, 
$$d = \frac{h}{2} \quad (\text{for symmetric beam})$$

And 
$$\frac{1}{\rho} = \frac{d^2 y}{dx^2} = -\frac{w}{\langle EI \rangle} \left(\frac{L}{2} - x\right) \quad (\text{from eqn. i})$$

$\therefore$  
$$\varepsilon = \frac{h}{2} \frac{d^2 y}{dx^2}$$

So, Strain at any point

$$\varepsilon_c = \frac{-w \cdot h}{2\langle EI \rangle} \left(\frac{L}{2} - x\right) \dots\dots\dots (v)$$

Since , 
$$w = -\frac{12\langle EI \rangle y}{x^2} \frac{1}{(3L-2x)} \quad (\text{from equation iv})$$

$$\varepsilon_c = \frac{h(3L-6x)y}{x^2(3L-2x)} \dots\dots\dots (vi)$$

From equation (v), it can be said that maximum positive strain occurs at  $x = 0$ , the strain value becomes 0 when  $x = \frac{L}{2}$  and maximum negative strain occurs at  $x = L$ .

### 3.5.3.2 Fatigue Damage Index

Fatigue damage index is a parameter to measure the extent of the damage caused by the cyclic fatigue, usually denoted by  $D$  and defined as:

$$D = 1 - \frac{E_r}{E_0} \quad (3.3)$$

Where,  $E_r$  and  $E_0$  are the modulus of the samples after and before the fatigue test, i.e.  $E_0$  refers to the undamaged state and  $E_r$  refers to the residual value after a certain fatigue cycle. So it is obvious that the value of  $D$  would always be less than 1 and a lower value indicates that fatigue damage is less in that sample. After 200,000 and 300,000 fatigue cycles, the flexural storage modulus of all samples was measured using the DMA 983. Then fatigue damage index  $D$  was calculated using equation 3.3.

# Chapter 4

## Vibration Test Results

### 4.1 DMA Analysis

Dynamic Mechanical Analysis (DMA) was carried out to measure the dynamic mechanical performance of pristine and nano-clay incorporated epoxy and glass/epoxy composite system. In the DMA test, a flexural oscillatory force is applied to the sample and the response to the applied force is measured as a function of temperature. In this analysis two different moduli can be determined. The first one is storage modulus or elastic modulus usually denoted by  $E'$  which represents the ability of the material to store energy. The second one is the loss modulus which indicates the ability of the material to dissipate energy and is usually defined by  $E''$ . The ratio of loss modulus  $E''$  and storage modulus  $E'$  is called Tan delta ( $\tan \delta$ ) which represents the damping property of the material. The temperature dependence of the flexural storage modulus, loss modulus and  $\tan \delta$  of all samples is described in the following sub-sections. In DMA analysis, the storage modulus gradually decreases and loss modulus gradually increases with the increase in temperature. At a certain temperature, the molecules of the material become unstable and there is relative motion between the molecules. At this point, the storage modulus falls sharply and the loss modulus reaches a maximum value. This temperature is called the glass transition temperature and is usually defined by  $T_g$ . Although  $T_g$  has a range, the temperature where  $\tan \delta$  is maximum, can be considered as the glass transition temperature. Below  $T_g$  the material is in glassy state and above  $T_g$  the material has a rubbery state.

#### 4.1.1 Neat epoxy and nano-clay incorporated epoxy

The temperature dependent curves of storage modulus, loss modulus and tan delta are shown in figure 4.1 as determined by flexural dynamic mechanical analysis. Within the entire heating range, three arbitrary temperatures (30°C, 60°C and 140°C) have been selected to compare the results in both glassy (30°C and 60°C) and rubbery (140°C) region. Table 4.1 shows the DMA properties of neat epoxy and nano-clay incorporated epoxy at these temperatures.

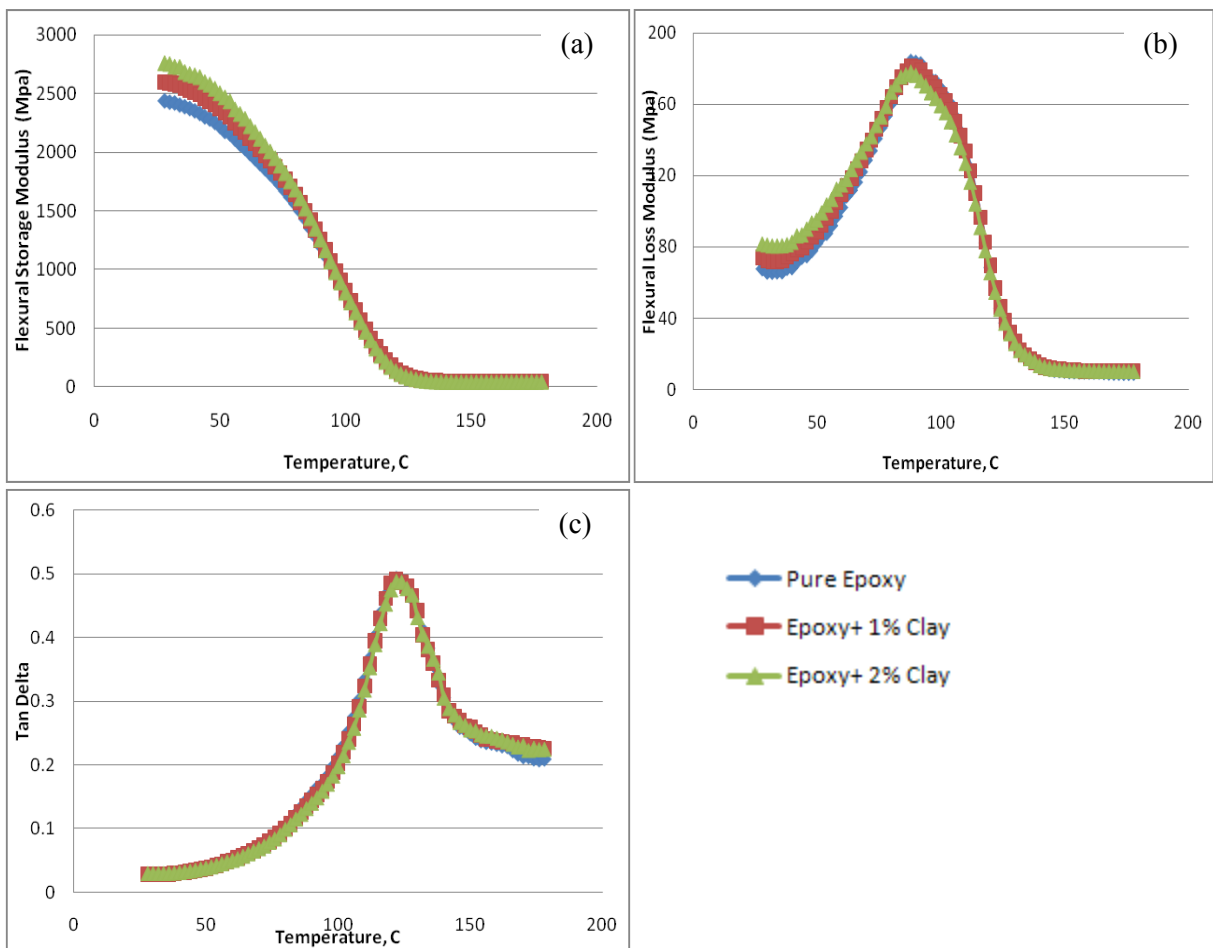


Figure 4.1 DMA curves of neat epoxy and nanoclay incorporated epoxy; (a) storage modulus, (b) loss modulus and (c) tan delta.

Table 4.1 DMA properties of neat epoxy and nanoclay incorporated epoxy

Material	Storage Modulus (GPa)			Tg (°C)
	30°C	60°C	140°C	
Epoxy	2.42	2.03	0.043	122
Epoxy + 1 wt.% Clay	2.59	2.17	0.044	122
Epoxy + 2 wt.% Clay	2.75	2.29	0.045	122
Material	Loss Modulus (MPa)			
	30°C	60°C	140°C	
Epoxy	65.88	102.22	13.13	
Epoxy + 1 wt.% Clay	72.31	109.42	13.84	
Epoxy + 2 wt.% Clay	81.30	115.00	13.71	

From figure 4.1(a), it can be clearly seen that nano-clay has a significant effect on flexural storage modulus. At room temperature the storage modulus is increased by 7% with only 1 wt.% of nano-clay I.30E compared to neat epoxy. At 2 wt.% of nano-clay, the improvement is 13.6%. At 60°C temperature similar trend is observed. But in the rubbery region, no significant change in the storage modulus is observed. So it can be said that the reinforcing effect of nano-clay is more dominant in the glassy region.

The DMA curve for the loss modulus is shown in figure 4.1(b). Maximum improvement in the loss modulus is observed at room temperature for both 1 and 2 wt.% incorporation of nano-clay. Here the improvement is 9.8% and 23.4% respectively. With the increase in temperature the percentage of improvement in the loss modulus is reduced. In the rubbery region, the change in the loss modulus is not significant.

Figure 4.1(c) represents the tan delta curve. There is no improvement observed in the tan delta value. Nano-clay improves both storage modulus and loss modulus. But the improvement in storage modulus is higher compared to the improvement in loss modulus. As tan delta is the ratio of loss modulus to storage modulus, the differences cancel out. Also, no change in the glass transition temperature was observed due to addition of nanoclay.

#### **4.1.2 Unidirectional Laminate**

The temperature dependent curves of storage modulus, loss modulus and tan delta for the unidirectional glass/epoxy laminate (with and without nanoclay) are shown in figure 4.2 as determined by flexural dynamic mechanical analysis. Table 4.2 shows the DMA properties at 30°C, 60°C and 140°C temperature. Temperature dependent curve of storage modulus in figure 4.2(a) shows that incorporation of nanoclay significantly improves the storage modulus both in glassy and rubbery region. At room temperature, 1 wt.% and 2 wt.% incorporation of nanoclay increased the storage modulus by 12.7% and 16.8% respectively.

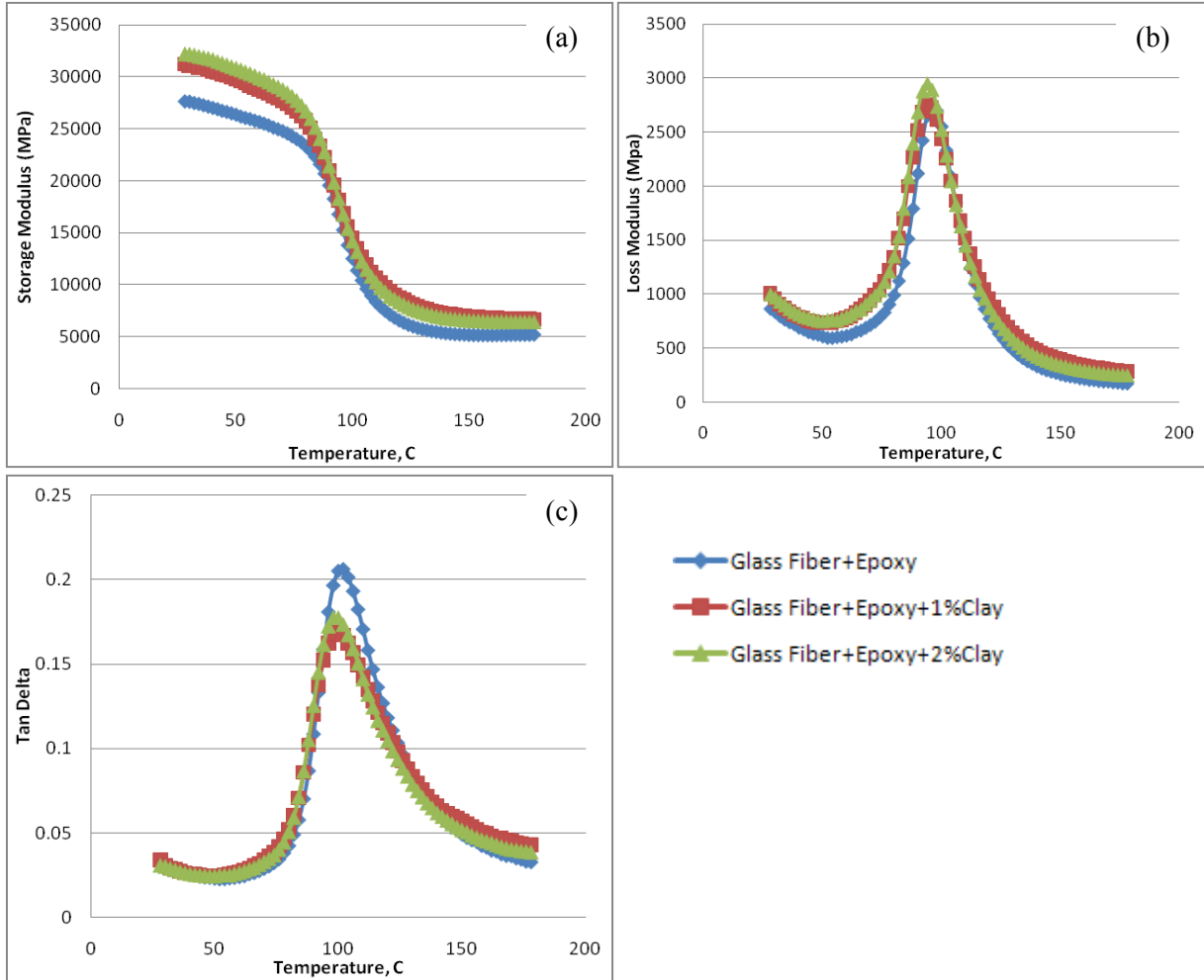


Figure 4.2 DMA curves of unidirectional laminates with different nanoclay contents; (a) storage modulus, (b) loss modulus and (c) tan delta.

Table 4.2 DMA properties of unidirectional laminates with different nanoclay contents

Laminate	Storage Modulus (GPa)			T <sub>g</sub> (°C)
	30°C	60°C	140°C	
Unidirectional	27.58	25.63	5.29	102
Unidirectional + 1 wt.% Clay	31.08	28.83	7.21	100
Unidirectional + 2 wt.% Clay	32.21	29.93	6.81	100
Laminate	Loss Modulus (MPa)			
	30°C	60°C	140°C	
Unidirectional	830.85	612.50	327.15	
Unidirectional + 1 wt.% Clay	958.50	780.15	479.60	
Unidirectional + 2 wt.% Clay	968.45	792.35	421.35	

Nanoclay has a similar positive effect on loss modulus in both glassy and rubbery region of unidirectional laminate shown in figure 4.2(b). The maximum improvement in the loss modulus is obtained at room temperature which are 15.4% and 16.6% for 1 wt.% and 2 wt.% nanoclay respectively. As both storage and loss modulus improve proportionally, the tan delta curves in figure 4.2(c) do not show any significant improvement and the peak of the tan delta curve with nanoclay reduced significantly compared to the laminate without nanoclay. At T<sub>g</sub>, energy dissipation ability due to friction is decreased because of relative motion between the molecules of the resin system. So the loss modulus falls quickly but due to the presence of glass fiber, the storage modulus still maintains some stiffness. This could be a possible reason why the peak of tan delta curves reduced successively at the glass transition temperature (T<sub>g</sub>).

### 4.1.3 Cross-Ply Laminate

The temperature dependent curves of storage modulus, loss modulus and tan delta for the cross-ply glass/epoxy laminate (with and without nanoclay) are shown in figure 4.3 as determined by flexural dynamic mechanical analysis. Table 4.3 shows the DMA properties at 30°C, 60°C and 140°C.

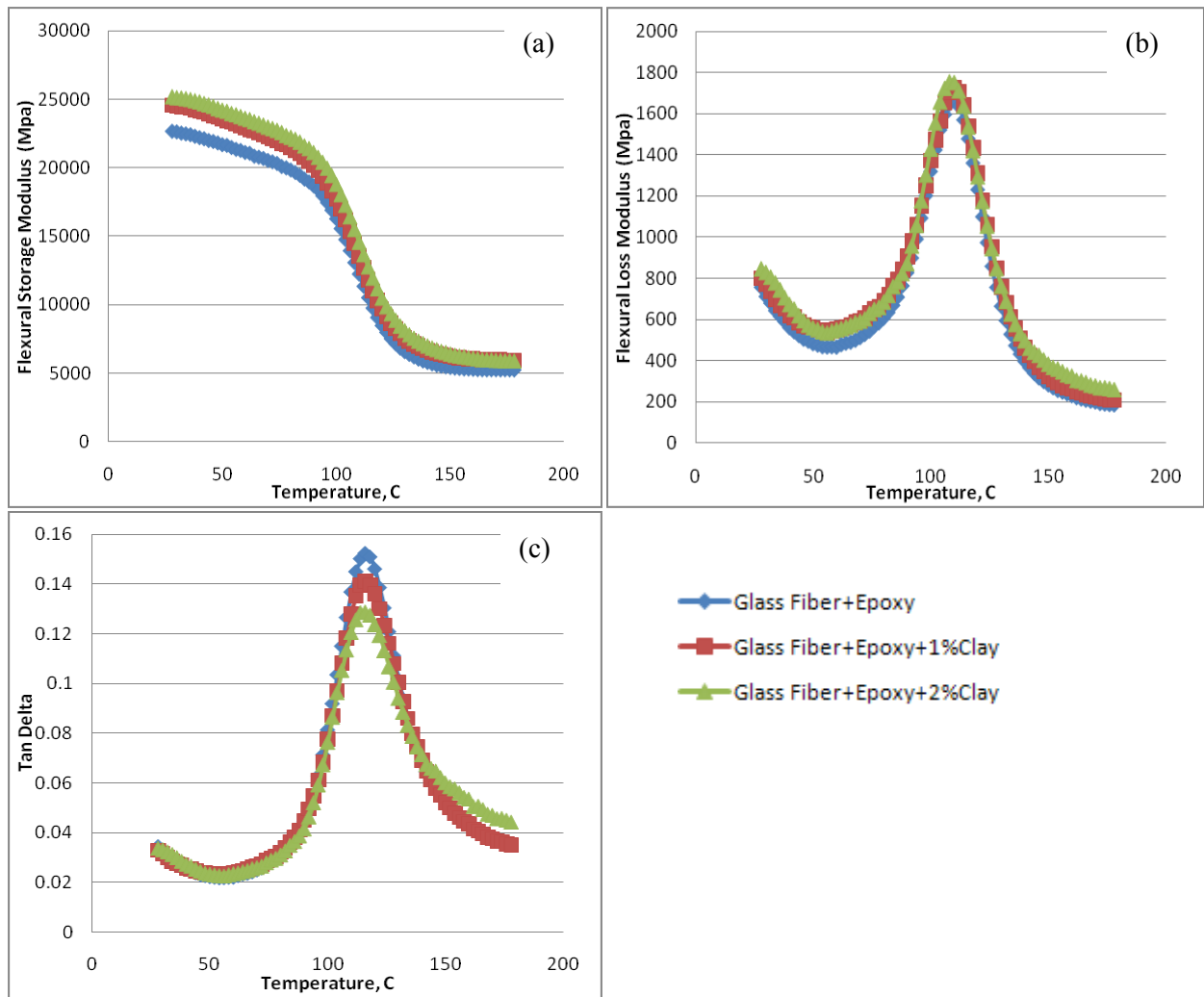


Figure 4.3 DMA curves of cross-ply laminates with different nanoclay contents; (a) storage modulus, (b) loss modulus and (c) tan delta.

Table 4.3 DMA properties of cross-ply laminates with different nanoclay contents

Laminate	Storage Modulus (GPa)			T <sub>g</sub> (°C)
	30°C	60°C	140°C	
Cross-ply	22.59	21.09	5.76	116
Cross-ply + 1 wt.% Clay	24.49	22.92	6.67	116
Cross-ply + 2 wt.% Clay	25.10	23.59	7.01	116
Laminate	Loss Modulus (GPa)			
	30°C	60°C	140°C	
Cross-ply	711.00	464.55	395.00	
Cross-ply + 1 wt.% Clay	770.30	551.35	461.70	
Cross-ply + 2 wt.% Clay	831.00	552.85	499.70	

Temperature dependent curve of storage modulus in figure 4.3(a) shows that similar to unidirectional laminate, incorporation of nanoclay fairly improves the storage modulus of cross-ply laminate in both glassy and rubbery region and the maximum improvement is observed at room temperature. At room temperature, 1 wt.% and 2 wt.% incorporation of nanoclay increased the storage modulus by 8.4% and 11.1% respectively. Nanoclay has a positive effect on loss modulus in both glassy and rubbery region of cross-ply laminate shown in figure 4.3(b). At room temperature the improvement in loss modulus is 8.3% and 16.9% respectively for 1 wt.% and 2 wt.% nanoclay contents. Again the improvement in the loss modulus is comparable to storage modulus. Thus like unidirectional laminate, the tan delta curve in figure 4.3(c) does not show any significant improvement in the glassy region and there was also a gradual reduction of peak in tan delta curves with increasing nanoclay content.

#### 4.1.4 Quasi-isotropic Laminate

The temperature dependent curves of storage modulus, loss modulus and tan delta for the quasi-isotropic glass/epoxy laminate (with and without nanoclay) are shown in figure 4.4 as determined by flexural dynamic mechanical analysis. Table 4.4 shows the DMA properties at 30°C, 60°C and 140°C.

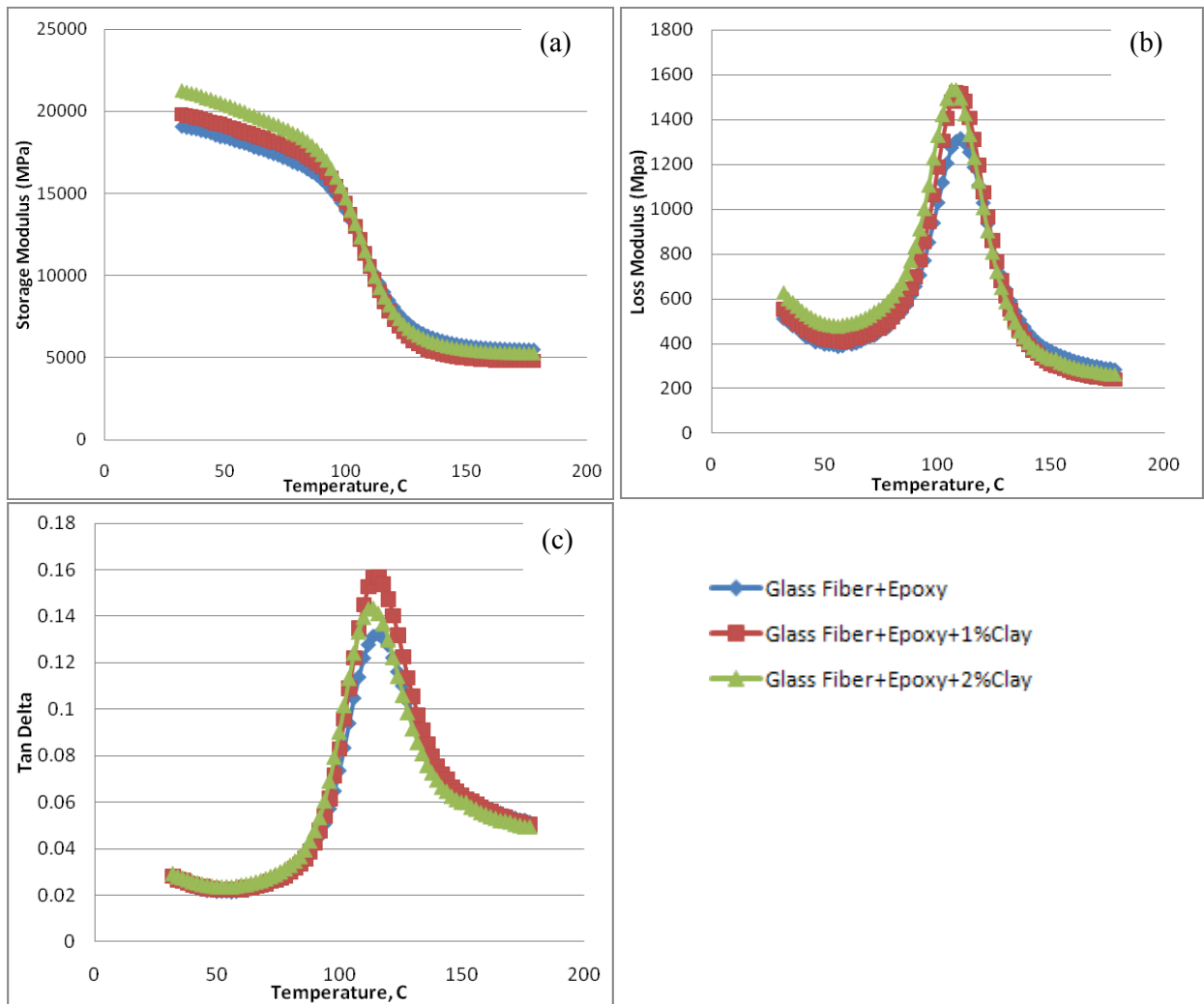


Figure 4.4 DMA curves of quasi-isotropic laminates with different nanoclay contents; (a) storage modulus, (b) loss modulus and (c) tan delta.

Table 4.4 DMA properties of quasi-isotropic laminates with different nanoclay contents

Laminate	Storage Modulus (GPa)			T <sub>g</sub> (°C)
	30°C	60°C	140°C	
Quasi-isotropic	19.07	17.94	6.06	116
Quasi-isotropic + 1 wt.% Clay	19.82	18.66	5.23	116
Quasi-isotropic + 2 wt.% Clay	21.28	19.81	5.81	114
Laminate	Loss Modulus (MPa)			
	30°C	60°C	140°C	
Quasi-isotropic	511.80	402.42	447.84	
Quasi-isotropic + 1 wt.% Clay	552.24	412.12	394.22	
Quasi-isotropic + 2 wt.% Clay	627.30	486.10	404.20	

The temperature dependent curve of storage modulus in figure 4.4(a) shows that similar to unidirectional and cross-ply laminate, incorporation of nanoclay significantly improves the storage modulus of quasi-isotropic laminate in the glassy region and the maximum improvement is observed at room temperature. At room temperature, 1 wt.% and 2 wt.% incorporation of nanoclay increased the storage modulus by 4% and 11.6% respectively. Nanoclay also has a positive effect on loss modulus in the glassy region of the quasi-isotropic laminate shown in figure 4.4(b). The improvements in the loss modulus are 8% and 22.5% at room temperature for the same clay contents. But in the rubbery region, both storage and loss modulus of laminates with nanoclay are slightly reduced compared to the laminates without nanoclay. The tan delta curve shown in figure 4.4(c) has a similar trend as observed in the case of unidirectional and cross-ply laminate.

## **4.2 Log Decrement Test**

Log decrement test results of different laminates are described in the following subsections.

### **4.2.1 Unidirectional Laminate**

The log decrement curves of unidirectional laminate with different nanoclay contents are shown in figure 4.5. It can be observed clearly that the amplitude of the laminates with nanoclay decays faster than the laminate without nanoclay and the damping effect is higher at higher nanoclay content. After 4.5 seconds, the amplitudes of laminate with 1 wt.% and 2 wt.% nanoclay have been reduced by 14.3% and 28.3% respectively. The log decrement value and the damping ratios of laminate with different nanoclay content are given in Table 4.5 which indicates that at 1 wt.% incorporation of nanoclay can improve the damping ratio by 12% and at 2 wt.% nanoclay content the improvement is 33%.

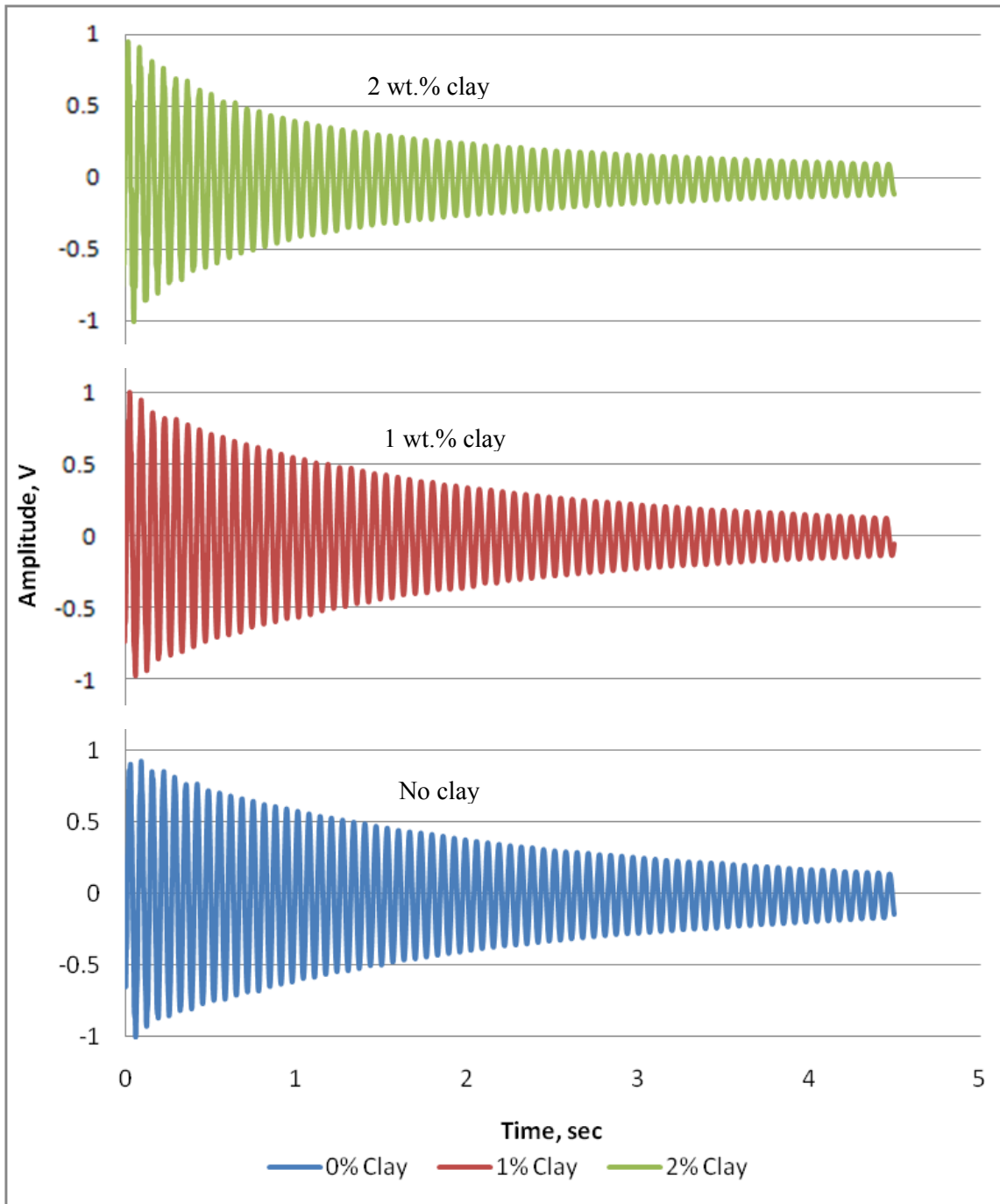


Figure 4.5 Free decay curves of unidirectional laminates with different nanoclay contents.

Table 4.5 Log decrement values and damping ratios of unidirectional laminates

Laminate	Logarithmic decrement, $\delta$	Damping ratio, $\zeta$ (eqn. 3.2)
Unidirectional (no clay)	0.033	0.00525
Unidirectional + 1 wt.% Clay	0.037	0.00588
Unidirectional + 2 wt.% Clay	0.044	0.00700

#### 4.2.2 Cross-Ply Laminate

The log decrement curves of cross-ply laminate with different nanoclay contents are shown in figure 4.6. It can be observed clearly that the amplitude of the laminates with nanoclay decay faster than the laminate without nanoclay and the damping effect is higher at higher nanoclay content. After 4.5 seconds, the amplitudes of laminate with 1 wt.% and 2 wt.% nanoclay have been reduced by 64.6% and 66.4% respectively. The log decrement value and the damping ratios of laminate with different nanoclay content are given in Table 4.6 which indicates that at 1 wt.% incorporation of nanoclay can improve the damping ratio by 41.7% and at 2 wt.% nanoclay content the improvement is 55.5%. Here the effect of nanoclay on damping property is even more than unidirectional laminate which could be because of less fiber dominated properties and more matrix dominated properties in the case of cross-ply laminate.

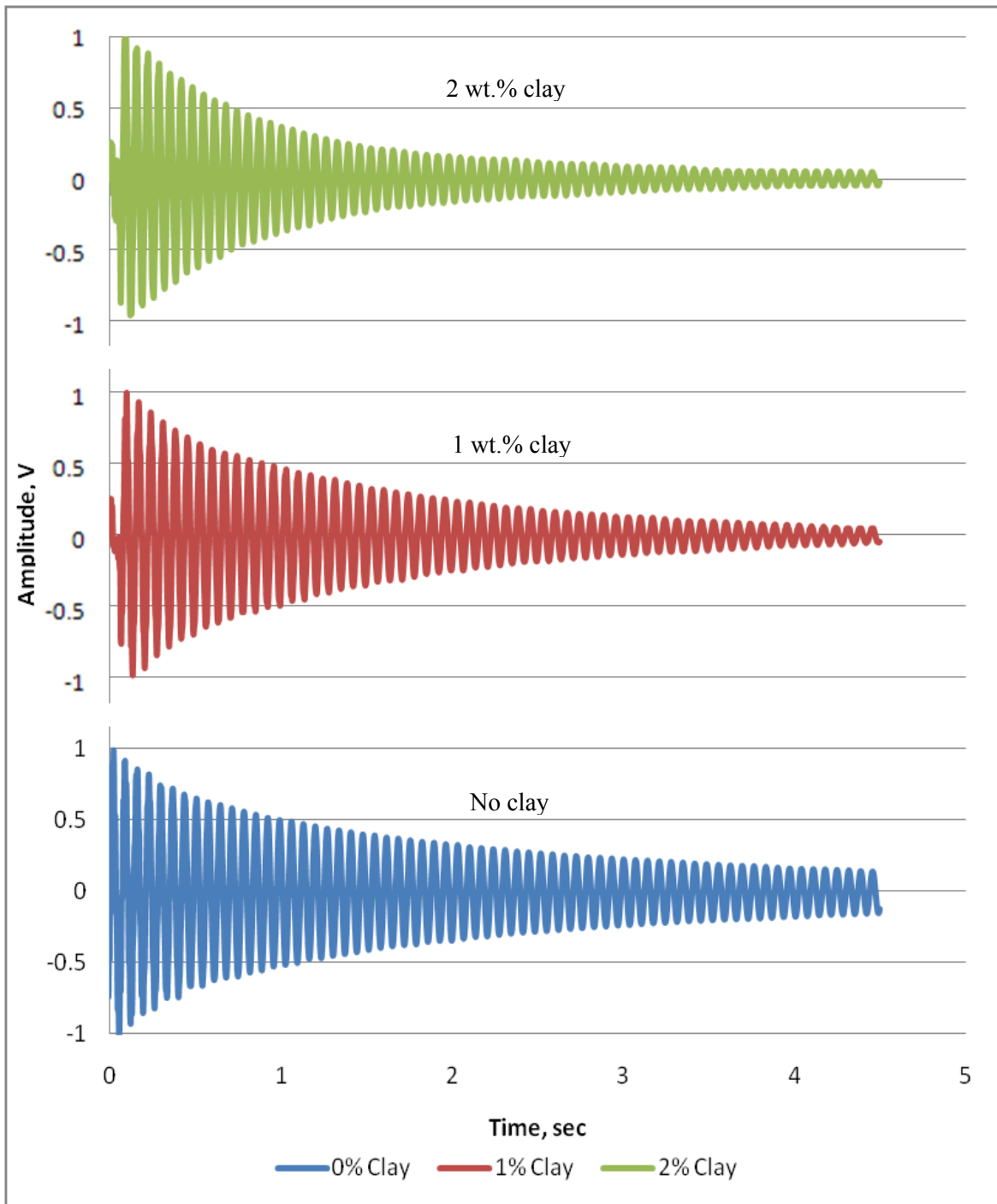


Figure 4.6 Free decay curves of cross-ply laminates with different nanoclay contents.

Table 4.6 Log decrement values and damping ratios of cross-ply laminates

Laminate	Logarithmic decrement, $\delta$	Damping ratio, $\zeta$ (eqn. 3.2)
Cross-ply (no clay)	0.036	0.00573
Cross-ply + 1 wt.% Clay	0.051	0.00812
Cross-ply + 2 wt.% Clay	0.056	0.00891

### 4.2.3 Quasi-isotropic Laminate

The log decrement curves of quasi-isotropic laminate with different nanoclay contents are shown in figure 4.7. Similar to unidirectional and cross-ply laminate, it can be observed clearly that the amplitude of the laminates with nanoclay decay faster than the laminate without nanoclay and the damping effect is higher at higher nanoclay content. After 4.5 seconds, the amplitudes of laminate with 1 wt.% and 2 wt.% nanoclay have been reduced by 32.2% and 49.1% respectively. The log decrement value and the damping ratios of laminate with different nanoclay content are given in Table 4.7 which indicates that at 1 wt.% incorporation of nanoclay can improve the damping ratio by 48.5% and at 2 wt.% nanoclay content the improvement is 57%. Because of more matrix dominated properties, the improvement in damping ratio in this case is higher than unidirectional and cross-ply laminate.

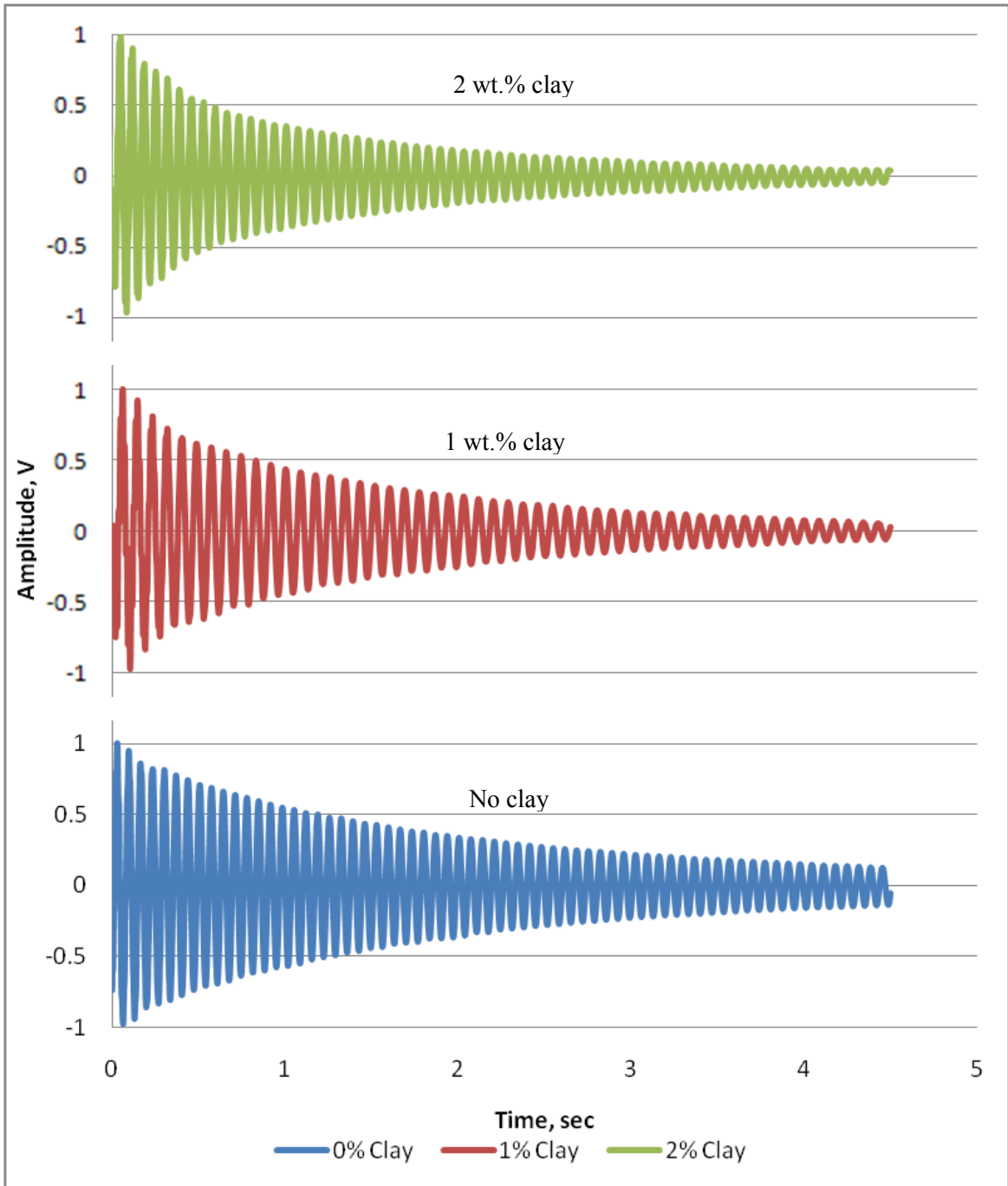


Figure 4.7 Free decay curves of quasi-isotropic laminates with different nanoclay contents.

Table 4.7 Log decrement values and damping ratios of quasi-isotropic laminates

Laminate	Logarithmic decrement, $\delta$	Damping ratio, $\zeta$ (eqn. 3.2)
Quasi-isotropic (no clay)	0.035	0.00557
Quasi-isotropic + 1 wt.% Clay	0.052	0.00827
Quasi-isotropic + 2 wt.% Clay	0.055	0.00875

### 4.3 Conclusion

The dynamic mechanical properties and free vibration test results are presented in this chapter. In the DMA analysis, it is found that nanoclay incorporation significantly improves the dynamic properties of both pristine epoxy and conventional glass/epoxy composites. The maximum improvement was observed in the glassy region around room temperature for all samples with different fiber orientation. At 1 wt.% clay content, a maximum of 12.7% improvement in storage modulus and 15.4% improvement in loss modulus was observed in the case of a unidirectional laminates. At 2 wt.% nanoclay incorporation, a maximum 16.8% improvement in storage modulus was found for unidirectional laminate and 22.5% improvement in loss modulus in the case of quasi-isotropic laminate was observed. As both storage and loss modulus were increased comparably, there was no significant improvement in tan delta values. From the DMA analysis, it was also found that nanoclay does not really affect the glass transition temperature of glass/epoxy composite laminate. The log decrement test which was carried out at higher frequency and amplitude compared to DMA analysis, indicates that

nanoclay has a very significant effect on vibration damping performance. In this free vibration test the amplitude of vibration of laminates with nanoclay decays much faster than laminates without nanoclay. But improvement in damping ratios were more significant in the case of cross-ply and quasi-isotropic laminate compared to unidirectional laminate. This could be because properties of cross-ply and quasi-isotropic laminates are less dominated by fiber (and more dominated by matrix) compared to unidirectional laminate. The maximum improvement in damping ratio for both 1 and 2 wt.% nanoclay incorporation are 48.5% and 57% respectively achieved in quasi-isotropic laminates.

# Chapter 5

## Fatigue Test Results and Fracture Behavior

### 5.1 Flexural Fatigue Test

The flexural fatigue test procedure was described in Chapter 3. Here a fixed frequency of 4 Hz was used. The amplitude of displacement was also fixed ( $\pm 6.67\text{mm}$ ) which produced a flexural stress that was much below the ultimate strength of the material. Hysteretic heating of samples was negligible, realized by physically touching the sample during the fatigue test. Thus the fracture that occurred in the laminate was due to mechanical fatigue rather than thermal failure. If there is any damage (crack or delamination) within the laminate due to fatigue, the stiffness will reduce and the maximum strain will increase. The number of fatigue cycles to induce strain value changes may be considered as a measure of flexural fatigue life. For repeatability of results, at least 3 samples of both cross-ply and quasi-isotropic laminate were tested. Table 5.1 represents the sample configurations for the fatigue test, where A, B and C indicates the percentage of nanoclay loading and 1, 2 and 3 indicates the number of samples manufactured in each different batches. To validate these results, log decrement tests were carried out after every 100,000 fatigue cycles and fatigue damage indexes were measured after 200,000 and 300,000 fatigue cycles. Flexural fatigue test results are described in the following sub-sections.

Table 5.1 Sample configurations for fatigue test

Sample		Description
A	1	No clay, Sample # 1
	2	No clay, Sample # 2
	3	No clay, Sample # 3
B	1	1 wt.% clay, Sample # 1
	2	1 wt.% clay, Sample # 2
	3	1 wt.% clay, Sample # 3
C	1	2 wt.% clay, Sample # 1
	2	2 wt.% clay, Sample # 2
	3	2 wt.% clay, Sample # 3

### 5.1.1 Cross-ply Laminate

Strain versus number of cycles curves of cross-ply laminate obtained from the flexural fatigue test are given in figures 5.1 to 5.3. Figure 5.1 represents the result of three different samples with the same nanoclay loading. On the other hand, figure 5.2 represent the results all type of samples (with different nanoclay loading) manufactured in the same batch that indicates the effect of clay contents on fatigue life. Figure 5.3 shows the average results with scatter in the strain values. Test results indicate that the maximum strain values remain the same up to certain fatigue cycles. Then there is a sudden increase in the strain values. As fatigue damage starts accumulating within the laminate, it loses its stiffness and the laminate tends to bend more. Thus the jump in maximum strain is observed. The number of fatigue cycles at which this change in strain value occurs, can be considered as a measure of the flexural fatigue life. The results clearly indicate that the presence of nanoclay significantly improves fatigue life of glass/epoxy laminate for all three samples. The maximum strain value of glass/epoxy laminate without nanoclay is quite consistent up to an average of 100,000 fatigue cycles. Then the strain increases rapidly. That means fatigue damage starts accumulating within the laminates after

approximately 100,000 fatigue cycles. On the other hand, the strain value starts changing after an average of 166,000 fatigue cycles for laminates with 1 wt.% nanoclay and the rate of increase in the strain value is slower compared to the laminate without nanoclay because of improved fatigue resistance. The laminates with 1 wt.% nanoclay have 66% improved flexural fatigue life. For the laminate with 2 wt.% nanoclay, a slight change in the strain value is observed after an average of 233,000 fatigue cycles.

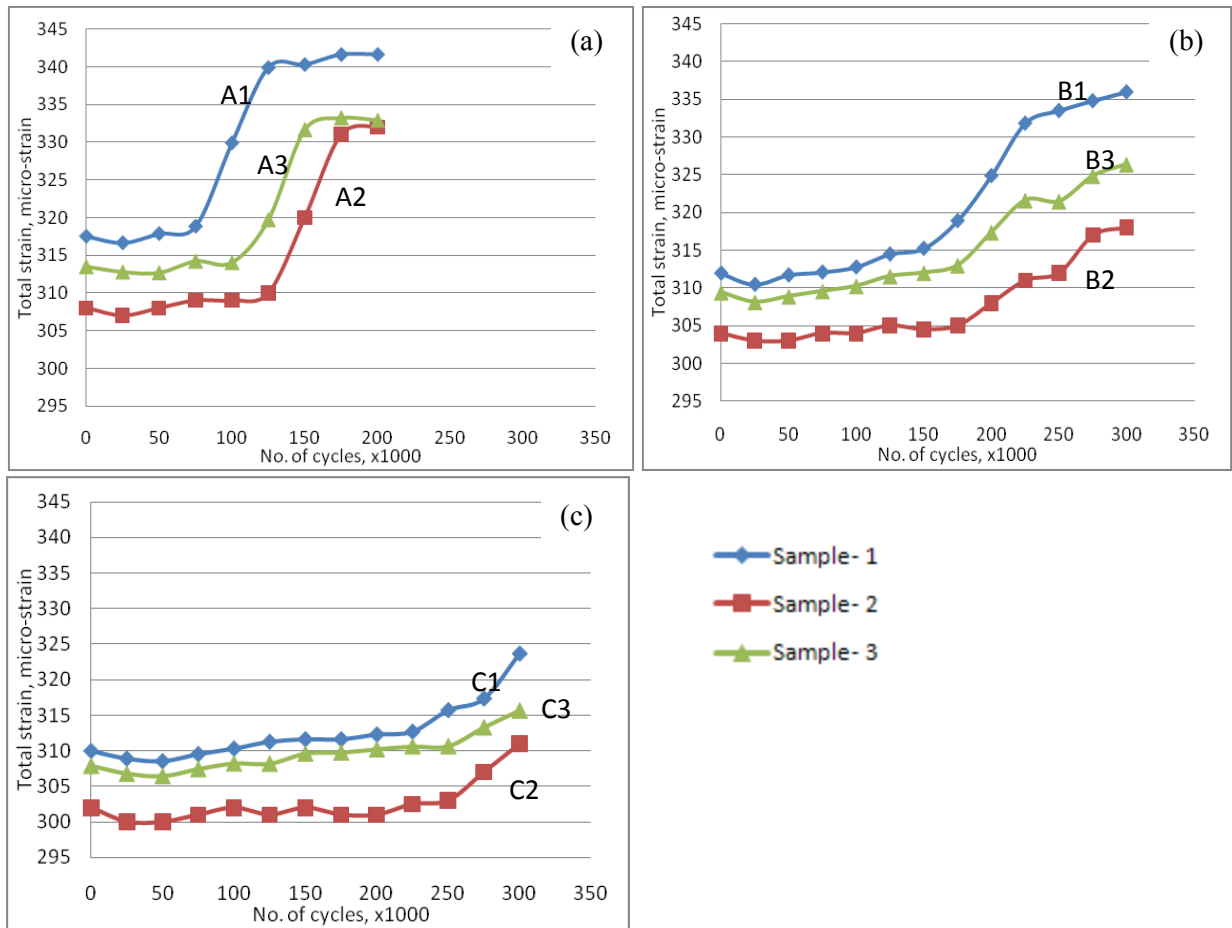


Figure 5.1 Flexural fatigue test results of cross-ply laminates: (a) no clay, (b) 1 wt.% nanoclay and (c) 2 wt.% nanoclay.

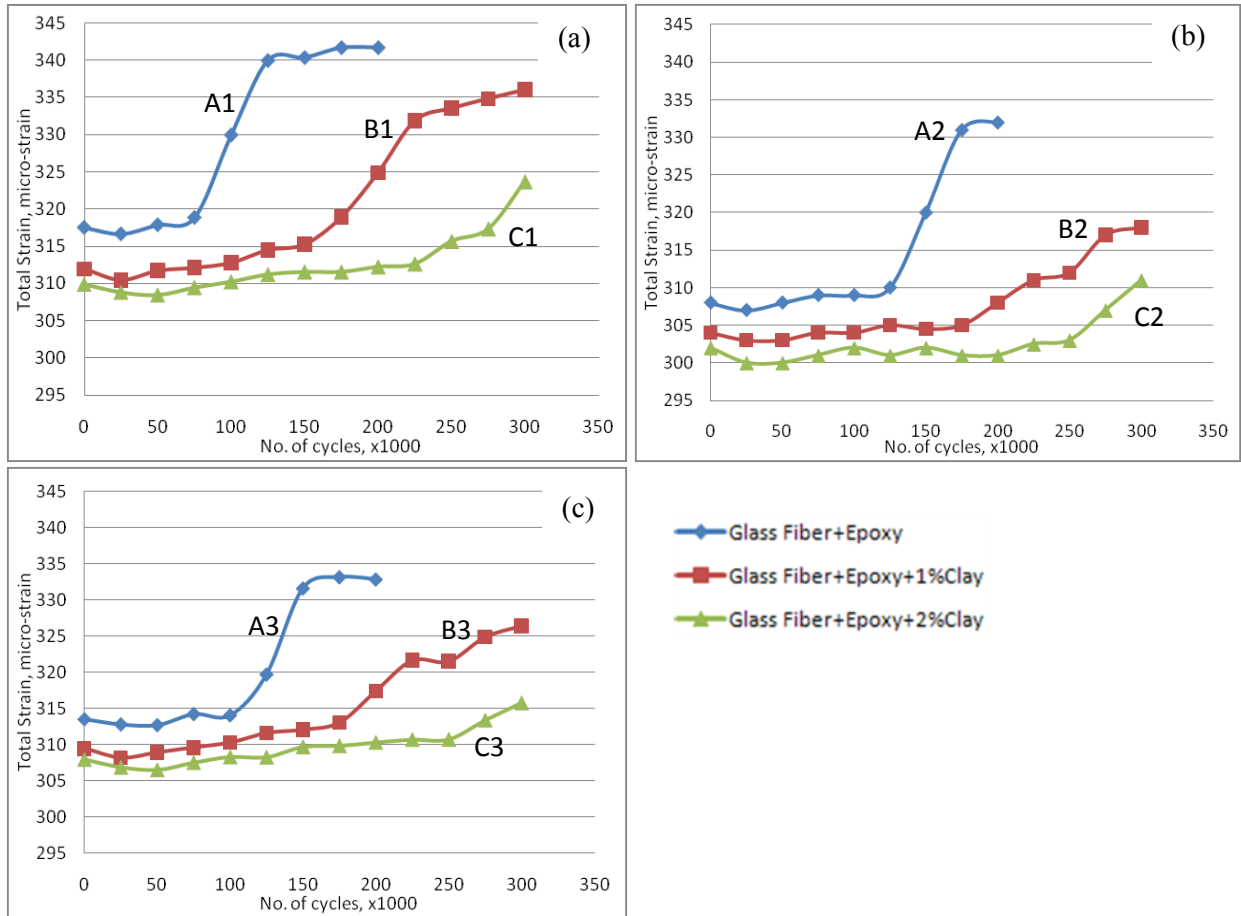
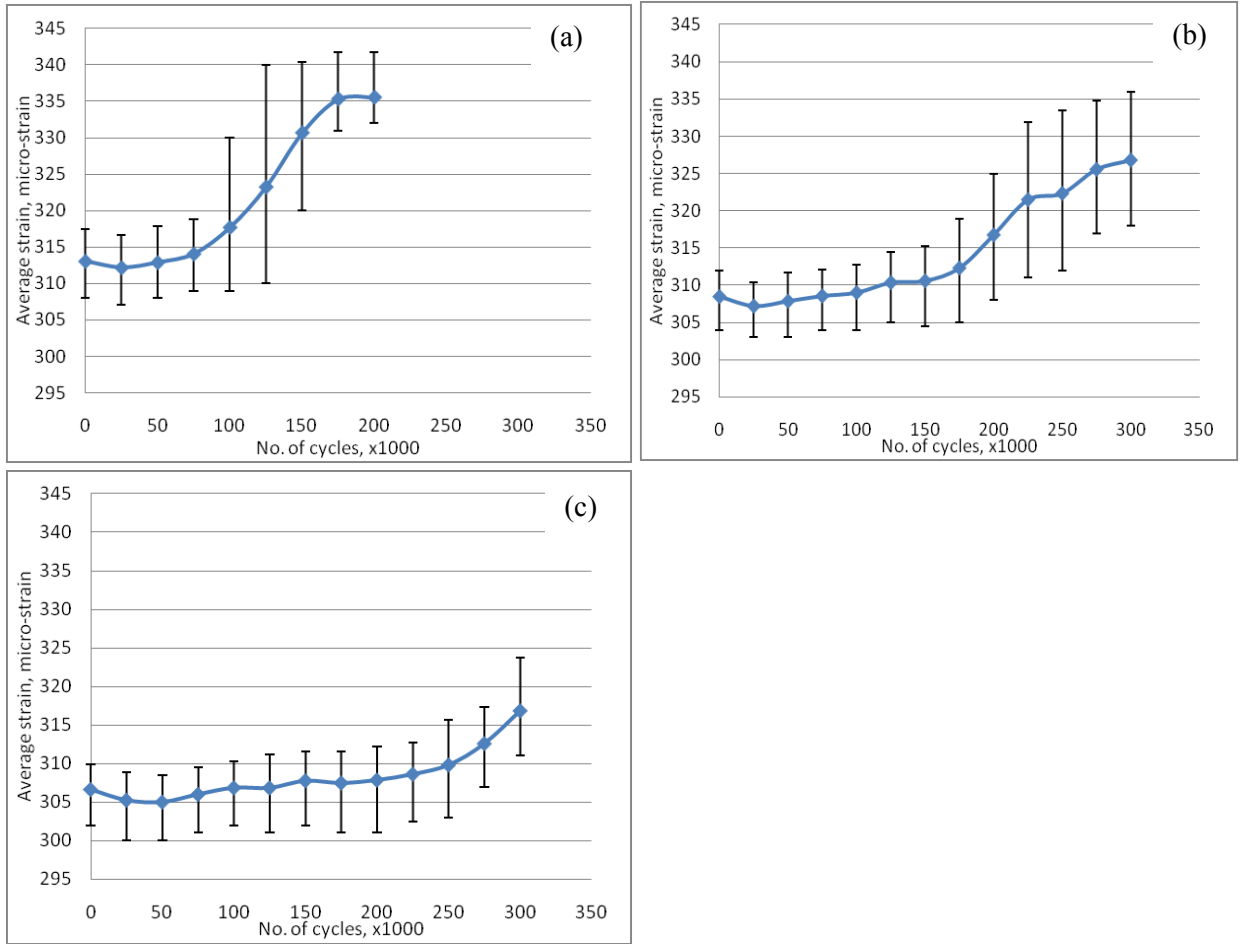


Figure 5.2 Flexural fatigue test results of cross-ply laminates: (a) Sample set# 1, (b) Sample set# 2 and (c) Sample set# 3.

At 2 wt.% incorporation of nanoclay, the flexural fatigue life of cross-ply laminates was increased by 133% compared to conventional glass/epoxy composites. Figure 5.3 shows the average strain values of the three samples with scatter. The scatter is more in the area where the strain values start increasing. This is possibly due to the uncontrolled nature of failure in composite materials. But all the curves have similar trend.



*Figure 5.3 Average test results of three cross-ply laminates with scatter in strain values: (a) no clay, (b) 1 wt.% nanoclay and (c) 2 wt.% nanoclay.*

The increase in the strain value occurred due to the accumulation of micro-cracks and delaminations inside the laminate. Figure 5.4a to 5.4c shows the optical microscopic image of the cross section the cross-ply laminate with different nanoclay contents after 200,000 fatigue cycles. After 200,000 fatigue cycles, the laminate without nanoclay has

the height concentration of cracks (shown by thin arrow) and delaminations (shown by thick arrow) within 3<sup>rd</sup> and 4<sup>th</sup> layer (transversely oriented fiber), those are clearly observable in figure 5.4a. The laminate with 1 wt.% nanoclay also has micro-cracks concentration within the same plane shown in figure 5.4b but the extent of damage is less than the laminate without nanoclay. Whereas the laminate with 2 wt.% nanoclay has very few cracks as shown in figure 5.4c.

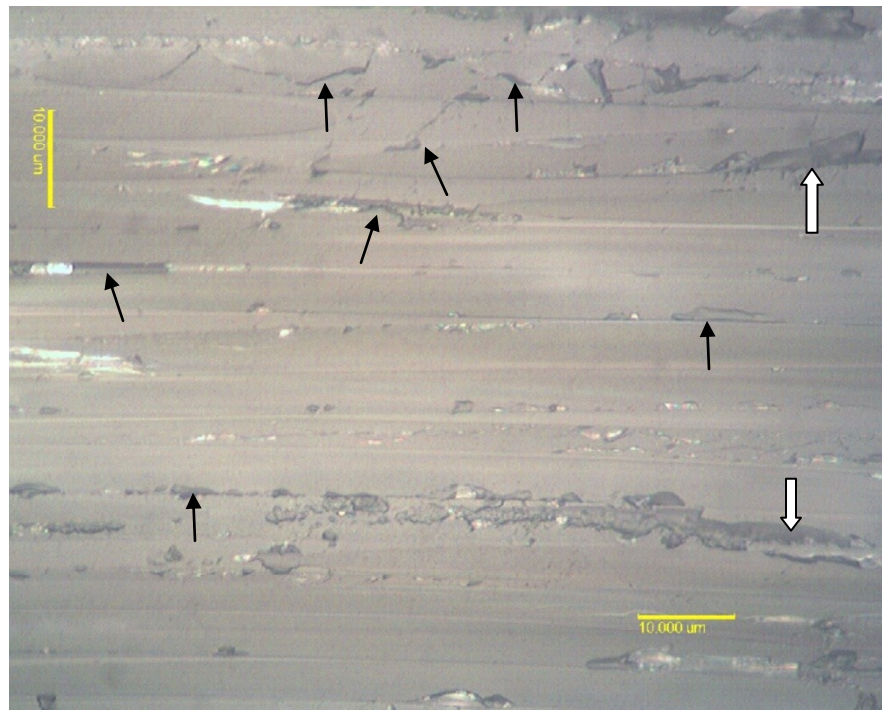


*Figure 5.4a Optical micro-graph of the cross section of cross-ply laminate without nanoclay after 200,000 fatigue cycles.*



*Figure 5.4b Optical micro-graph of the cross section of cross-ply laminate with 1 wt.% nanoclay after 200,000 fatigue cycles.*

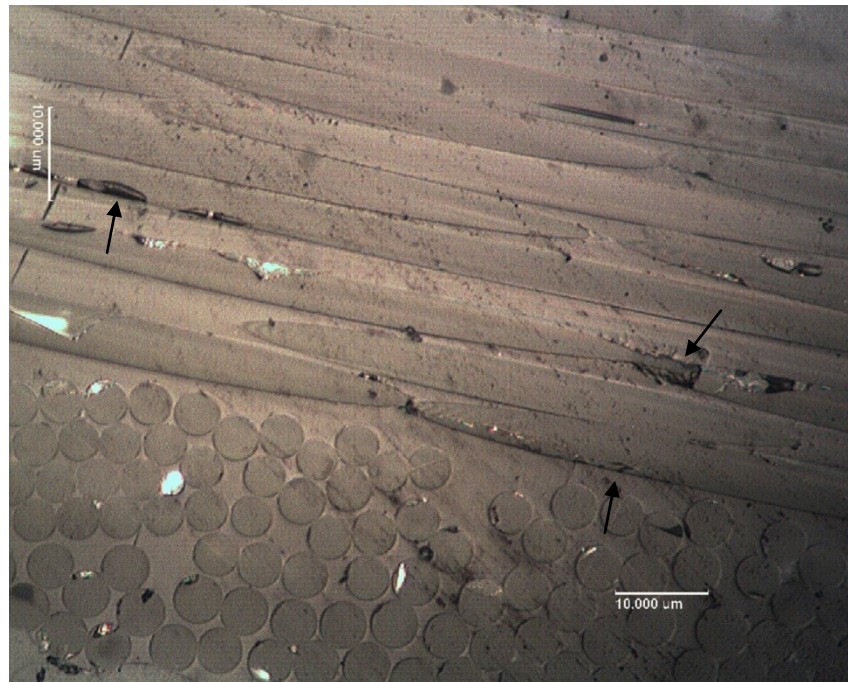


*Figure 5.4c Optical micro-graph of the cross section of cross-ply laminate with 2 wt.% nanoclay after 200,000 fatigue cycles.*

The concentration of micro-cracks lead to delaminations, thus the laminate loses its stiffness and its energy dissipation ability increases. In such condition, the amplitude of free vibration will decay much faster than non-fatigued samples. Log decrement tests were carried out after different fatigue cycles to validate the flexural fatigue test for the first sample. The free decay curves after every 100,000 fatigue cycles are presented in figure 5.5 (a, b and c) for cross-ply laminates with different nanoclay loadings and the log decrement values are presented in table 5.2. The free decay curve of laminate without clay shown in figure 5.5a indicates that the decay rate of amplitude sharply increased after 100,000 fatigue cycles because fatigue damage (micro-cracks and delaminations) already took place inside the laminate. Flexural fatigue test result of cross-ply laminate (figure 5.1a) also indicates that fatigue damage starts occurring within the laminate after 75,000 fatigue cycles. Figure 5.5b represents the free decay curve of cross-ply laminate with 1 wt.% nanoclay. Here the decay rate of amplitude is almost consistent up to 100,000 cycles but after 200,000 cycles of fatigue the amplitude decays very fast. Micro-cracks and subsequent delaminations have taken place within 100,000 to 200,000 fatigue cycles. The flexural fatigue test of cross-ply laminate with 1 wt.% nanoclay (figure 5.1b) also confirms this result. Free decay curves for cross-ply laminate with 2 wt.% nanoclay shown in figure 5.5c indicates that there is very insignificant change in the decay rate after 300,000 fatigue cycles. The flexural fatigue test shown in figure 5.1c also indicates similar trend but after 275,000 cycles there were a slight increase in the strain values.

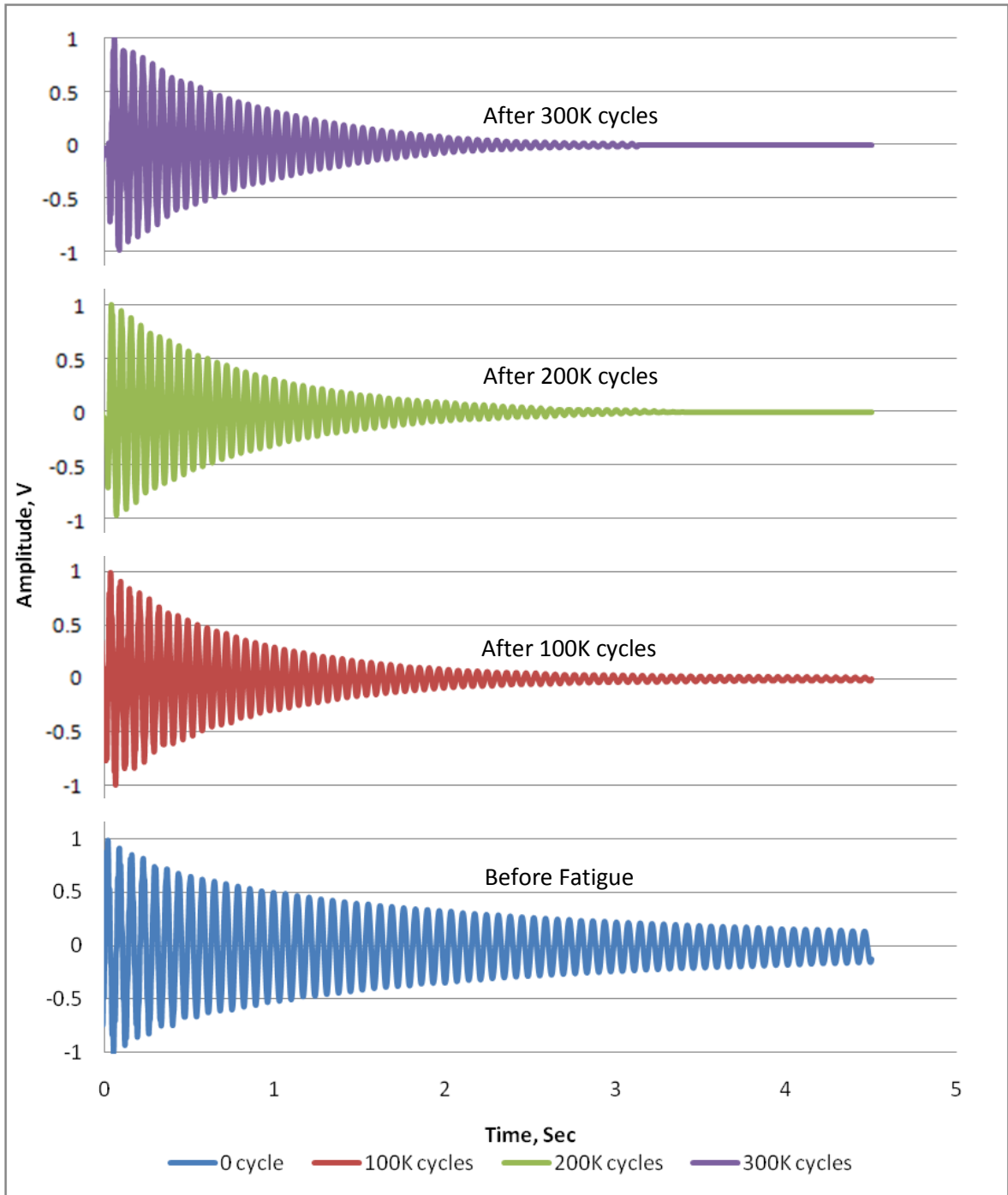


*Figure 5.5a Free decay curves for cross-ply laminate without nanoclay after different fatigue cycles.*

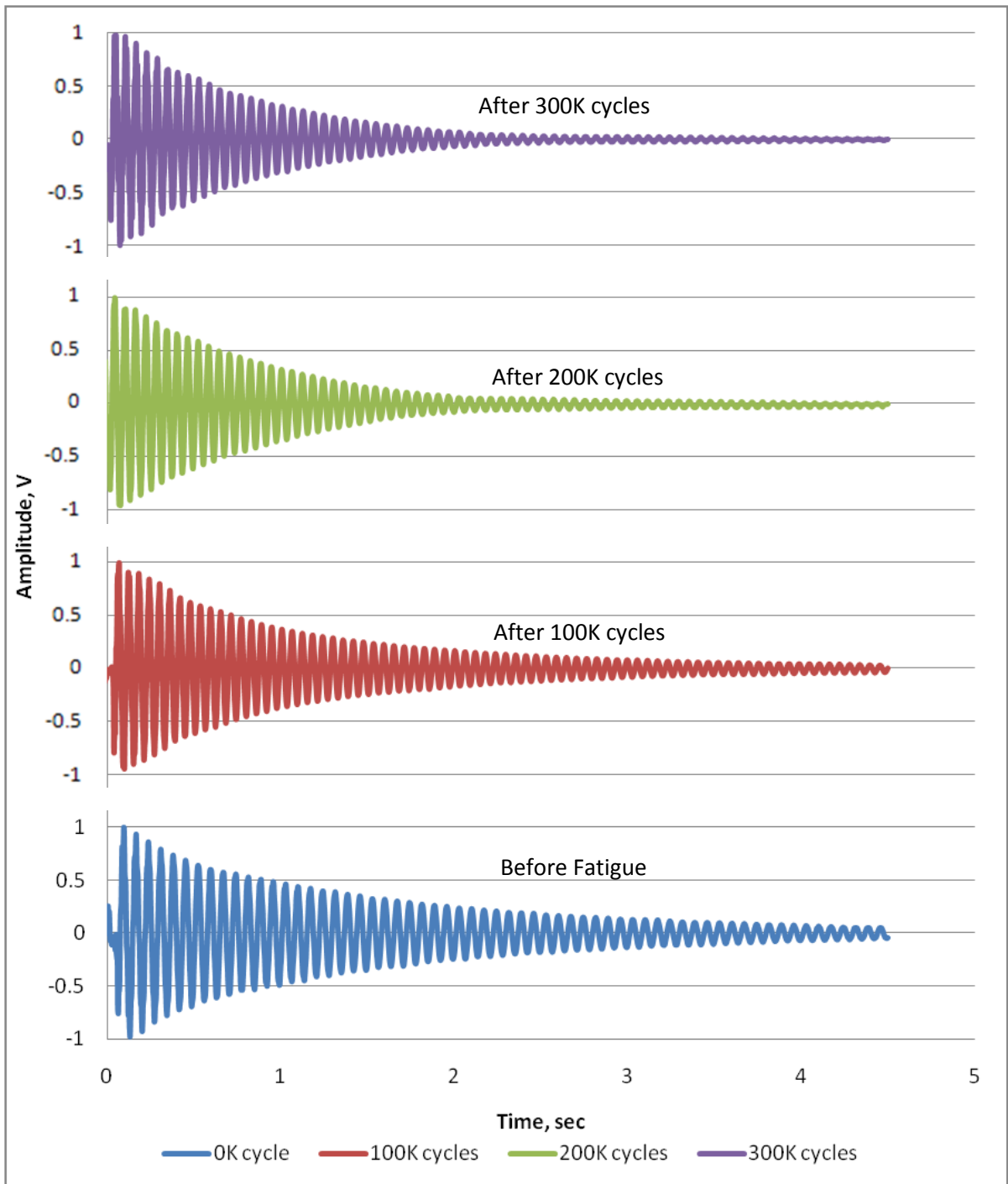


*Figure 5.5b Free decay curves for cross-ply laminate with 1 wt.% nanoclay after different fatigue cycles.*

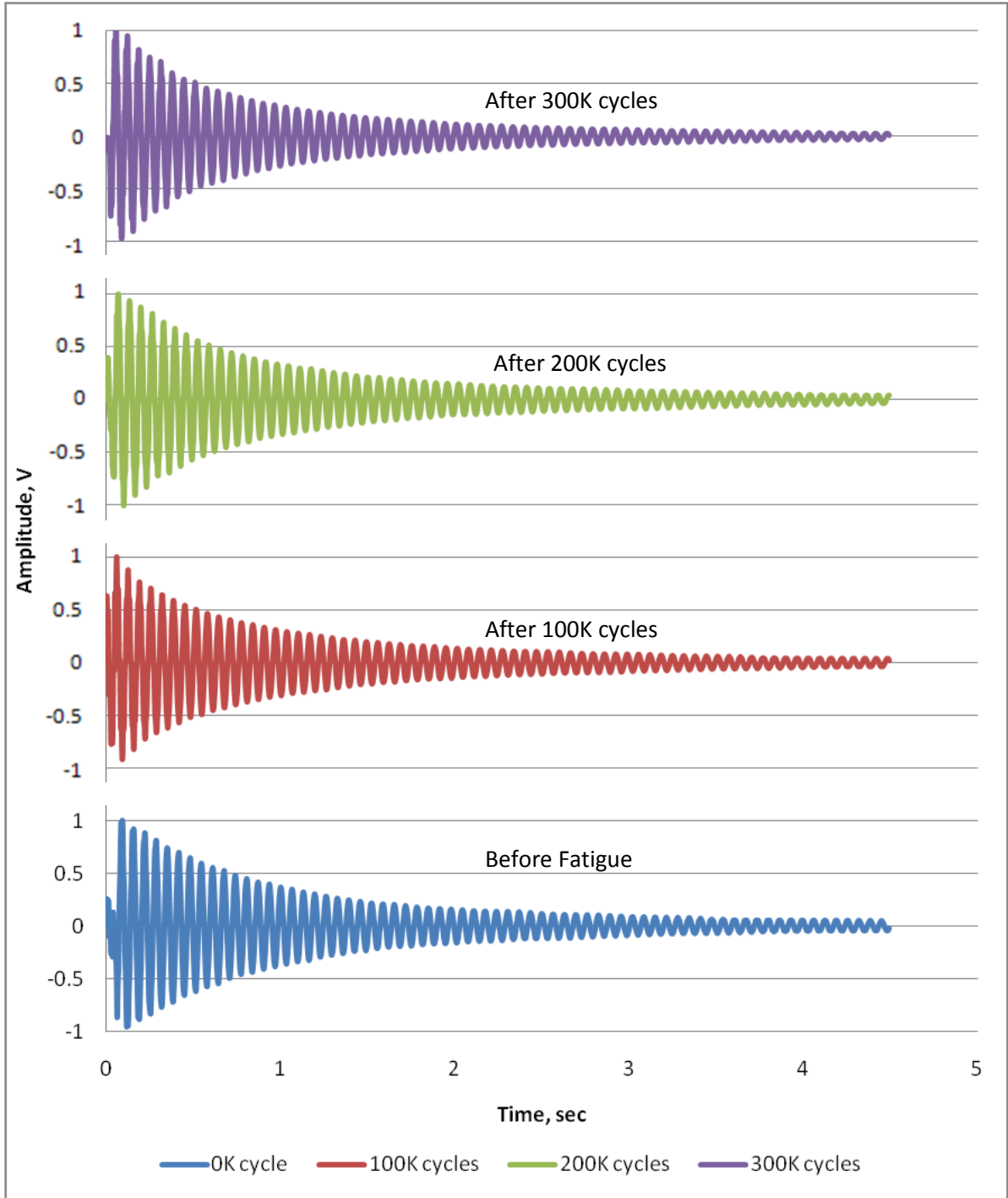


Figure 5.5c Free decay curves for cross-ply laminate with 2 wt.% nanoclay after different fatigue cycles.

Table 5.2 Log decrement values of cross-ply laminate after different fatigue cycles

Cross-ply Laminate	Logarithmic decrement, $\delta$			
	0 cycle	100,000 cycles	200,000 cycles	300,000 cycles
No clay	0.036	0.071	0.076	0.083
1 wt.% clay	0.051	0.056	0.073	0.076
2 wt.% clay	0.056	0.059	0.062	0.069

Table 5.3 Storage modulus and Fatigue damage index of cross-ply laminate after different fatigue cycles

Cross-ply Laminate	Storage Modulus, GPa			Fatigue Damage Index	
	0 cycle	200,000 cycles	300,000 cycles	200,000 cycles	300,000 cycles
No clay	22.7	13.4	7.7	0.41	0.66
1 wt.% clay	24.8	21.5	12.7	0.13	0.49
2 wt.% clay	25.2	23.4	17.6	0.07	0.30

To quantify the extent of damage within the laminates, flexural storage moduli of the laminates were measured after 200,000 and 300,000 fatigue cycles and using formula 3.3 the fatigue damage index were calculated. Table 5.3 shows the storage modulus and fatigue damage index of cross-ply laminates after 200,000 and 300,000 fatigue cycles with different nanoclay contents. Here, it can be seen that the storage modulus of the laminate without nanoclay is reduced significantly with a high damage index of 0.41 after 200,000 fatigue cycles where as samples with 1 and 2 wt.% nanoclay retains their stiffness with low damage indexes of 0.13 and 0.07 respectively. After 300,000 fatigue cycles, stiffness of laminate with 1 wt.% nanoclay falls but laminate with 2 wt.% nanoclay still maintain some stiffness with a low damage index of 0.30. This also agrees with the result from flexural fatigue test.

### 5.1.2 Quasi-isotropic Laminate

Figure 5.6 to 5.8 represents the strain versus number of cycles curves of quasi-isotropic laminates obtained from flexural fatigue tests. Like cross-ply samples, the results indicate that the presence of nanoclay significantly improves fatigue life of quasi-isotropic glass/epoxy laminate for all three samples. The maximum strain value of glass/epoxy laminate without nanoclay is quite consistent up to an average of 108,000 fatigue cycles. Then the strain increases rapidly.

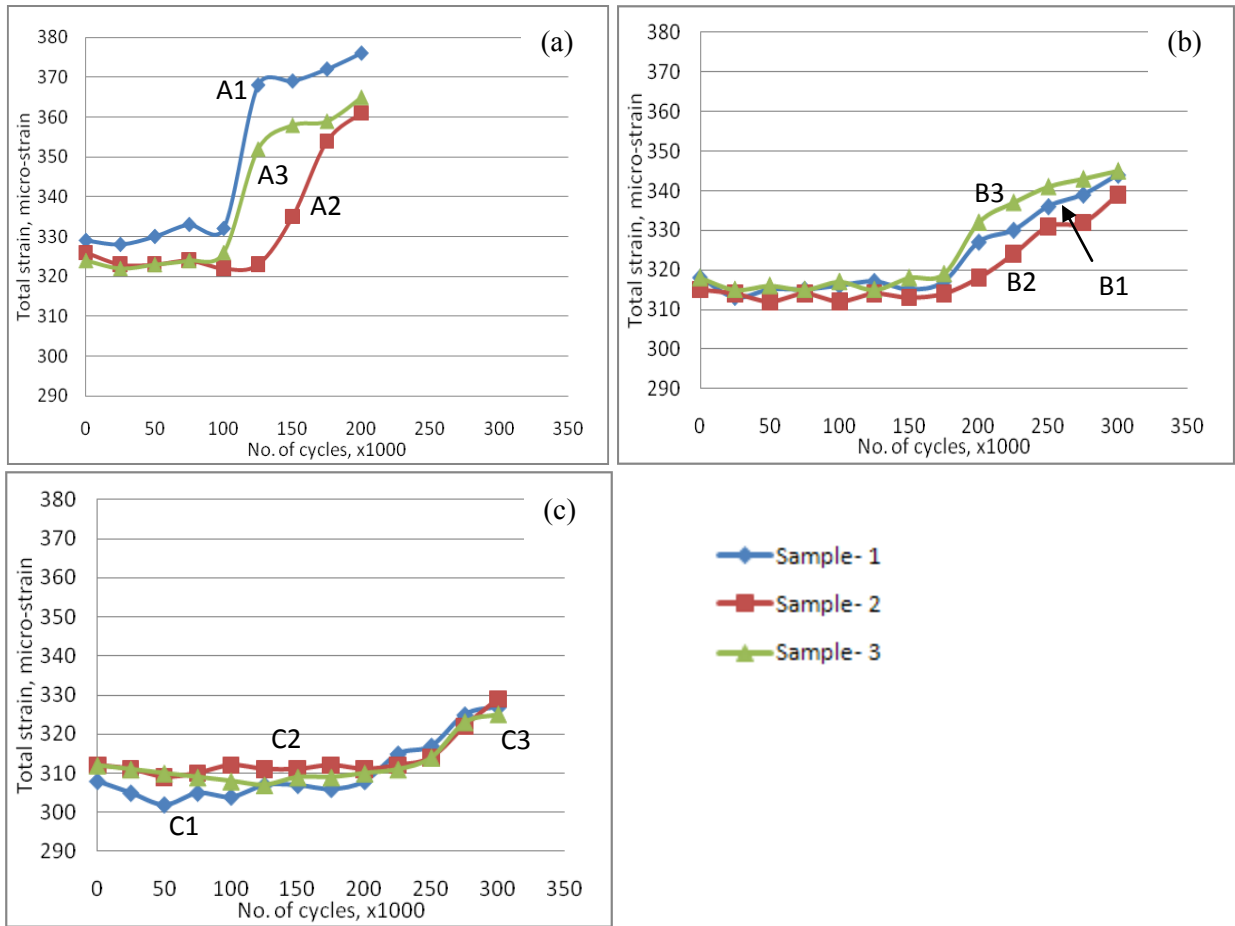


Figure 5.6 Flexural fatigue test results of quasi-isotropic laminates: (a) no clay, (b) 1 wt.% nanoclay and (c) 2 wt.% nanoclay.

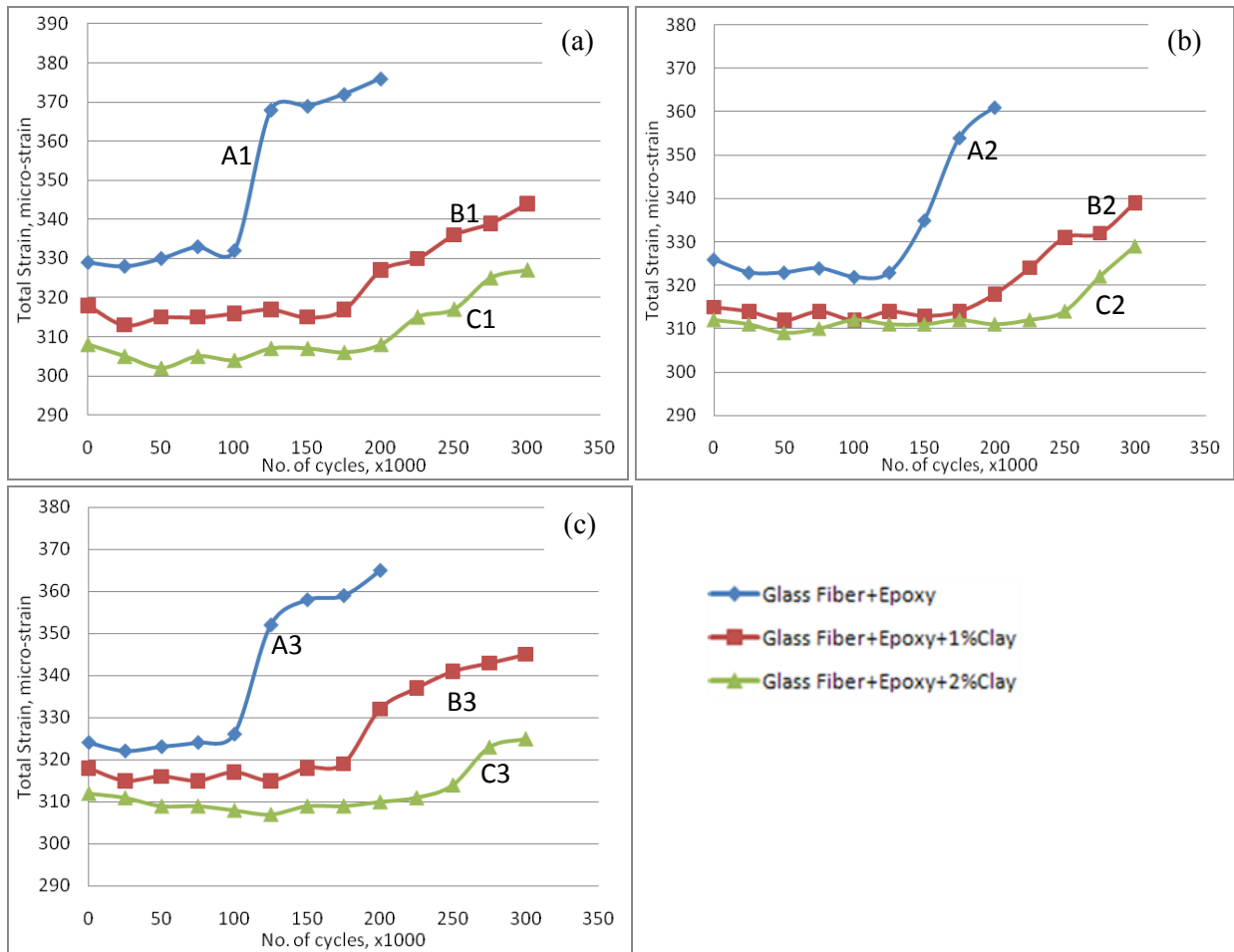


Figure 5.7 Flexural fatigue test results of quasi-isotropic laminates: (a) Sample set# 1, (b) Sample set# 2 and (c) Sample set# 3.

The increase in the strain value indicates that fatigue damage starts accumulating within the laminates after approximately 108,000 fatigue cycles. The optical micro-graph in figure 5.9a shows the concentration of micro-cracks (thin arrow) and delaminations (thick arrow) within the 2<sup>nd</sup> and 3<sup>rd</sup> layer of quasi-isotropic laminate after 200,000 fatigue

cycles. On the other hand, the strain value starts changing after an average of 175,000 fatigue cycles for laminates with 1 wt.%

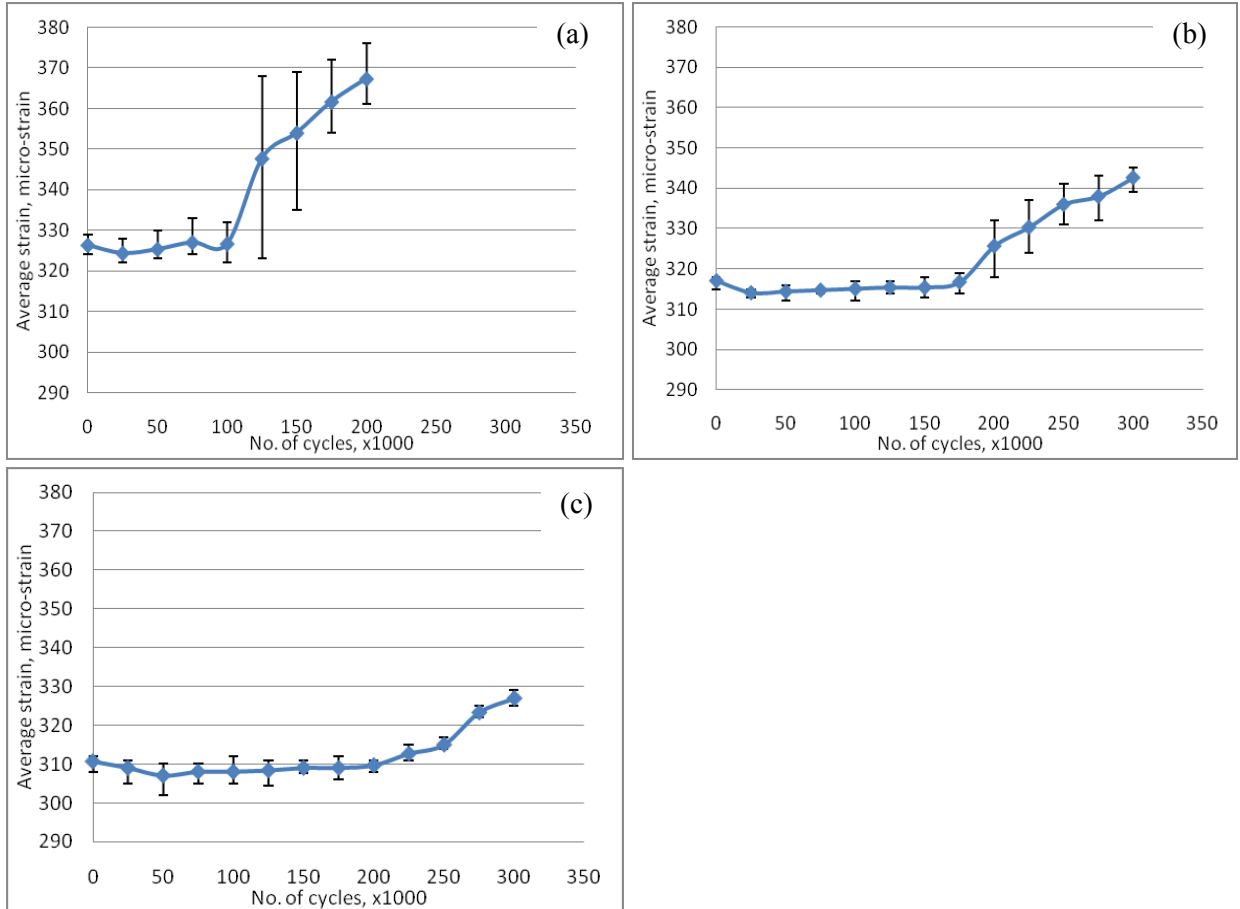
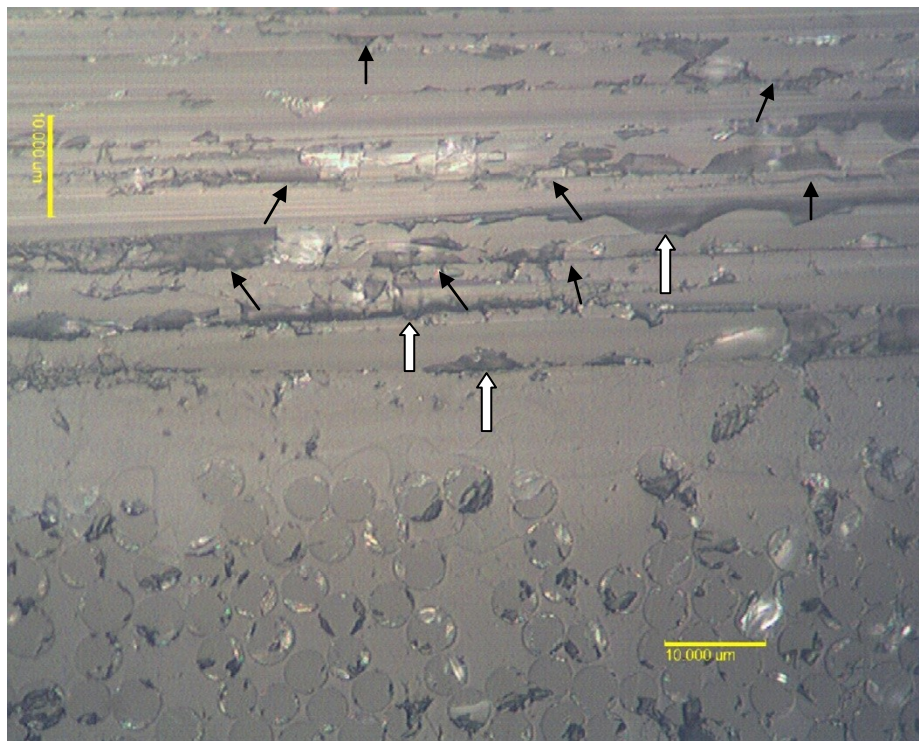


Figure 5.8 Average test results of three quasi-isotropic laminates with scatter in strain values: (a) no clay, (b) 1 wt.% nanoclay and (c) 2 wt.% nanoclay.

nanoclay and the rate of increase in the strain value is slower compared to the laminate without nanoclay. The amount of fatigue damage is also less compared to laminate

without nanoclay as shown in figure 5.9b. The laminates with 1 wt.% nanoclay have 62% improved flexural fatigue life. For the laminate with 2 wt.% nanoclay, a slight change in the strain value is observed after an average of 225,000 fatigue cycles. At 2 wt.% incorporation of nanoclay, the flexural fatigue life of quasi-isotropic laminates were increased by 108% compared to conventional glass/epoxy composites. Fatigue damage is very less for the case of laminate with 2 wt.% nanoclay content shown in figure 5.9c.



*Figure 5.9a Optical micro-graph of the cross section of quasi-isotropic laminate without nanoclay after 200,000 fatigue cycles.*

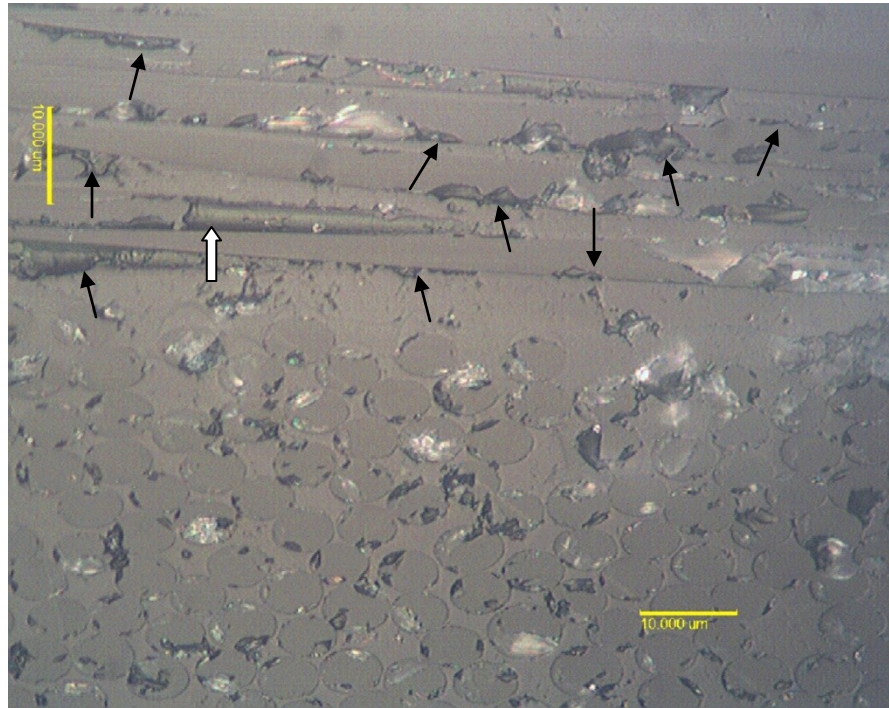


*Figure 5.9b Optical micro-graph of the cross section of quasi-isotropic laminate with 1 wt.% nanoclay after 200,000 fatigue cycles.*

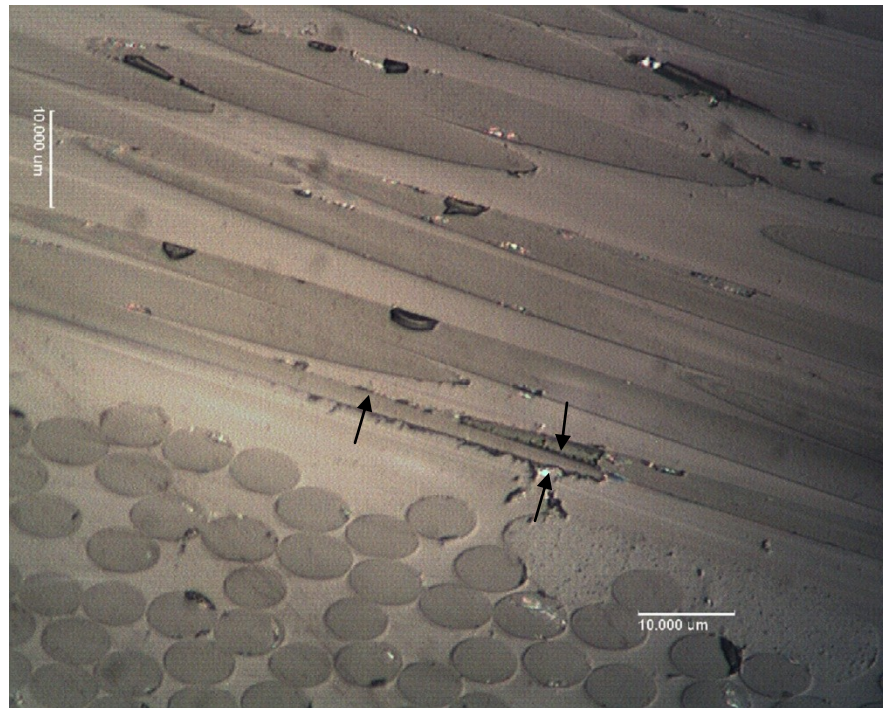


*Figure 5.9c Optical micro-graph of the cross section of quasi-isotropic laminate with 2 wt.% nanoclay after 200,000 fatigue cycles.*

The free decay curves after every 100,000 fatigue cycles are presented in figure 5.10 (a, b and c) for quasi-isotropic laminates with different nanoclay loading and the log decrement values are presented in table 5.4. The free decay curve of laminate without clay shown in figure 5.10a that indicates the decay rate of amplitude sharply increased after 100,000 fatigue cycles, because fatigue damage (micro-cracks and delaminations) have already taken place inside the laminate. The flexural fatigue test results of the quasi-isotropic laminate (figure 5.6a) also indicate that fatigue damage starts occurring within the laminate after 100,000 cycles of fatigue loading. Figure 5.10b represents the free decay curve of the quasi-isotropic laminate with 1 wt.% nanoclay. Here the decay rate of amplitude is almost consistent up to 100,000 cycles but after 200,000 cycles of fatigue the amplitude decays very fast. Micro-cracks and subsequent delaminations may have taken place within 100,000 to 200,000 fatigue cycles. The flexural fatigue test of quasi-isotropic laminate with 1 wt.% nanoclay (figure 5.6b) also agrees with this result. Free decay curves for quasi-isotropic laminate with 2 wt.% nanoclay shown in figure 5.10c indicate that the decay rate slightly increases after 200,000 fatigue cycles. The flexural fatigue test with 2 wt.% nanoclay shown in figure 5.6c also indicates that after 200,000 cycles there was some increase in the strain values.

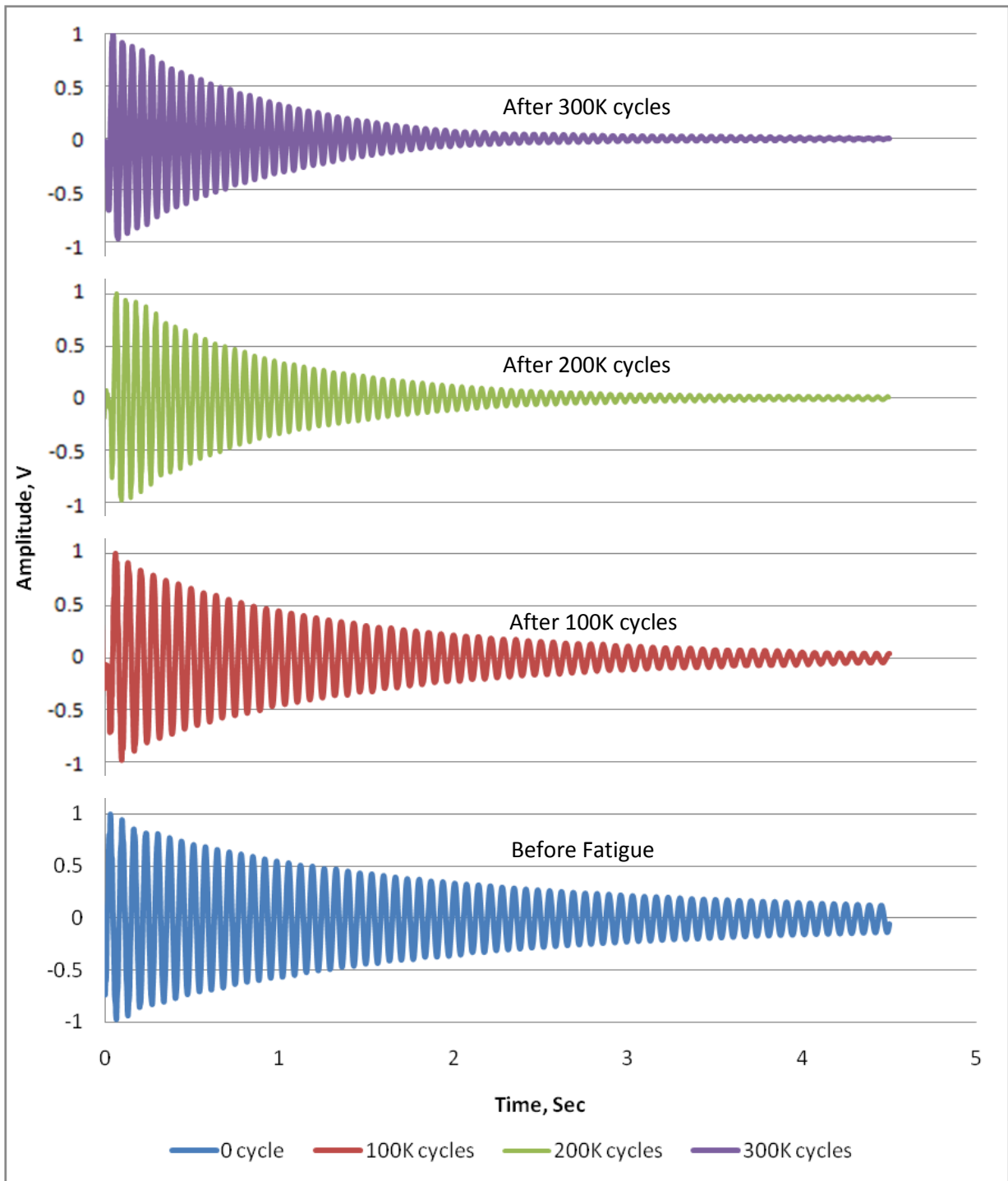


Figure 5.10a Free decay curves for quasi-isotropic laminate without nanoclay after different fatigue cycles.

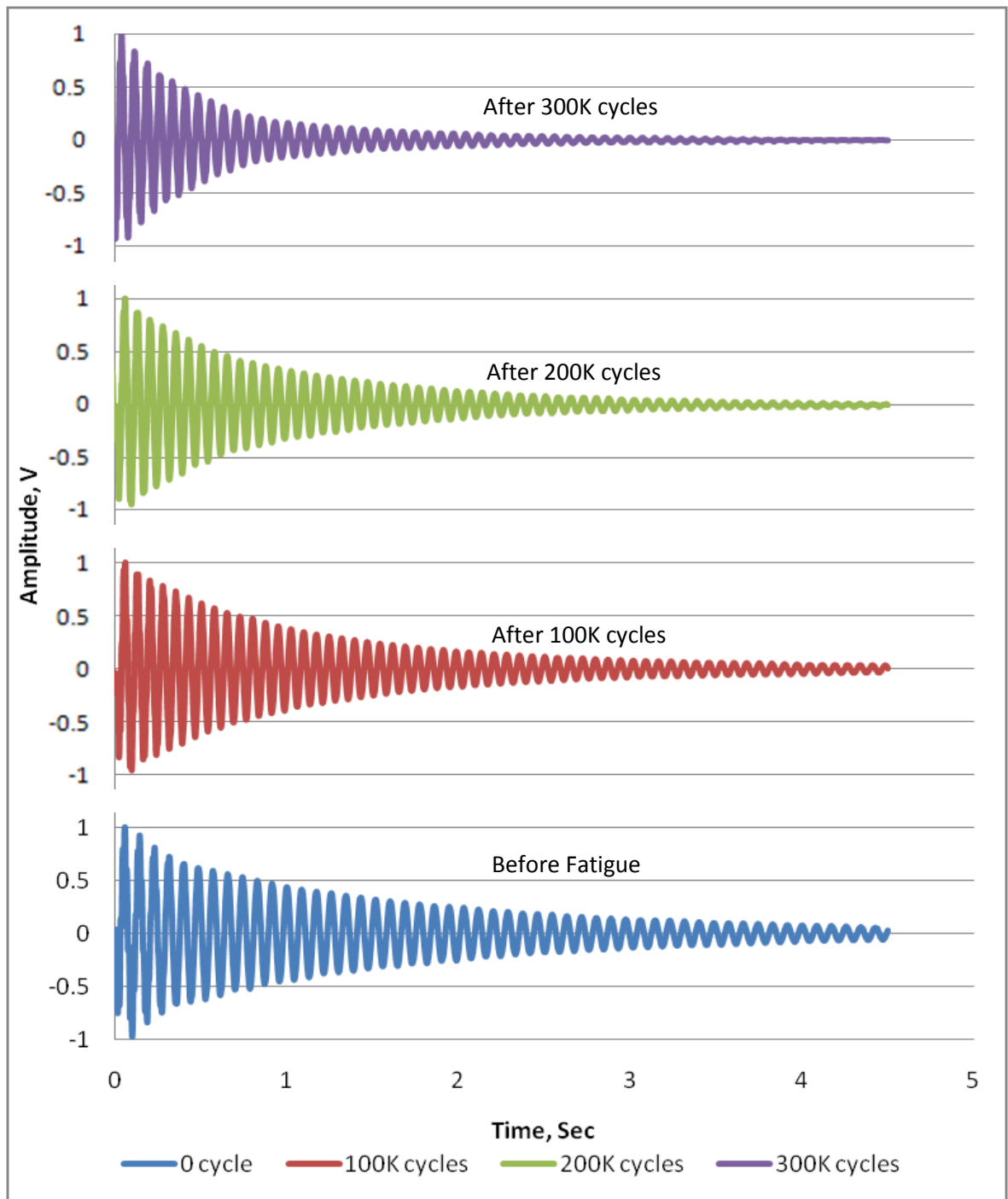


Figure 5.10b Free decay curves for quasi-isotropic laminate with 1 wt.% nanoclay after different fatigue cycles.

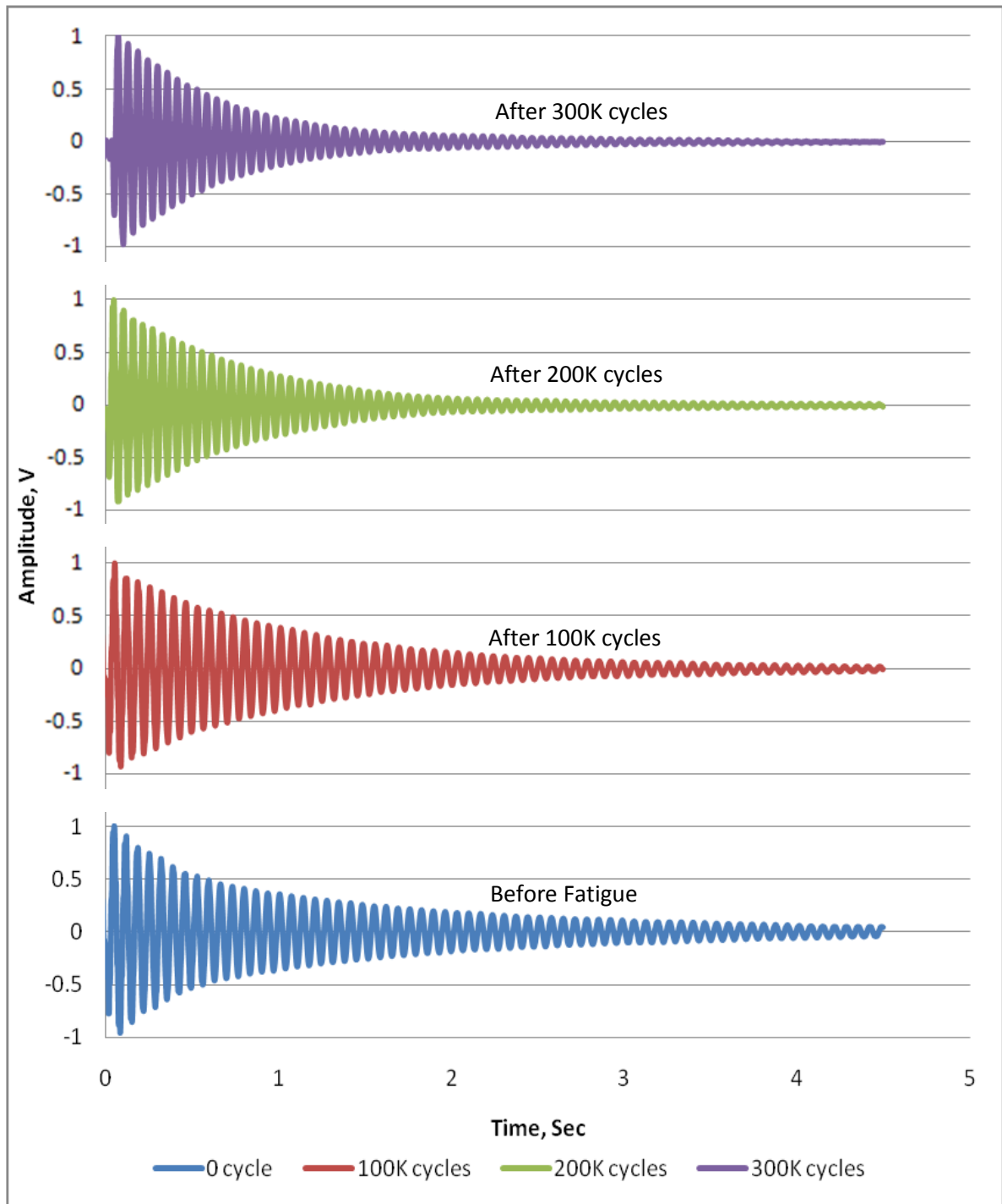


Figure 5.10c Free decay curves for quasi-isotropic laminate with 2 wt.% nanoclay after different fatigue cycles.

Table 5.4 Log decrement values of quasi-isotropic laminate after different fatigue cycles

Quasi-isotropic Laminate	Logarithmic decrement, $\delta$			
	0 cycle	100,000 cycles	200,000 cycles	300,000 cycles
No clay	0.035	0.047	0.068	0.073
1 wt.% clay	0.052	0.057	0.069	0.086
2 wt.% clay	0.055	0.058	0.068	0.077

Table 5.5 Storage modulus and Fatigue damage index of quasi-isotropic laminate after different fatigue cycles

Quasi-isotropic Laminate	Storage Modulus, GPa			Fatigue Damage Index	
	0 cycle	200,000 cycles	300,000 cycles	200,000 cycles	300,000 cycles
No clay	18.2	9.8	7.3	0.46	0.59
1 wt.% clay	20.1	17.9	11.9	0.11	0.41
2 wt.% clay	21.5	19.7	15.7	0.08	0.27

Table 5.5 shows the storage modulus and fatigue damage index of quasi-isotropic laminates after 200,000 and 300,000 fatigue cycles with different nanoclay content. Similar to cross-ply laminate, the storage modulus of laminate without nanoclay is reduced to almost half with a remarkably high damage index 0.46 after 200,000 fatigue cycles where as samples with 1 and 2 wt.% nanoclay retains their stiffness sufficiently. After 200,000 fatigue cycles laminates with 1 and 2 wt.% nanoclay have damage index of 0.11 and 0.08 respectively. After 300,000 fatigue cycles, the stiffness of the laminate with 1 wt.% nanoclay falls but the laminate with 2 wt.% nanoclay still maintain some stiffness (15.7 GPa) with 0.27 damage index. This agrees quite well with flexural fatigue test results.

## 5.2 Fracture Behavior

To characterize the fatigue damage within the laminates, scanning electron microscopic (SEM) images of the cross sections at different locations of the cross-ply laminates were analyzed after 300,000 fatigue cycles. For the scanning electron microscopy, the fatigued laminates were cut using a high speed diamond cutter and the cross sections were polished to remove any cracks if induced during cutting with diamond cutter. As nanoclay/glass/epoxy samples are entirely non-conductive, a conductive coating of Au-Pd was done using a sputtering machine in an inert environment for 3 minutes. SEM images of the cross-section of laminate were taken at three different locations; (i) Location A (within 1 cm from fixed end), (ii) Location B (3 cm from the fixed end) and (iii) Location C (6 cm from the fixed end) as shown in figure 5.11.

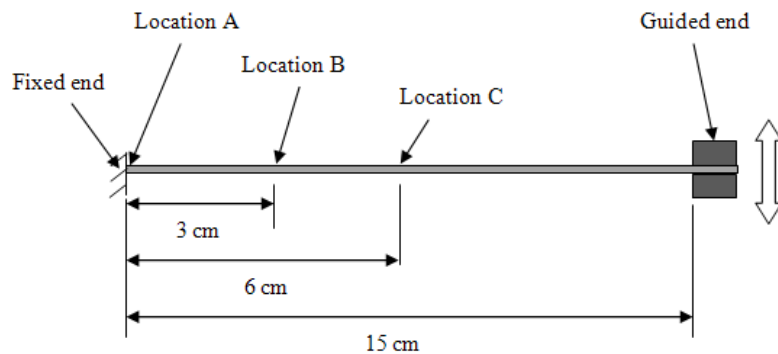


*Figure 5.11 schematic illustration of the location of the beam cross-section for SEM.*

### 5.2.1 Location A

Figure 5.12 represents the SEM images of cross-section within 1 cm of fixed end of cross-ply laminates with different nanoclay contents after 300,000 fatigue cycles. This is the area where maximum bending moment is applied. Figure 5.12a shows the SEM images of fatigued laminate without nanoclay where it can be seen that there is a big

delamination throughout the image (shown by thick white arrow) taken place within 3<sup>rd</sup> and 4<sup>th</sup> layers (90° layers) along with some micro-cracks (shown by thin black arrow)

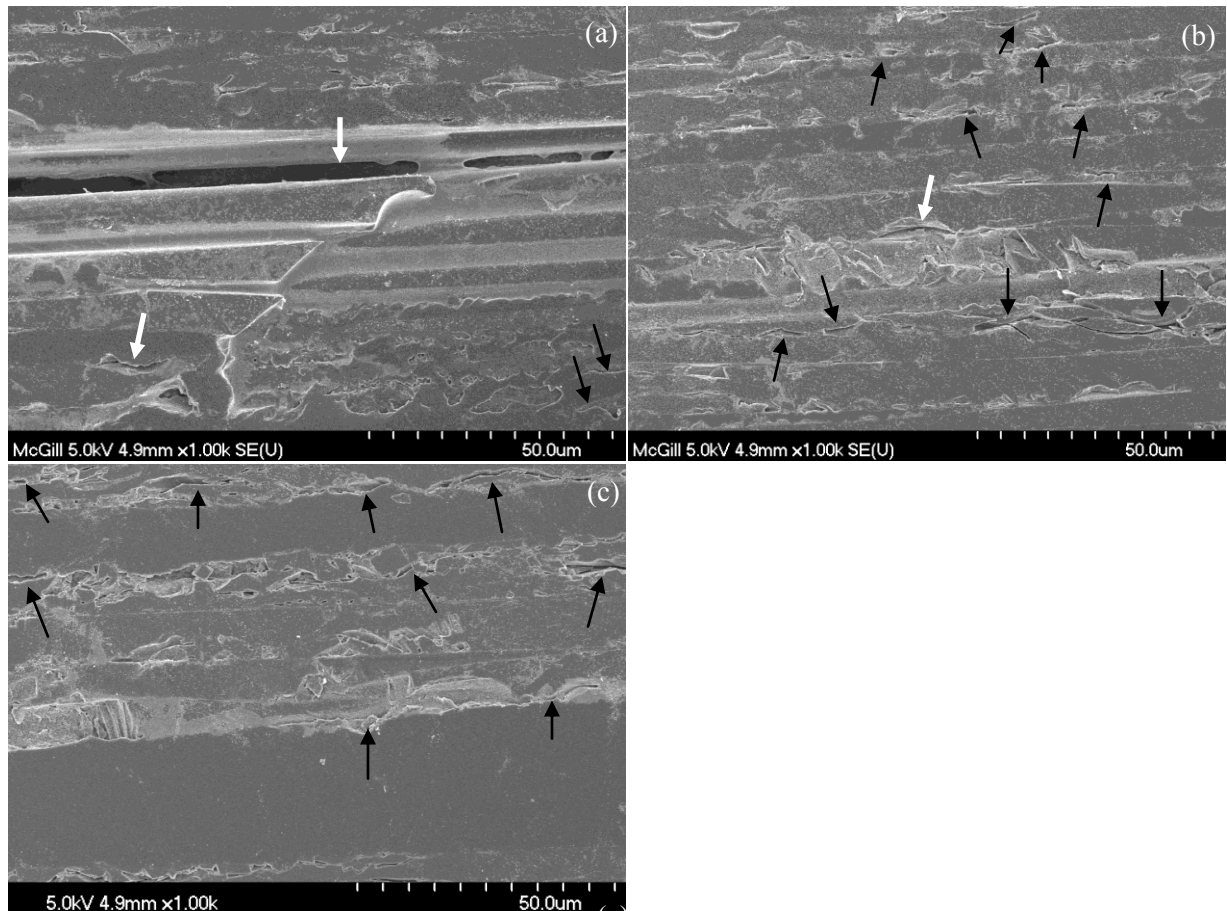


*Figure 5.12 SEM images of cross-section of laminate at location A; (a) without nanoclay, (b) 1 wt.% nanoclay and (c) 2 wt.% nanoclay.*

and the delamination has taken place parallel to the crack propagation direction. This is a typical fractography feature of unfilled polymer having low fracture toughness thus brittle in nature. On the contrary, SEM images of laminate with 1 wt.% nanoclay shown in figure 5.12b has improved fracture behavior. Although there are some delaminations and micro-cracks observable within 3<sup>rd</sup> and 4<sup>th</sup> layers but the length of delamination and

micro-cracks is considerably less than the laminate without nanoclay. The laminate with 2 wt.% nanoclay shown in figure 5.12c has no delamination and less micro-cracks observable within the same plane. Also the micro-cracks within laminate with 1 and 2 wt.% nanoclay mostly have curved shape that means the direction of propagation has been changed. This is may be because of improved fracture toughness of matrix system due to the presence of nanoclay that usually induces a rough fracture surface thus distorting the crack propagation direction frequently. The nanoclay platelet and nanoclay aggregate easily interact with a growing crack front to distort its direction of propagation and eventually stops it. Similar trend was also observed by some other investigators [13,59]. As the samples were polished, the interaction of nanoclay with a growing crack front was not clearly observable in the SEM images. It is also remarkable here that the damages (in the form of micro-cracks leading to delaminations) have mostly taken place within the 3<sup>rd</sup> and 4<sup>th</sup> layers (90° layers). The 1<sup>st</sup> and 2<sup>nd</sup> layers are not much affected by the fatigue load. This indicates that fibers take the major portion of flexural load and damages within the 0° layers are minimal.

### **5.2.2 Location B**

Figure 5.13a to 5.13c represents the SEM images of cross sections at 3cm from the fixed end. Here the bending moment and shear stress within the laminate due to applied deflection is less compared to location A. The images indicate similar trend of fracture behavior as location A but only the extent of fracture concentration is less due to low applied bending moment.

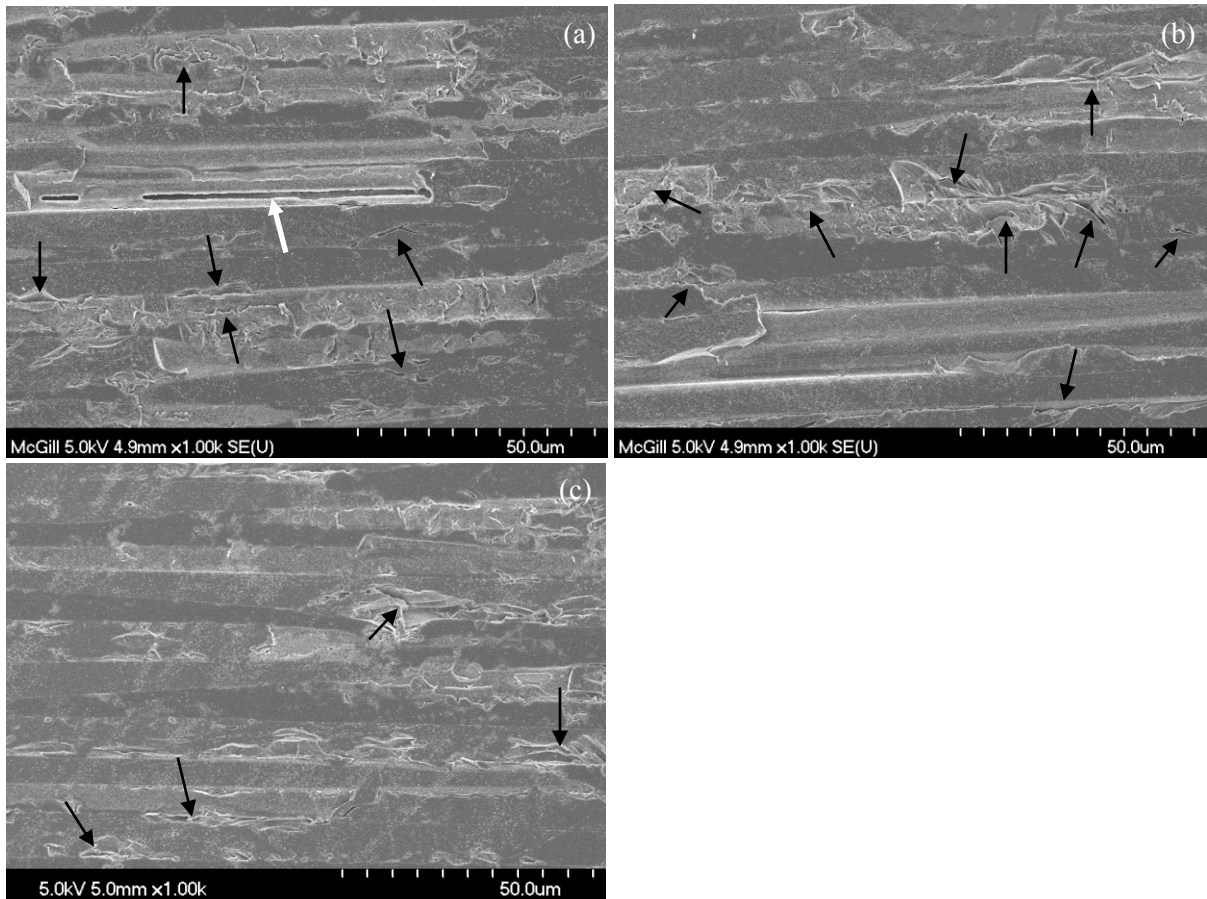


*Figure 5.13 SEM images of cross-sections of laminate at location B; (a) without nanoclay, (b) 1 wt.% nanoclay and (c) 2 wt.% nanoclay.*

Laminates with 1 and 2 wt.% nanoclay in figure 5.13b and 5.13c have successively less amount of micro-cracks than the laminate without nanoclay in figure 5.13a. Within the area of SEM image of the laminate without nanoclay in figure 5.13a, a delamination of approximately  $75\mu\text{m}$  has taken place. Whereas, the laminates with 1 and 2 wt.% nanoclay in figure 5.13b and 5.13c do not have any delaminated area but some micro-cracks. This is a clear indication of improvement and it can be said that nanoclay incorporation significantly improve flexural fatigue behavior and fracture characteristics.

### 5.2.3 Location C

Figure 5.14a to 5.14c represents the SEM images of cross sections at 6 cm from the fixed end and this is the location where strain gages were attached during flexural fatigue test. Here the bending moment and shear stress within the laminate due to applied deflection is less compared to location B. Similar to previous case, the images indicate similar trend of fracture behavior as location B but the extent of micro-crack concentration is less due to

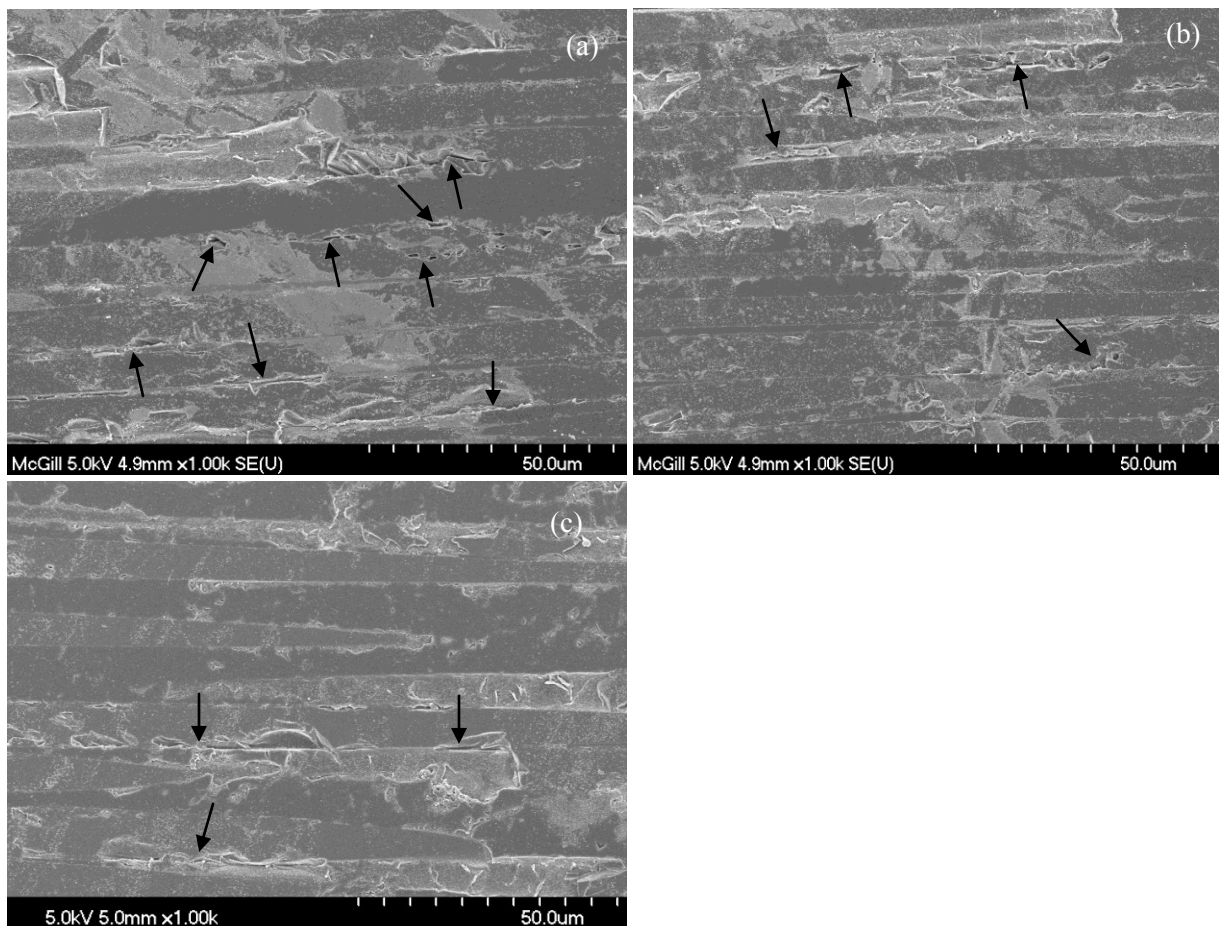


*Figure 5.14 SEM images of cross-sections of laminate at location C; (a) without nanoclay, (b) 1 wt. % nanoclay and (c) 2 wt. % nanoclay.*

low applied bending moment at this position. Laminates with 1 and 2 wt.% nanoclay in figure 5.14b and 5.14c have successively less amount of micro-cracks than the laminate without nanoclay in figure 5.14a.

### **5.3 Conclusion**

In this chapter the flexural fatigue test results are presented. Flexural fatigue test results indicate that nanoclay incorporation significantly improves the flexural fatigue life of glass/epoxy composite materials. At only 1 wt.% nanoclay loading, the flexural fatigue life of cross-ply laminate was increased by an average of 66% while at 2 wt.% nanoclay loading the average improvement is 133%. For quasi-isotropic laminate, the improvement is 62% and 108% respectively. To validate the test results, free vibration tests were done after every 100,000 fatigue cycles to see the decay of amplitude of vibration over time. If there is any damage within the laminate, the amplitude would decay faster. The free vibration test results considerably agree with the flexural fatigue test results. Fatigue damage index was calculated after 200,000 and 300,000 fatigue cycles which also satisfy the flexural fatigue test results. Optical and scanning electron microscopy was done to see the fracture behavior after fatigue test. The optical and SEM images indicate that damages occur within the laminate in the form of micro-cracks and gradually lead to delaminations. It also indicates that nanoclay significantly improve fractographic characteristics of glass/epoxy composite laminates and extend its service life.

# Chapter 6

## Conclusion, Contributions and Future Work

### 6.1 Conclusion

In this research, vibration damping and flexural fatigue behavior of glass/epoxy/nanoclay composite were studied. Organically modified nanoclay was dispersed in epoxy resin by high speed mixing method using a high speed homogenizer. Good dispersion was achieved using this method and SEM images of the fracture surface indicate that an exfoliated/intercalated structure was obtained.

To measure the vibration damping property, DMA analysis and log decrement tests were carried out. DMA analysis indicates that nanoclay incorporation significantly improve both storage modulus and loss modulus. That means, nanoclay enhances the energy dissipation capability of glass/epoxy composite material and at the same time increases its stiffness. A maximum of 16.8% improvement in storage modulus was obtained at 2 wt.% nanoclay incorporation in unidirectional laminate. Maximum improvement in loss modulus was 22.5% in quasi-isotropic laminate for same nanoclay loading. Also the glass transition temperature was not affected due to nanoclay incorporation. In the log decrement test, a maximum of 57% improvement in damping ratio was observed at 2 wt.% nanoclay incorporation in quasi-isotropic laminate. Thus it can be said that nanoclay significantly improves vibration damping property.

Flexural fatigue tests were done on cross-ply and quasi-isotropic laminate to see the effect of nanoclay on flexural fatigue behavior. A low amplitude flexural fatigue test was

designed so that fatigue could be attributed from vibration and free from thermal effect. Test results show that nanoclay significantly improves flexural fatigue life. Flexural fatigue life of cross-ply laminate was increased by 66% and 133% at only 1 and 2 wt.% nanoclay incorporation respectively. This improvement might be attributed from the improvement in vibration damping due to nanoclay incorporation. It may also be attributed from the improved fracture toughness and improved strength of resin system due to addition of nanoclay. Nanoclay and nanoclay aggregate can easily interact with a growing crack front and distort its direction of propagation. Thus the presence of nanoclay makes crack propagation more difficult compared to the laminate without nanoclay. The SEM images of cross-section of fatigued sample indicate that nanoclay addition successfully reduce micro-crack formation within the laminate thus improving its fatigue life.

## **6.2 Contributions**

This study has the following contributions.

- Demonstrated the effect of addition of nanoclay on the improvement of vibration damping of glass/epoxy composites.
- Demonstrated the effect of addition of nanoclay on the improvement of flexural fatigue lives of glass/epoxy composites.

### **6.3 Future work**

This project could lead to following further investigations.

- Log decrement tests were carried out in air thus test results include air damping. To get exact material damping property, the test can be done in vacuum to avoid the effect of air damping.
- The experiments can be done on actual parts (i.e. helicopter yoke, blade etc.) to see the effect of nanoclay on actual components.

## References:

- [1] Chandra R, Singh S P, Gupta K, “A study of damping in fiber-reinforced composites”, *J. of Sound and Vibration*, 262, 475-496, 2003.
- [2] Chandra R., Singh S.P., Gupta K., “Damping studies in fiber-reinforced composites- a review”, *Composite structure*, 46, 41-51, 1999.
- [3] Helmy A K, Ferreiro E A, Bussetti S G de, “Surface area evaluation of Montmorillonite”, *Journal of Colloid and Interface Science*, 210, 167–171, 1999.
- [4] Zhou X, Shin E, Wang K W, Bakis C E, “Interfacial damping characteristics of carbon nanotube-based composites”, *Composites Sci. and Technol.*, 64, 2425-2437, 2004.
- [5] Mohan T P, Kumar M R, Velmurugan R, “Thermal, mechanical and vibration characteristics of epoxy-clay nanocomposites”, *J. Mater Sci.*, 41, 5915-5925, 2006.
- [6] Sarathi R, Sahu R, Danikas M G, “Understanding the mechanical properties of epoxy nanocomposites insulating materials”, *J. Electrical Engineering*, 60, 358-361, 2009.
- [7] Mantena P R, Al-Ostaz A, Cheng A H D, “Dynamic response and simulations of nanoparticle-enhanced composites”, *Composites Sci. and Technol.*, 69, 772-779, 2009.
- [8] Usuki A, Kojima Y, Kawasumi M, Okada A, Fukushima Y, et al. “Synthesis of nylon 6-clay hybrid”, *Journal of Materials Research*, 8, 1179-1184, 1993.

- [9] Deer W A, Howie R A, "Rock-forming minerals", Wiley, 3, 240, 1962.
- [10] Ray S S, Okamoto M, "Polymer/layered silicate nanocomposites: a review from preparation to processing", Prog. Polym. Sci., 28, 1539-1641, 2003.
- [11] Alexandre M, Dubois P, "Polymer-layered silicate nanocomposites: preparation, properties and uses of a new class of materials", Materials Science and Engineering, 28, 1-63, 2000.
- [12] Vaia R A, Teukolsky R K, Giannelis E P, "Interlayer structure and molecular environment of Alkylammonium layered silicates", Chem. Mater., 6, 1017-1022, 1994.
- [13] Ngo T D, "Understanding the effect of adding nanoclays into epoxies", PhD thesis, Concordia University, 2007.
- [14] Vaia R A, Jandt K D, Kramer E J, Giannelis E P, "Microstructural evolution of melt intercalated polymer-organically modified layered silicates nanocomposites", Chem. Mater., 8, 2628-2635, 1996.
- [15] Vaia R A, Ishii H, Giannelis E P, "Synthesis and properties of two-dimensional nanostructures by direct intercalation of polymer melts in layered silicates", Chem. Mater., 5, 1694-1696, 1993.
- [16] Ngo T D, Ton-That M T, Hoa S V, Cole K C, "Effect of temperature, duration, and speed of pre-mixing on the dispersion of clay/epoxy nanocomposites", Composites Science and Technology, 69, 1831-1840, 2009.

- [17] Gianni A D, Amerio E, Monticelli O, Bongiovanni R, "Preparation of polymer/clay mineral nanocomposites via dispersion of silylated montmorillonite in a UV curable epoxy matrix", *Applied Clay Science*, 42, 116-124, 2008.
- [18] Kornmann X, Thomann R, Mulhaupt R, Finter J, Berglund L A, "High performance epoxy-layered silicate nanocomposites", *Polymer Engineering and Science*, 42, 1815-1826, 2002.
- [19] Munzy C D, Butler B D, Hanley H J M, Tsvetkov F, Peiffer D G, "Clay platelet dispersion in a polymer matrix", *Materials Letters*, 28, 379-384, 1996.
- [20] Lam C, Lau K, Cheung H, Ling H, "Effect of ultrasound sonication in nanoclay/epoxy composites", *Materials Letters*, 59, 1369-1372, 2005.
- [21] Mitra Y, Hossien T, Daulton T L, Lin J-S, Pittman C U, "Clay delamination in clay/ poly(dicyclopentadiene) nanocomposites quantified by small angle neutron scattering and high resolution transmission electron microscopy", *Macromolecules*, 38, 818-831, 2005.
- [22] Hernandez M, Sixou B, Duchet J, Sautereau H, "The effect of dispersion state on PMMA-epoxy-clay ternary blends", *Polymer*, 48, 4075-4086, 2007.
- [23] Park J H, Jana S C, "The relation between nano- and micro-structures and mechanical properties in PMMA-epoxy-nanoclay composites", *Polymer*, 44, 2091-2100, 2003.
- [24] Liu W P, Hoa S V, Pugh M, "Organoclay-modified high performance epoxy nanocomposites", *Composites Science and Technology*, 65, 307-316, 2005.

- [25] Liu W P, Hoa S V, Pugh M, “Fracture toughness and water uptake of high performance epoxy/nanoclay nanocomposites”, *Composites Science and Technology*, 65, 2364-2373, 2005
- [26] Adams R D, Bacon D G C, “Effect of fiber-orientation and laminate geometry on properties of CFRP”, *J. Comp. Mater.*, 7, 402-428, 1973.
- [27] Ni R G, Adams R D, “The damping and dynamic moduli of symmetric laminated composite beams-Theoretical and experimental results”, *J. Comp. Mater.*, 18, 104-121, 1984.
- [28] Adams R D, Maheri M R, “Dynamic flexural properties of anisotropic fibrous composite beams”, *Composite Science and Technology*, 50(4), 497-514, 1994.
- [29] Yim J H, “A damping analysis of composites using the closed form expression for the basic damping of poisson’s ratio”, *Composite Structures*, 46, 405-411, 1999.
- [30] Suarez S A, Gibson R F, Sun C T, Chaturvedi S K, “The influence of fiber length and fiber orientation on damping and stiffness of polymer composite materials”, *Experimental Mechanics*, 26(2), 175-184, 1986.
- [31] Gibson R F, Chaturvedi S K, Sun C T, “Complex moduli of aligned discontinuous fiber-reinforced polymer composites”, *Journal of Materials Science*, 17, 3499-3509, 1982.
- [32] Cox H L, “The elasticity and strength of paper and other fibrous materials”, *British Journal of Applied Physics*, 3, 72-79, 1952.

- [33] Saravanos D A, Chamis C C, “Unified micromechanics of damping for unidirectional and off-axis fiber composites”, *Journal of Composites Technology & Research*, 12(1), 31-40, 1990.
- [34] White R G, Abdin E M Y, “Dynamic properties of aligned short carbon fiber-reinforced plastic in flexure and torsion”, *Composites*, 16(4), 293-306, 1985.
- [35] Hwang S J, Gibson R F, “Micromechanical modeling of damping in discontinuous fiber composites using a strain energy/finite element approach”, *Journal of Materials Science and Technology*, 109, 47-52, 1987.
- [36] Chaturvedi S K, Tzeng G Y, “Micromechanical modeling of material damping in discontinuous fiber three-phase polymer composites”, *Composite Engineering*, 1(1), 49-60, 1991.
- [37] Tzeng G Y, “Micromechanical modeling of damping and stiffness of three phase polymer composites” Master’s Thesis, Ohio State University, 1989.
- [38] Finegan I C, Tibbetts G G, Gibson R F, “Modeling and characterization of damping in carbon nanofiber/polypropylene composites”, *Composites Science and Tech.*, 63, 1629-1635, 2003.
- [39] Sun C T, Wu J K, Gibson R F, “Prediction of material damping in randomly oriented short fiber polymer matrix composites”, *Journal of Reinforced Plastics and Composites*, 4, 162-272, 1985.
- [40] Adams R A, Bacon D G C, “Measurement of the flexural damping capacity and dynamic Young’s modulus of metals and reinforced plastics”, *J. Phys. D: Appl. Phys.*, 6, 27-41, 1973.

- [41] Guild F J, Adams R D, "A new technique for the measurement of the specific damping capacity of the beams in flexure", *J. Phys. E: Sci. Instrum.*, 14, 355-363, 1981.
- [42] Gibson R F, "Modal vibration response measurements for characterization of composite materials and structures", *Comp. Sci. Technol.*, 60, 2769-2780, 2000.
- [43] Pant R H, Gibson R F, "Analysis and testing of dynamic micromechanical behavior of composite materials at elevated temperatures", *J. of Engineering Materials and Technology*, 118, 554-560, 1996.
- [44] Wei C Y, Kukureka S N, "Evaluation of damping and elastic properties of composites and composites structures by the resonance technique", *J. Materials Science*, 35, 3785-3792, 2000.
- [45] Riviere A, "Measurement of high damping: techniques and analysis", *J. of Alloys and Compounds*, 355, 201-206, 2003.
- [46] Moser K, Lumassegger M, "Increasing the damping of flexural vibration of laminated FPC structures by incorporation of soft intermediate plies with minimum reduction of stiffness", *Composite Structures*, 10, 321-333, 1988.
- [47] Liao F, Su A, Hsu T J, "Vibration damping of interleaved carbon fiber-epoxy composite beams", *J. Composite Mater.*, 28(18), 1840-1854, 1994.
- [48] Berthelot J, Sefrani Y, "Damping analysis of unidirectional glass fiber composites with interleaved viscoelastic layers: experimental investigation and discussion", *J. Composite Mater.*, 40(21), 1911-1931, 2006.

- [49] Tanimoto T, “A new vibration damping CFRP material with interlayers of dispersed piezoelectric ceramic particles”, *Composites Sci. and Technol.*, 67, 213-221, 2007.
- [50] Oshima N, Inui D, Fukuda T, “Improvement of damping property of CFRP composite beam interleaved with shape memory polymer using CFRP laminate as a heater”, *Mem. Fac. Eng., Osaka City Univ.*, 38, 1-6, 1997.
- [51] Romberg O, Tausche M, Pereira C, Panning L, “Passive damping of spacecraft sandwich panels”, 10th European Conference on Spacecraft Structures, Materials & Mechanical Testing, 10-13 Sep 2007, Berlin.
- [52] Messersmith P B, Giannelis E P, “Synthesis and characterization of layered silicate-epoxy nanocomposites”, *Chem. Mater.*, 6, 1719-1725, 1994.
- [53] Chen C, Curliss D, “Processing and morphological development of montmorillonite epoxy nanocomposites”, *Nanotechnology*, 14, 643-648, 2003.
- [54] Hudnut S W, Chung D D L, “Use of submicron diameter carbon filaments for reinforcement between continuous carbon fiber layers in a polymer-matrix composite”, *Carbon*, 33(11), 1627-1631, 1995.
- [55] Haque A, Shamsuzzoha M, “S2-glass/epoxy polymer nanocomposites: manufacturing, structures, thermal and mechanical properties”, *J. Composite Materials*, 37(20), 1821-1837, 2003.
- [56] Avila A F, Donadon L V, Duarte H V, “Modal analysis on nanoclay epoxy-based fiber-glass laminates”, *Composite Structures*, 83, 324-333, 2008.

- [57] Chandradass J, Kumar M R, Velmurugan R, “Effect of nanoclay addition on vibration properties of glass fibre reinforced vinyl ester composites”, *Materials Letters*, 61, 4385-4388, 2007
- [58] Velmurugan R, Jeyaprakash P, Balaganesan G, “Damping study of hybrid nano composites by low velocity impact”, *Proceedings of International Conference on Aerospace Science and Technology, India*, 26-28 June 2008.
- [59] Varadharajan B R, “Fatigue behavior of  $\alpha$ -Zirconium Phosphate/epoxy nanocomposites”, Master’s thesis, Texas A&M University, 2005.
- [60] Song M, Yao K J, “X-ray diffraction detection of compliance in polyurethane-organoclay nanocomposites”, *Materials Science and Technology*, 20, 989-993, 2004.
- [61] Blackman B R K, Kinloch A J et al., “The fracture and fatigue behavior of nano-modified epoxy polymers”, *J. Mater. Sci.*, 42, 7049-7051, 2007.
- [62] Wetzel B, Rosso P et al., “Epoxy nanocomposites – fracture and toughening mechanisms”, *Engineering Fracture Mechanics*, 73, 2375-2398, 2006.
- [63] Chisholm N, Mahfuz H, Rangari V K, Ashfaq A, Jeelani S, “Fabrication and mechanical characterization of carbon/SiC-epoxy nanocomposites”, *Composite Structures*, 67, 115-124, 2005.
- [64] Grimmer C S, Dharan C K H, “High-cycle fatigue of hybrid carbon nanotube/glass fiber/ polymer composites”, *J. Mater. Sci.*, 43, 4487-4492, 2008.
- [65] <http://www.agy.com/>
- [66] <http://www.nanocor.com/>
- [67] <http://www.hexion.com/>

[68] <http://www.ika.net/>

[69] 983 Dynamic Mechanical Analyzer, Operator's Manual, Du Pont Company, Wilmington, DE, 1986.